SPATIAL DIVERSITY FOR ATMOSPHERIC OPTICAL COMMUNICATIONS

James Harwood Churnside
B.S., Whitworth College, 1974

A dissertation submitted to the faculty
of the Oregon Graduate Center
in partial fulfillment of the
requirements for the degree
Doctor of Philosophy
in
Applied Physics

April, 1978

This dissertation has been examined and approved by the following Examination Committee:

Charles M. McIntyre, Thesis Advisor
Assistant Professor

Richard A. Elliott
Associate Professor

Douglas F. Barofsky
Associate Professor

J. Richard Kerr
Professor

Acknowledgements

This work was supported in part by the National Science Foundation under NSF grant ENG73-08221.

I would like to acknowledge the help and guidance received from everyone connected with atmospheric propagation at the Oregon Graduate Center. In addition, I would like to thank the members of my examining committee, and Dr. J. Richard Kerr in particular, for their efforts.

To my thesis advisor Dr. Charles M. McIntyre, and to my loving wife Karen, I owe a special debt of gratitude for making this work possible.

TABLE OF CONTENTS

6. N-Fold Probability Distribution of an Optical Heterodyne Receiver Array in the Turbulent Atmosphere

List of Figures

ABSTRACT

This work presents results pertinent to the study of spatial diversity as a means for partially overcoming the deleterious effects of the clear-air turbulent atmosphere on direct detection and heterodyne optical communication systems. For photon counting receivers, an averaged threshold receiver is presented, which is seen to be simpler to implement and to provide consistantly lower bit error rates than optimized memoryless receivers. The heterodyne results include the introduction of a partial tracking heterodyne array; a discussion, both theoretical and experimental, of IF signal magnitude probability distributions for static heterodyne arrays; and a theoretical treatment of the probability distribution for a single heterodyne element with angle-of-arrival tracking.

1. INTRODUCTION

The concept of using optical beams for communications through the atmosphere is not a new one. As early as 458 B.C.E., the Greek Playwrite Aeschylus described how news of the defeat of Troy was returned to Argos by a relay system of beacon fires.[1] From this rather crude beginning, sophisticated systems have been developed, with lasers being used in place of bonfires and complex photoelectric devices in place of the eyes of Greek slaves. This work is an investigation into certain aspects of refinements in these detectors, based on improved understanding of the effects of the clear-air turbulent atmosphere on optical propagation.

In 1905, Einstein proposed that, while light behaves as an electromagnetic wave in some respects, in other cases it behaves like a particle.[2] In one view, the most fundamental detection process involves counting the individual photons, or particles of the received signal. In the other view, the received wave can be amplified by heterodyning, or mixing it with a strong optical wave generated in the receiver structure. Both of these detection processes will be considered here.

The optical signal reaching a detector, however, can be severely distorted by propagation through the atmosphere.[3,4] Although fog, rain, snow, dust, atmospheric molecules, and turbulence all can contribute to this distortion, the effects of turbulence are probably the most pervasive, due to the relatively minor contribution of molecular scattering and to the intermittent nature of particulate scattering. Concentrating on the effects of turbulence, one finds that the instantaneous distortion varies from point to point in the detection plane. This leads to the concept of spatial diversity. By judiciously combining the signals from several photon counting or heterodyne detectors, one can partially overcome the deleterious effects of atmospheric turbulence.

The investigation of what is meant by "judiciously combining the signals" is, in general, a four step process consisting of the following stages of development:

1) evaluation of the probability distribution of the signals to be combined,
2) evaluation of optimum "memoryless" combining structure and resulting bit error rate,
3) evaluation of simplified "memoryless" structures and associated bit error rates,
4) evaluation of systems with memory - structures and bit error rates,

where a system with memory is one which uses information from previous bits to evaluate the present one. It should be noted that, in discussing bit error rates, the topic of interest has been limited to digital communication systems.

For the case of photon counting elements, the theory of the first three steps of this process has been developed by Teich, et. al.[5-8] The final stage is covered in Chapter 2 of this work.

The heterodyne case is complicated by a number of possible receiver configurations, which must be considered separately. The first choice to be made is whether to combine the signals after IF demodulation or before. For the former case, the probability distribution of the IF signal magnitudes must be evaluated in step 1. The latter requires knowledge of the magnitude and phase statistics of the IF signals and will not be considered in this work. The second choice is whether to track angle-of-arrival fluctuations at each array element, to track the average instantaneous angle-of-arrival over the array, or to employ no tracking at all. The second configuration is introduced in Chapter 3 of this work, and compared, in terms of total array SNR, with the other two previously presented receiver types.

In Chapters 4 through 6 of this work, the investigation of signal combining structures for these six heterodyne receiver configurations is begun. What has been accomplished is presented in Table I.

	pre demodulation combining	post demodulation combining
non tracking		step 1 independent fading theory - Chap. 4 independent fading experimental - Chap. 5 correlated fading theory and experiment - Chap. 6
partial tracking		
full tracking		step 1 independent fading theory - Chap. 4

Table I. Status of diversity heterodyne investigation.

2. AVERAGED THRESHOLD RECEIVER FOR DIRECT DETECTION OF OPTICAL COMMUNICATIONS THROUGH THE LOGNORMAL ATMOSPHERIC CHANNEL

I. Introduction

Several authors[7,9] have looked at the problem of developing efficient, practical, diversity receivers for direct detection of low power optical communication signals. In this chapter, a different receiver structure is developed that is simpler to implement than either the optimum or the *maximum a posteriori* (MAP) receivers developed by Teich and Rosenberg; it is seen to result in a lower bit error rate than these previous receivers under a wide range of conditions.

A block diagram of the general system under consideration is given in Figure 2.1. The signal to the receiver will be assumed to come from an array of high gain, photon counting detectors, so that shot noise and background radiation are the major sources of noise introduced in the detection process.[10,11] The optical field at each detector consists of the signal after fading caused by the atmosphere plus an independent additive component due to background radiation.[10,11]

Several assumptions have been made in order to reduce the number of parameters to a manageable level. These have been chosen, however, so that the results will be applicable to most practical systems. Independent fading at each detector in the array is assumed for the most efficient use of low signal levels.[8] Under usual conditions, the background radiation, due to band-limited Gaussian thermal sources, can be considered to be a constant additive intensity at each detector.[5,12] The transmitter is assumed to be of constant intensity; for most practical systems, the sampling rate imposed by modulation will be unable

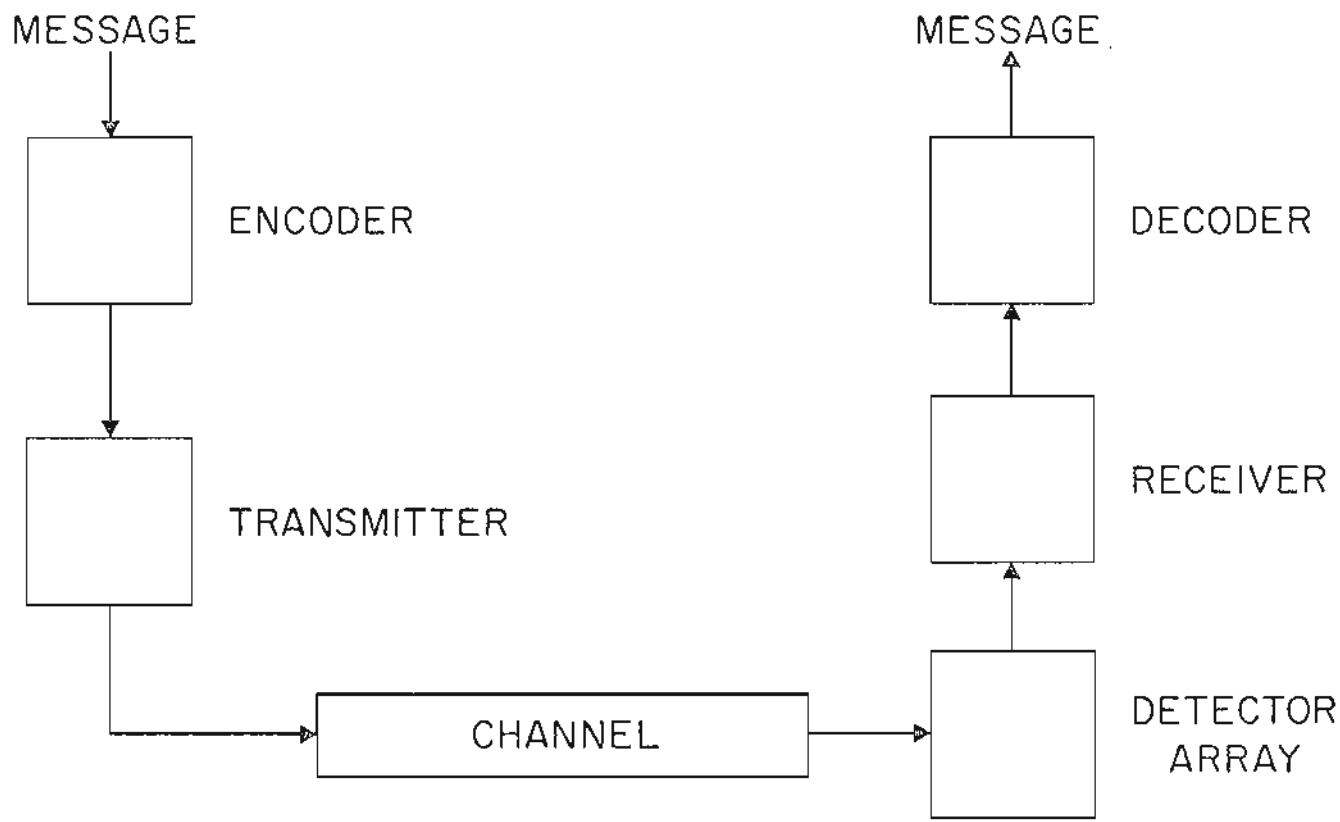

Fig. 2.1. Block diagram of general optical communication system. Specific receiver structures will be examined for channels through the clear-air turbulent atmosphere.

to resolve source intensity fluctuations,[8] justifying this assumption. For simplicity, only symmetric, binary, pulse-code modulation is considered, with bit rates faster than atmospheric fluctuations (~ 500 Hz).[4]

In Section 2.II, those characteristics of the signal, the channel, and the detection process pertinent to the receiver structure are described in detail. Section 2.III is a review of the approximate optimum and MAP receivers, along with a derivation of the new averaged threshold receiver and a limit to its applicability. Section 2.IV compares bit error rates of these three receivers for various combinations of turbulence strength, background radiation level, signal to noise ratio, number of diversity channels, and number of bits used for threshold averaging.

II. General System Considerations

The effects of turbulence on the signal are described by the normalized fading parameter, defined as $Z = I_S'/I_S$,[3] where I_S' is the instantaneous optical signal intensity at a point in the receiver plane, and I_S is the intensity that would be present at that point in the absence of turbulence. Based on both experimental and theoretical evidence,[3,13] Z is considered to be a lognormal random variable, with probability density function:

$$p(Z) = \frac{1}{\sqrt{2\pi}\sigma Z} \exp\left[-\frac{\left(\ln(Z) + \frac{1}{2}\sigma^2\right)^2}{2\sigma^2}\right] \qquad (1)$$

where σ^2 is the normalized log-intensity variance. Scattering and absorption by the atmosphere are neglected except for a possible uniform reduction of the signal strength reaching the receiver plane.

In addition to the received signal ZI_S, a uniform (unresolved) background illumination of intensity I_B may be present so that, at a point in the receiver plane, the optical intensity is given by:

$$I = ZI_S + I_B \qquad \text{if 1 is sent} \qquad (2a)$$

$$I = I_B \qquad \text{if 0 is sent} \qquad (2b)$$

Note that, for simplicity, I_S, I_B, and σ^2 are assumed to be the same at all detectors in the array.

An array of D photon counting detectors is mounted in the receiver plane. The relative performance of receivers using 1, 2, and 4 channel spatial diversity detector arrays will be explored in Section 2.IV. The detectors in the array are assumed to be spaced so that the fading at each detector is independent of that at any other. This is an easy condition to meet in practice. Eliminating non-zero correlation between adjacent detectors improves bit error rates,[8] and, by decoupling necessary calculations, also results in simplified receiver structures.[7]

In order to easily find the integrated intensity over each detector area and over the period of each bit, it is assumed that 1) the area of each detector is smaller than the coherence area of the fading, and 2) the duration of each bit is shorter than the coherence time. Actually, these conditions are not rigorously required in practice. If Z is replaced by its average value over the detector area and bit period, then this new random variable retains much of the log-normal characteristic.[14] This averaged

value of Z obviously satisfies the conditions of limited spatial and temporal coherence just described. Note, however, that the log-intensity variance, σ^2, must then be calculated differently.[3,13]

The number of photoelectrons emitted during a time T from a photocathode of area A is a Poisson random variable[15] described by the conditional density function:

$$p(n|W) = \frac{1}{n!} W^n e^{-W} \tag{3}$$

In this expression W, the integrated rate parameter, is defined as:

$$W = \frac{\eta}{h\nu} \int_T \int_A I(\vec{r},t)\, d\vec{r}\, dt \tag{4}$$

where η is the quantum efficiency of the photocathode, h is Planck's constant, ν is the frequency of the signal, and $I(\vec{r},t)$ is the irradiance at $\vec{r}$, at time t. Using the assumptions of limited spatial and temporal coherence of the fading, the integration reduces to multiplication by T and A so that W is given by:

$$W = ZN_S + N_B \qquad \text{if 1 is sent} \tag{5a}$$

$$W = N_B \qquad \text{if 0 is sent} \tag{5b}$$

Here N_B is defined as $(\eta/h\nu)$ A T I_B and is equal to the mean number of photocounts due to background radiation, and similarly, $N_S = (\eta/h\nu)$ A T I_S is the mean photocount due to signal intensity. It has been assumed that individual photoelectrons can be resolved and counted.

If H_1 is the hypothesis that a one was sent (signal is present) and H_0 is the hypothesis that a zero was sent (no signal), then the

receiver, for an array of D independent detectors with independent fading, must choose between H_o and H_1. The decision is based on $\vec{n}$, which is a D-dimensional vector having components n_i giving the photocount from each detector and having the following conditional density functions:

$$p(\vec{n}|H_o) = \prod_{i=1}^{D} p(n_i|H_o) = \prod_{i=1}^{D} \frac{1}{n_i!} (N_B)^{n_i} \exp(-N_B) \tag{6a}$$

or

$$p(\vec{n}|H_1) = \prod_{i=1}^{D} p(n_i|H_1) \tag{6b}$$

$$= \prod_{i=1}^{D} \int_o^\infty \frac{1}{n_i!} (Z_i N_S + N_B)^{n_i} \exp(-Z_i N_S - N_B)\, p(Z_i)\, dZ_i$$

An approximation, for log-normal $p(Z_i)$, has been applied to this integral by Diament and Teich[5] and by Teich and Rosenberg.[7] Using the method of steepest descents, they find that:

$$p(n_i/H_1) =$$

$$\frac{\frac{1}{n_i!} (Z_{io} N_S + N_B)^{n_i} \exp(-Z_{io} N_S - N_B) \exp\left(\frac{-\left(\ln(Z_{io}) + \frac{1}{2}\sigma^2\right)^2}{2\sigma^2}\right)}{\left[1 + \sigma^2 Z_{io} N_s \left(1 - \frac{n_i N_B}{(Z_{io} N_S + N_B)^2}\right)\right]^{1/2}} \tag{7a}$$

where the D-dimensional vector $\vec{Z}_o$ is found from the condition that:

$$\frac{n_i Z_{io} N_S}{Z_{io} N_S + N_B} - Z_{io} N_S - \frac{\ln(Z_{io}) + \frac{1}{2}\sigma^2}{\sigma^2} = 0 \text{ for } i = 1, 2, \ldots D \tag{7b}$$

III. Receiver Structures

The purpose of the receiver processor is to decide between H_o and H_1, and, based on a simple Bayes criterion calculation, it can be shown that this decision should be made according to the likelihood ratio test in order to minimize the total probability of error.[16] In this test, the function L is defined as:

$$L(\vec{n}) = \ln \frac{p(\vec{n}|H_1)}{p(\vec{n}|H_o)} \tag{8}$$

and H_1 (H_o) is chosen for $L(\vec{n}) > (<) 0$. In the event that $L(\vec{n}) = 0$, either H_1 or H_o can be chosen at random without affecting the total probability of error. This type of receiver results in a total probability of error given by:

$$P(E) = \frac{1}{2}\left[P(L < 0|H_1) + P(L > 0|H_o)\right] \tag{9}$$

A. Optimum Processor

Based on the exact photocount density functions (6a,b), the lowest probability of error is seen to result from the likelihood function:

$$L = \sum_{i=1}^{D} \int_0^{\infty} \left(\frac{ZN_S}{N_B} + 1\right)^{n_i} \exp\left(-ZN_S\right) p(Z)\, dZ \tag{10}$$

However, this implies a degree of signal processing that may be difficult to achieve in many real-time situations. If the steepest descents approximation to $p(\vec{n}|H_1)$ is used instead of the exact expression, the processor no longer needs to evaluate the integrals in (10), and this results in a simplified likelihood function given by:

$$L = \sum_{i=1}^{D} \left\{ n_i \ln\left(\frac{Z_{io}N_S}{N_B} + 1\right) - Z_{io}N_S - \frac{\left(\ln Z_{io} + \frac{1}{2}\sigma^2\right)^2}{2\sigma^2} - \frac{1}{2}\ln\left[1 + \sigma^2 Z_{io}N_S\left(1 - \frac{n_i N_B}{\left(Z_{io}N_S + N_B\right)^2}\right)\right]\right\} \tag{11}$$

with the Z_{io} points found from the set of equations (7b). A block diagram of this receiver, given in Figure 2.2, shows that it is still a fairly complicated structure, requiring independent measurement of σ^2 in addition to *a priori* knowledge of N_S and N_B.

B. MAP Processor

A simpler processor structure than the approximate optimum described above would have several advantages. Speed and reliability generally increase as complexity decreases and, at the same time, the cost of the system tends to decrease. One obvious simplification is to assume that an estimate of the fading can be used as if the fading were known exactly; then the likelihood function reduces to:

$$L = \ln \frac{p(\vec{n}|Z,H_1)}{p(\vec{n}|Z,H_o)} = \sum_{i=1}^{D} n_i \ln\left(\frac{\hat{Z}_i N_S}{N_B} + 1\right) - \hat{Z}_i N_S \tag{12}$$

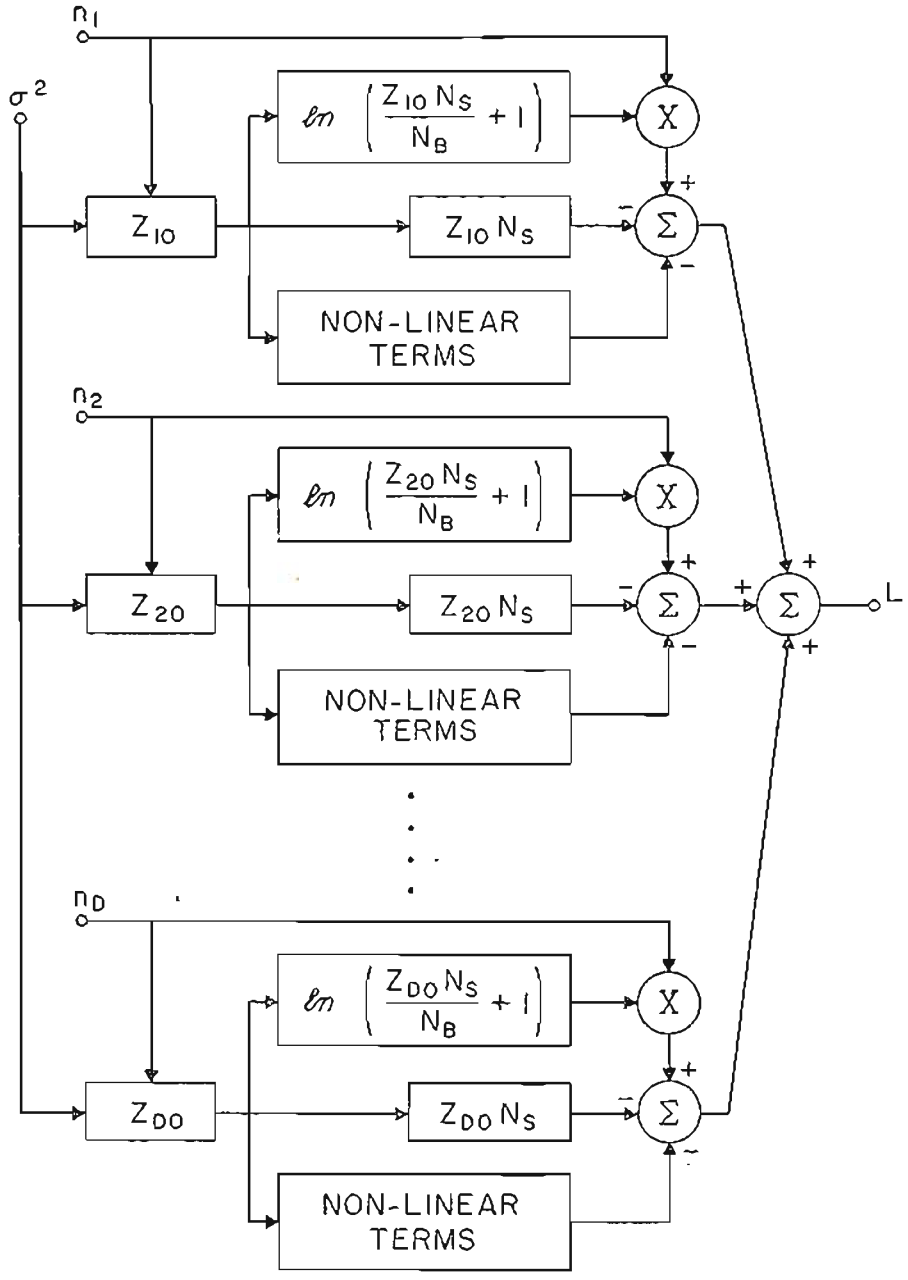

Fig. 2.2. Block diagram of approximate optimum receiver

where $\hat{Z}_i$ is the receiver estimate of the fading at the i'th detector. In the MAP receiver as described by Van Trees,[16] the $\hat{Z}_i$ are given by those values which maximize the *a posteriori* probability of the fading at each detector, given that n_i photocounts were received at that detector. In other words, the $\hat{Z}_i$ are found from the condition that:

$$\frac{\partial}{\partial Z_i}\left(p(Z_i|n_i)\right)_{Z_i = \hat{Z}_i} = 0 \quad i = 1, 2, \ldots D \tag{13}$$

which is easily seen to reduce to the condition that equation (7b) be satisfied for $Z_{io} = \hat{Z}_i$. In this approximation, the receiver structure has been simplified, as shown in Figure 2.3, even though the same inputs are still required.

C. Averaged Threshold Processor

The performance of the receivers described so far will remain constant whether the message consists of long strings of data or of a single bit. In practice, however, single bit messages are rare and a large number of bits will be received, in many applications, while the fading remains essentially constant. Where this holds, the signal can be averaged over several bits, and the $\hat{Z}_i$ can then be found from the extended MAP condition:

$$\frac{\partial}{\partial Z_i}\left(p(Z_i|\bar{n}_i)\right)_{Z_i = \hat{Z}_i} = 0 \quad i = 1, 2, \ldots D \tag{14}$$

where the average photocount over N bits is given by:

$$\bar{n}_i = \frac{1}{N}\sum_{j=1}^{N} n_{ij} \qquad i = 1, 2, \ldots D \tag{15}$$

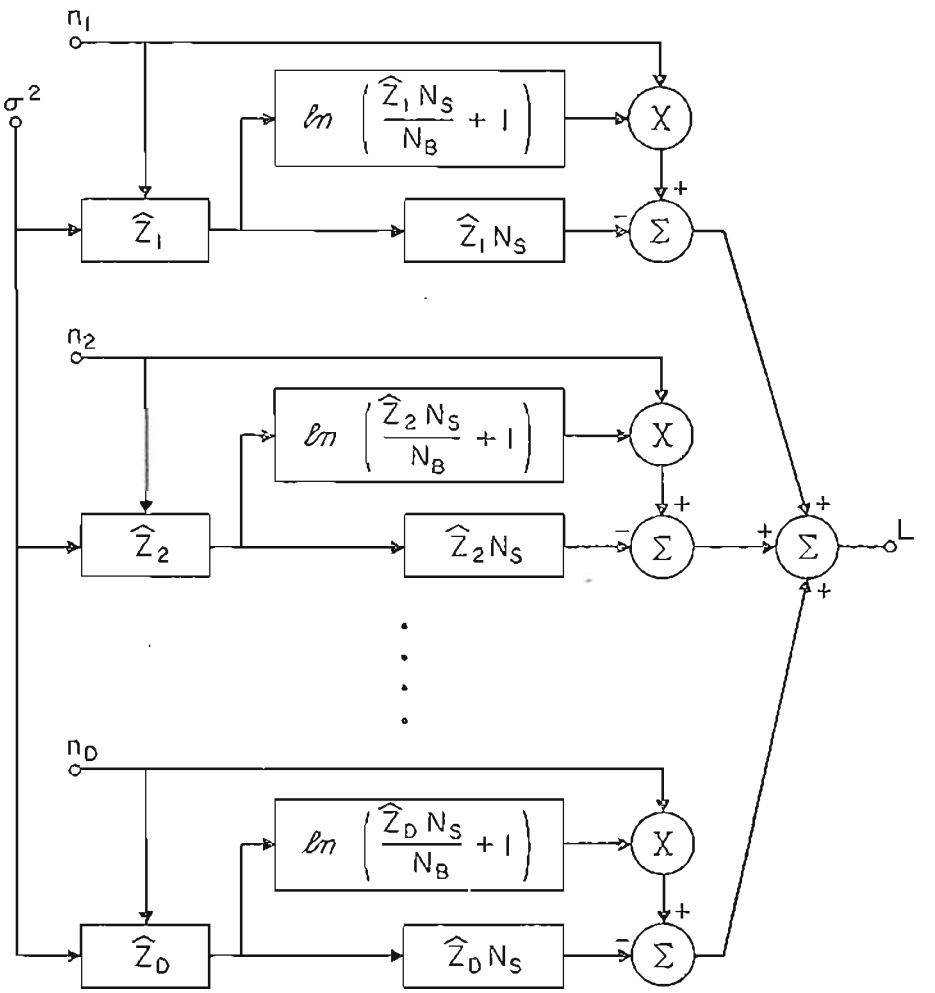

Fig. 2.3. Block diagram of MAP receiver

Note that, once the data rate has been specified, the number of averaging bits must be chosen carefully. It must be large enough that, with high probability, the number to "ones" seen and the number of "zeros" seen are each very close of $\frac{1}{2}N$ and, at the same time, it must be small enough that the fading changes very little during N bits. These factors will be explored in greater depth below. Assuming, however, that N has been judiciously chosen, equation (14) is easily reduced to the condition that:

$$\frac{N\bar{n}_i \hat{Z}_i N_S}{\hat{Z}_i N_S + 2N_B} - \frac{1}{2} N\hat{Z}_i N_S - \frac{\ln(\hat{Z}_i) + \frac{1}{2}\sigma^2}{\sigma^2} = 0 \qquad (16)$$

As N becomes large, the first two terms in equation (16) dominate, and the expression approaches the asymptotic form:

$$\bar{n}_i - \frac{1}{2} \hat{Z}_i N_S - N_B = 0 \qquad (17)$$

Using this approximation in the likelihood function of equation(12) results in a simplified function given by:

$$L = n_i \ln\left(\frac{2\bar{n}_i}{N_B} - 1\right) - 2\bar{n}_i + 2N_B \qquad (18)$$

It can be seen from the block diagram, Figure 2.4, that when compared to "single bit" receivers, this is a very simple processor, since measurement of σ^2 has been replaced by the more direct measurement of the $\bar{n}_i$ and knowledge of N_S is no longer necessary.

While the averaged threshold receiver, described by equation (18), can be used in a great many practical applications, there certainly exist situations in which it is not applicable, since it was assumed

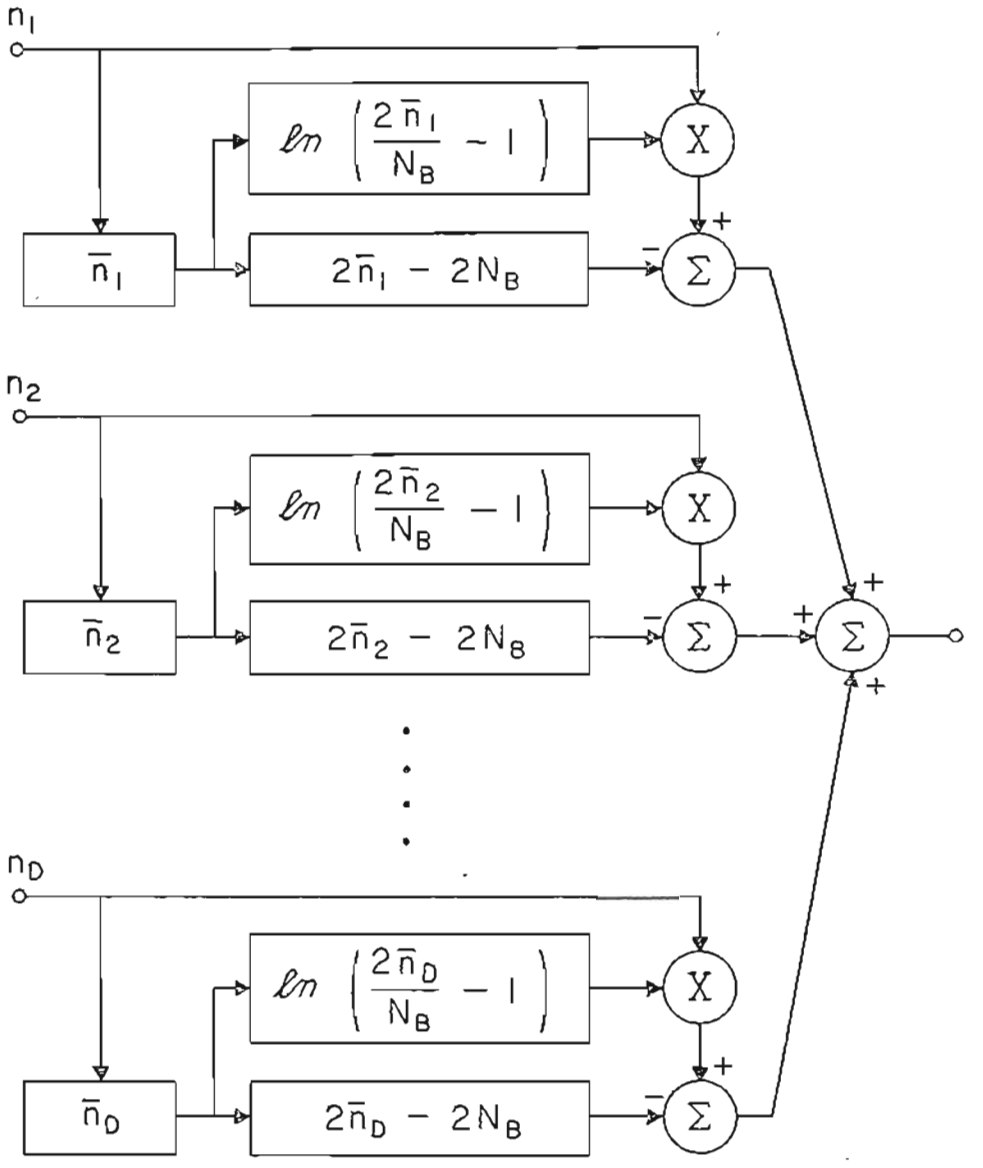

Fig. 2.4. Block diagram of averaged threshold receiver.

in the derivation that each Z_i is constant during the time that N bits are received. If "constant" is taken to mean that the fluctuations in the fading should be much less than the uncertainty in the receiver estimate of the fading, this assumption can be transformed into an upper bound on the number of averaging bits. In particular, it is shown in Appendix A that the condition:

$$N << 0.546\, N_B^{1/3}\, (\lambda L)^{5/18}\, l_o^{1/9} \left(\frac{R}{N_S \sigma v_\perp}\right)^{2/3} \left(\frac{1}{2} N_S + N_B + e^{\sigma^2} N_S^2\right) \tag{19}$$

must be satisfied, where $\sqrt{\lambda L}$ is the Fresnel zone size, l_o is the inner scale of turbulence, R is the data rate, and $v_\perp$ is the component of wind velocity perpendicular to the path.

IV. Bit Error Rates

The total probability of error for these receivers has been calculated for a variety of parameter values, and is presented as a function of signal to noise ratio in Figures 2.5 through 2.15 where signal to noise ratio is defined by $\gamma = N_S/N_B$. In the absence of turbulence ($\sigma^2 = 0$), all of the receivers here reduce to the same structure. Curves for this structure have been calculated for comparison and are designated by 0.

The MAP and approximate optimum curves are denoted by 1 and 2 respectively. In Figures 2.5 through 2.9, they were obtained from Reference 8 and, in Figures 2.10 through 2.15, they were calculated using the steepest descents approximation to $p_1(\vec{n})$.

The curves denoted by 3 are values for the averaged threshold processor with infinite threshold averaging. In other words, the value of P(E) reported in curve 3 for any set of parameters is found by taking the limit as N goes to infinity of P(E) for the averaged threshold processor with N bit averaging. For the two and four channel diversity cases, the Hermite approximation[17] to the integral over $p(\vec{Z})$ was used.

In case of finite averaging, the extended MAP receiver of equations (14) and (15) turned out to result in a greater probability of error than the simpler averaged threshold receiver of equation (18) and Figure 2.4; for this reason, the former was ignored and the latter was included with 10 bit (curves 4) and 25 bit (curves 5) averaging. The Central Limit Theorem was used here in assuming that the conditional density of $\bar{n}_i$, given Z_i and the number of "ones" received, is approximately Gaussian. Numerical calculations of these curves for the four channel diversity cases turned out to be prohibitively complex. The manner in which finite averaging receivers approach the limiting case with increasing N appears, however, to be relatively insensitive to whether D = 1 or D = 2, and one would not expect from this that it would be greatly different for D = 4.

The main conclusion to be drawn from the graphs is that the infinite averaged threshold receiver results in lower bit error rates than either the MAP or the approximate optimum in all cases reported here. Moreover, these bit error rates can be very closely

approximated by realizable finite averages. In cases where D N_B = 4, for example, it was found that $N \approx 25/\sigma^2$ gives P(E) values within 20% of the limiting values at $\Upsilon = 20$. For lower Υ, convergence is even faster and, while increasing D N_B to 40 decreases the rate of convergence, the decrease is slight.

If the inequality of Appendix A is not rigorously satisfied, the performance of the averaged threshold receiver will be degraded somewhat. This effect is of great practical importance and deserves further investigation; it is, however, beyond the scope of this work.

The following caption is an explanation of Figures 2.5 - 2.15:

Figs. 2.5-2.15: Total probability of error, P(E), vs. SNR, Υ, for various receiver structures. For each combination of background radiation level, N_B, number of diversity channels, D, and log-intensity standard deviation, σ, P(E) curves are denoted by:

0 for $\sigma = 0$

1 for MAP receiver

2 for approximate optimum receiver

3 for infinite averaged threshold receiver

4 for 10 bit averaged threshold receiver

5 for 25 bit averaged threshold receiver

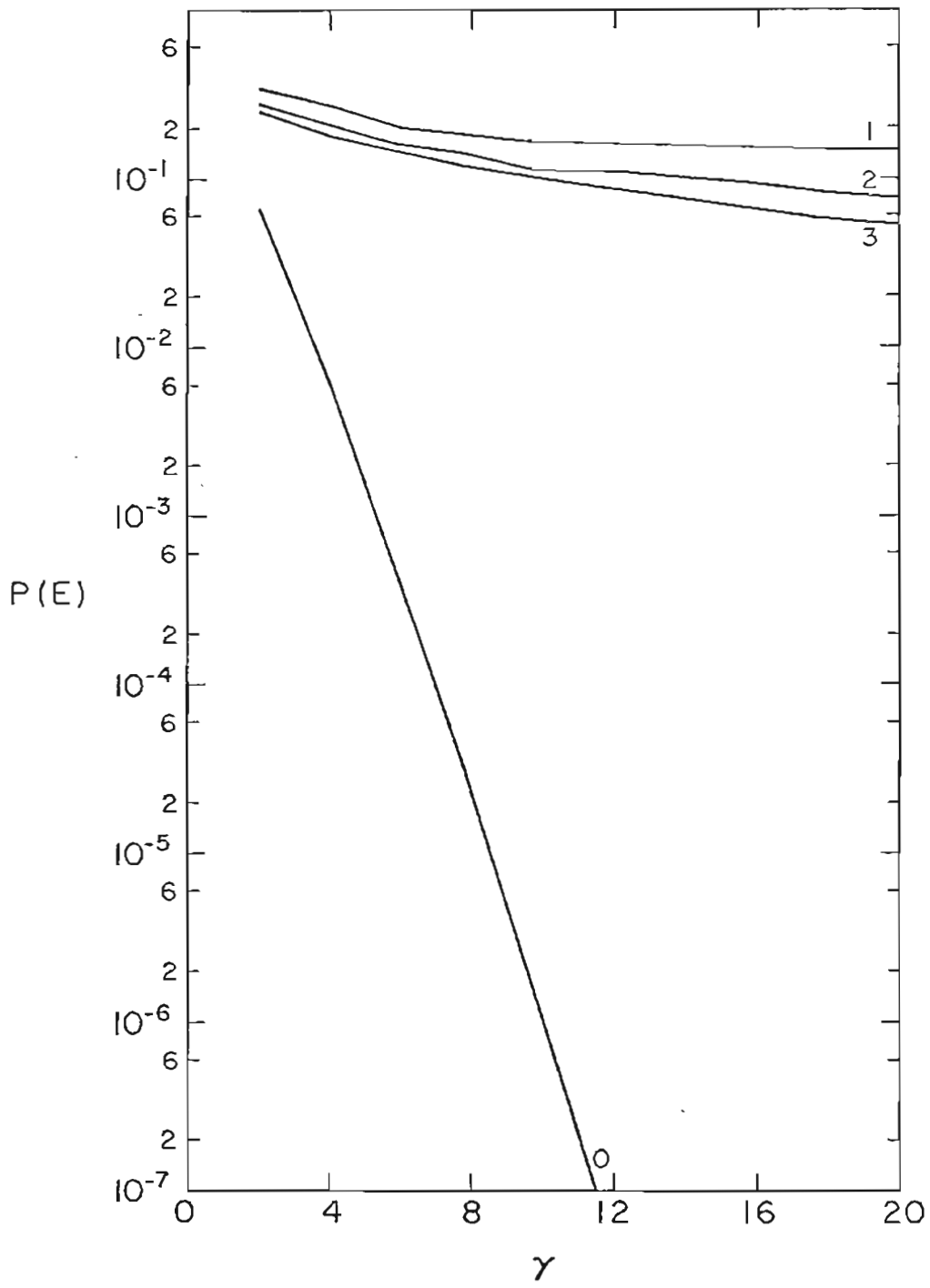

Fig. 2.5. $N_B = 4$, $D = 1$, $\sigma = 1.5$

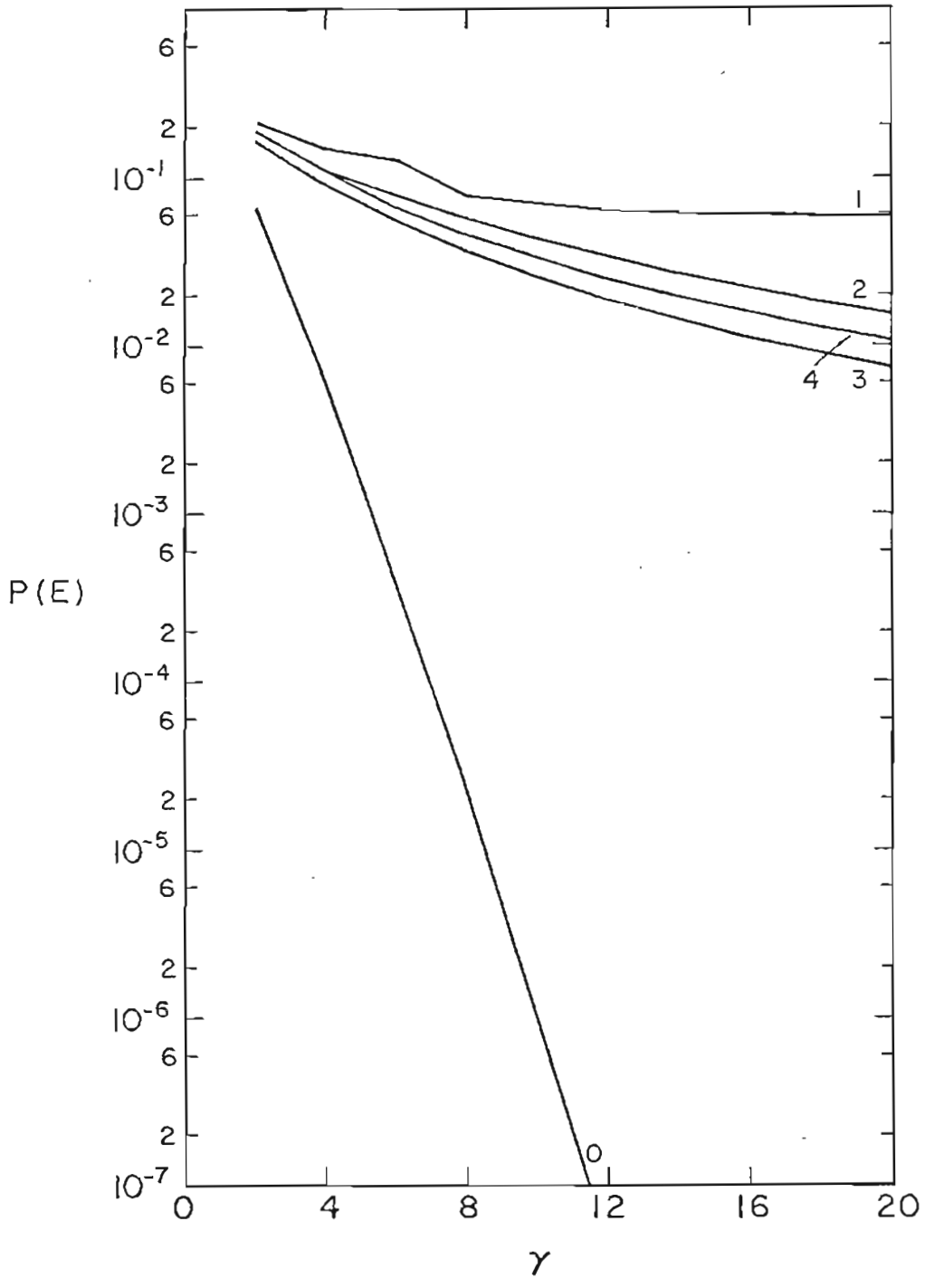

Fig. 2.6. $N_B = 4$, $D = 1$, $\sigma = 1.0$

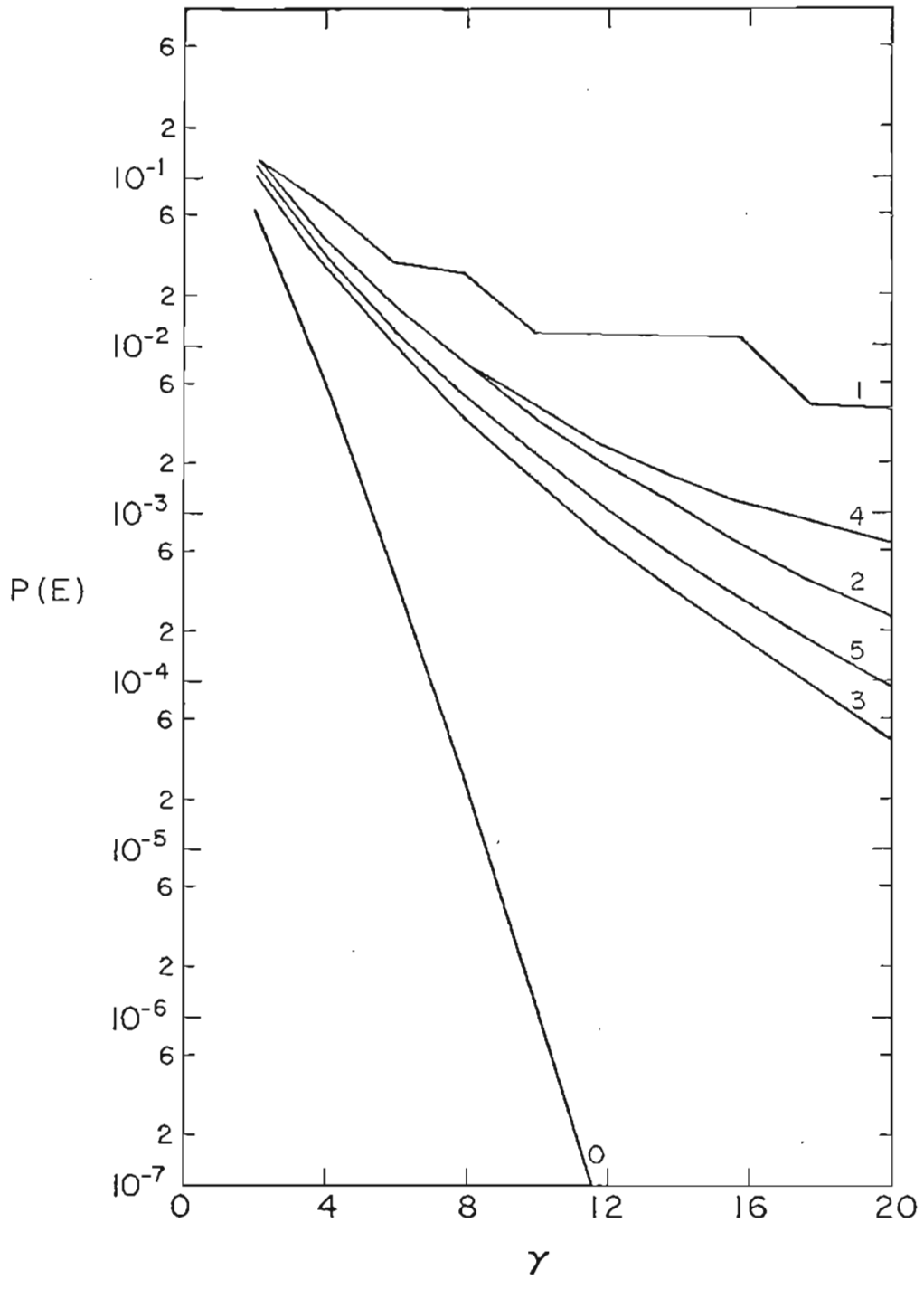

Fig. 2.7 $N_B = 4$, $D = 1$, $\sigma = 0.5$

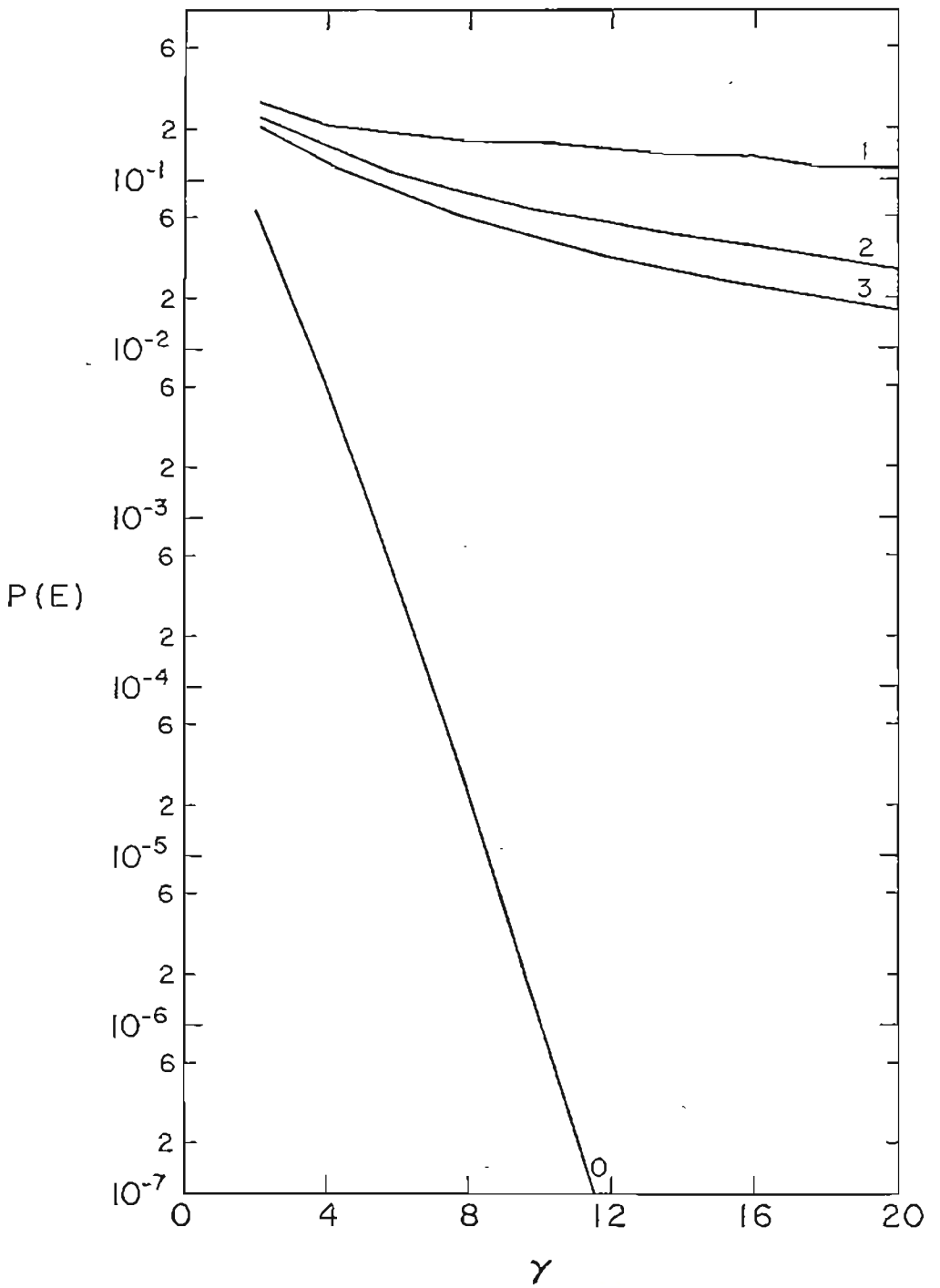

Fig. 2.8. $N_B = 2$, $D = 2$, $\sigma = 1.5$

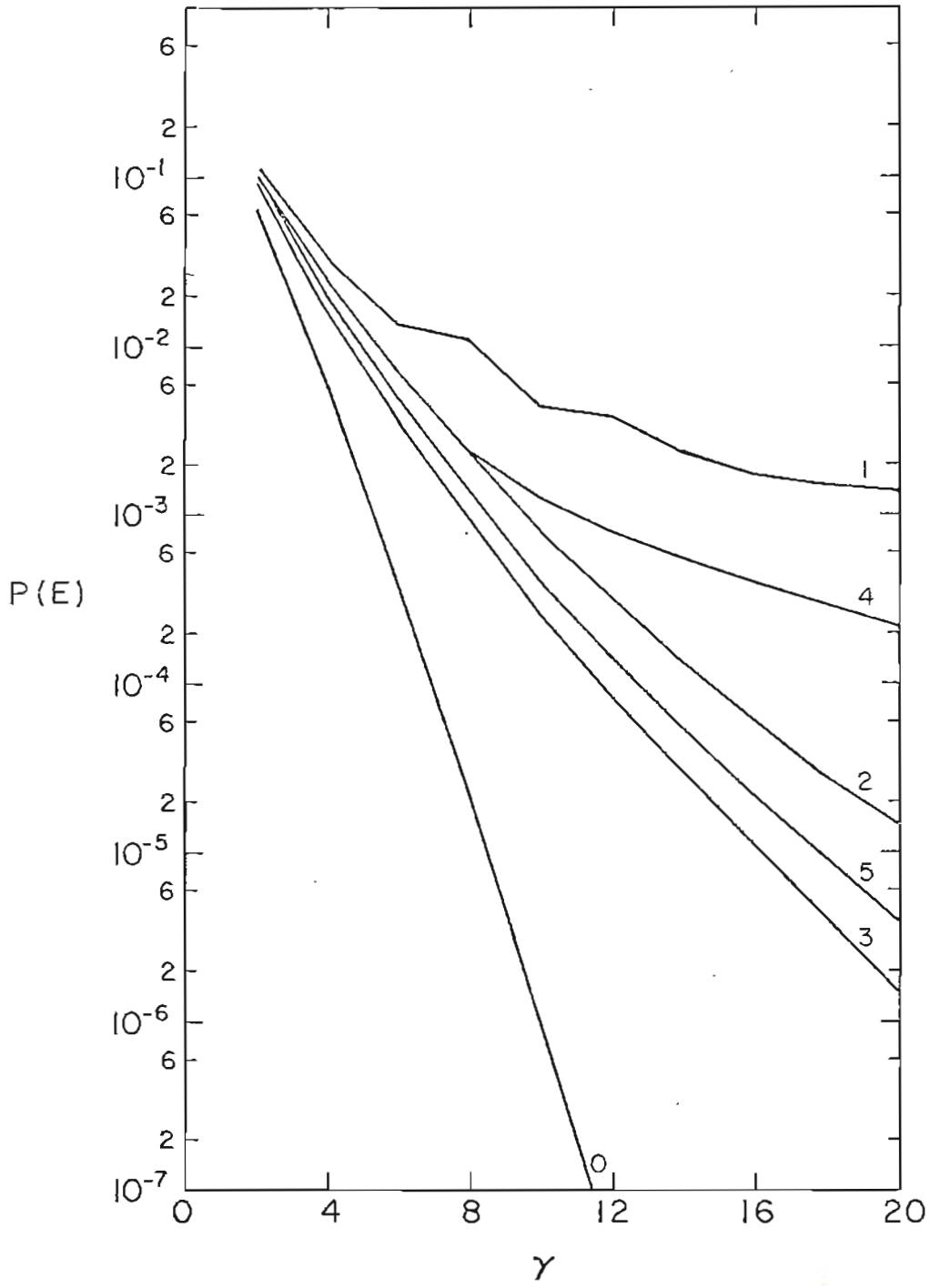

Fig. 2.9. $N_B = 2$, $D = 2$, $\sigma = 0.5$

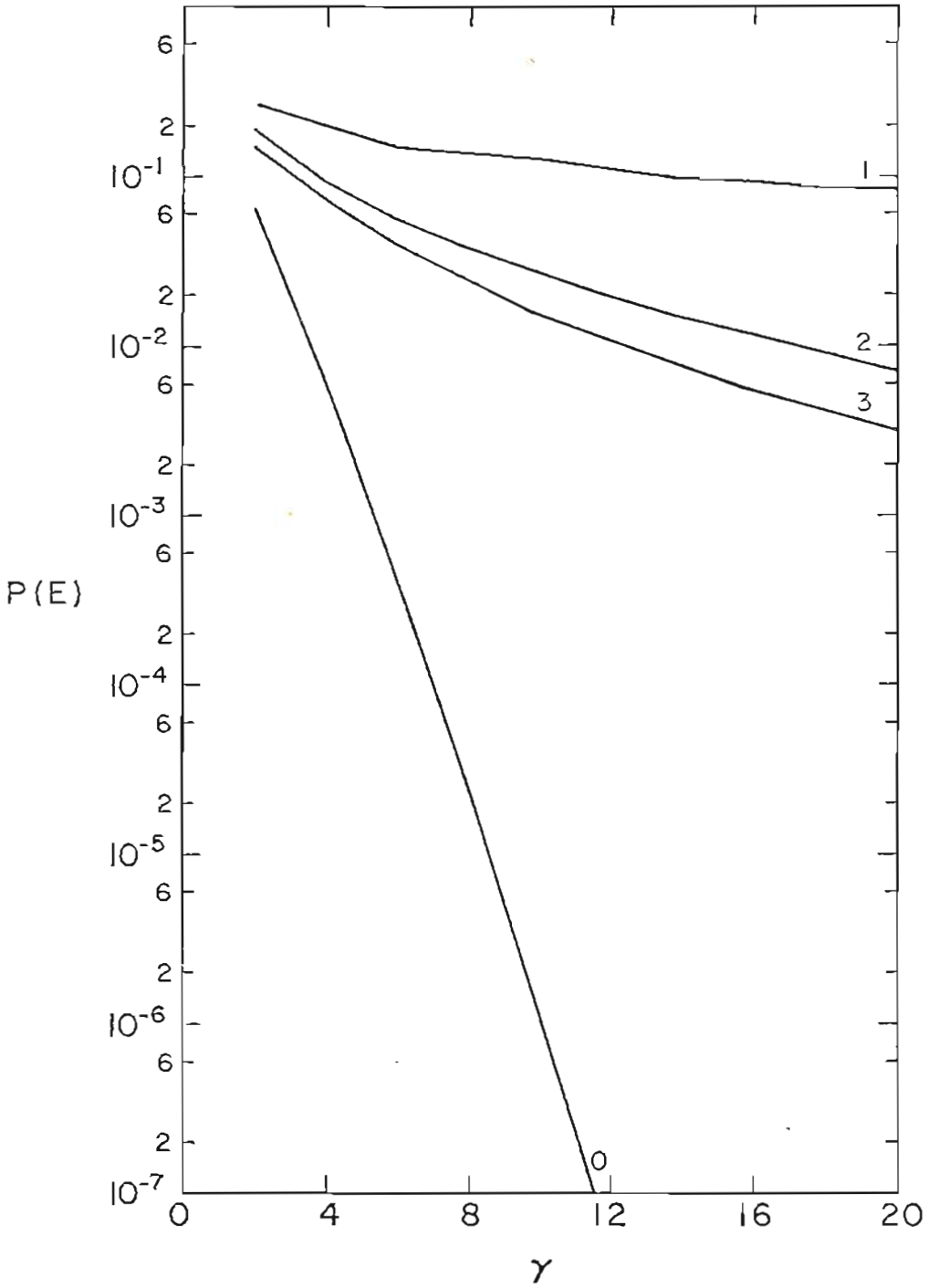

Fig. 2.10. $N_B = 1$, $D = 4$, $\sigma = 1.5$

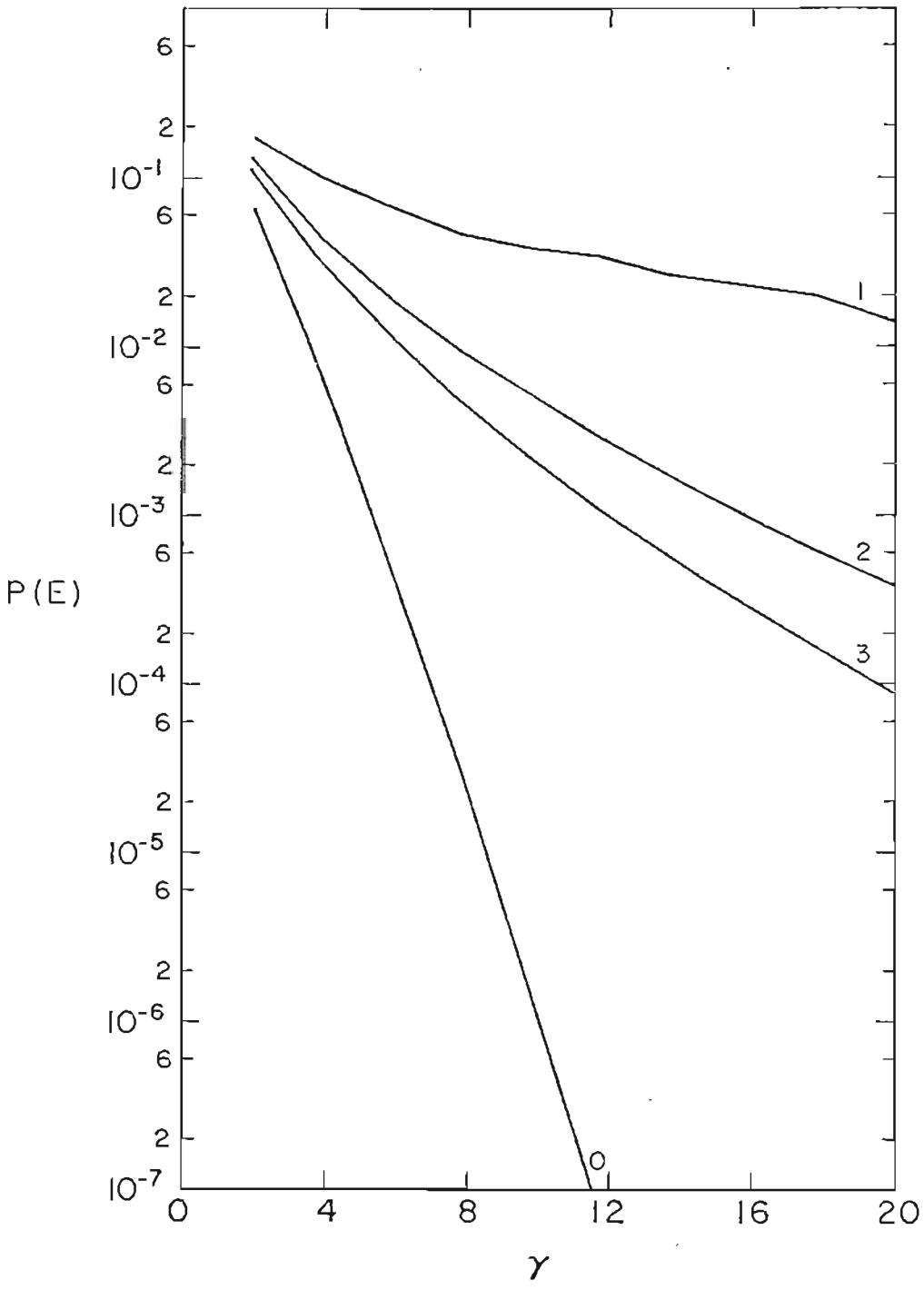

Fig. 2.11. $N_B = 1$, $D = 4$, $\sigma = 1.0$

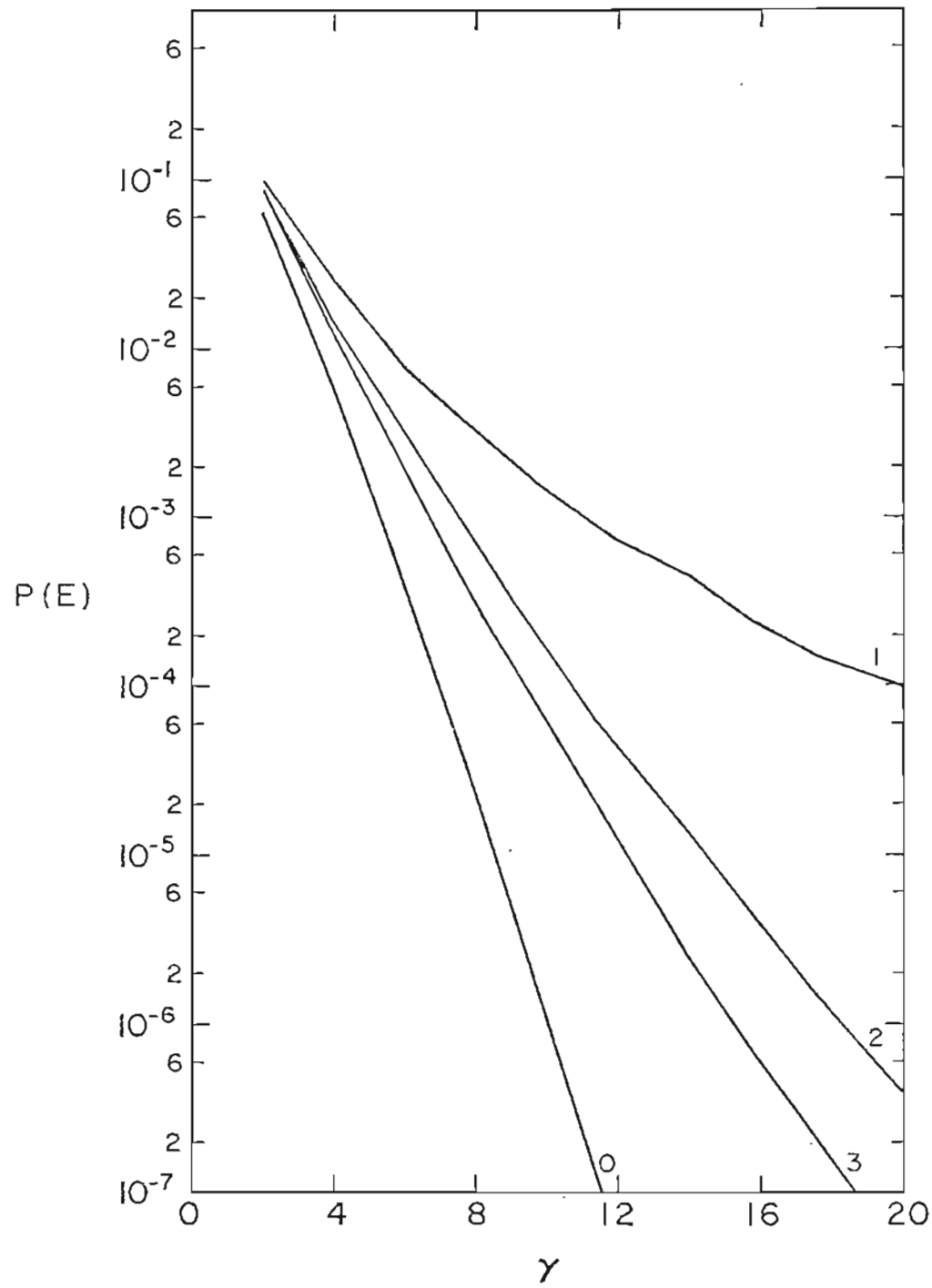

Fig. 2.12. $N_B = 1$, $D = 4$, $\sigma = 0.5$

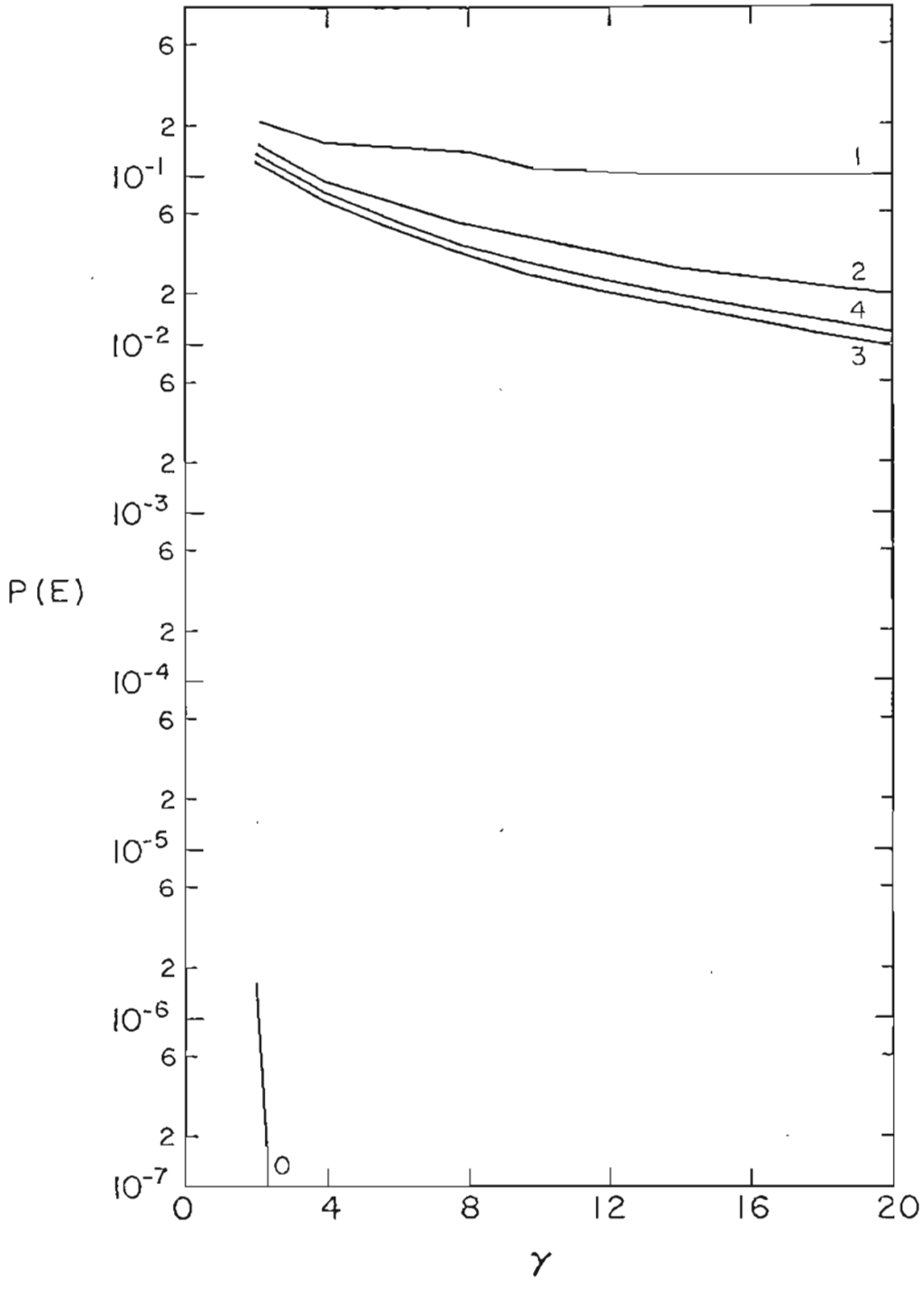

Fig. 2.13. $N_B = 40$, $D = 1$, $\sigma = 1.5$

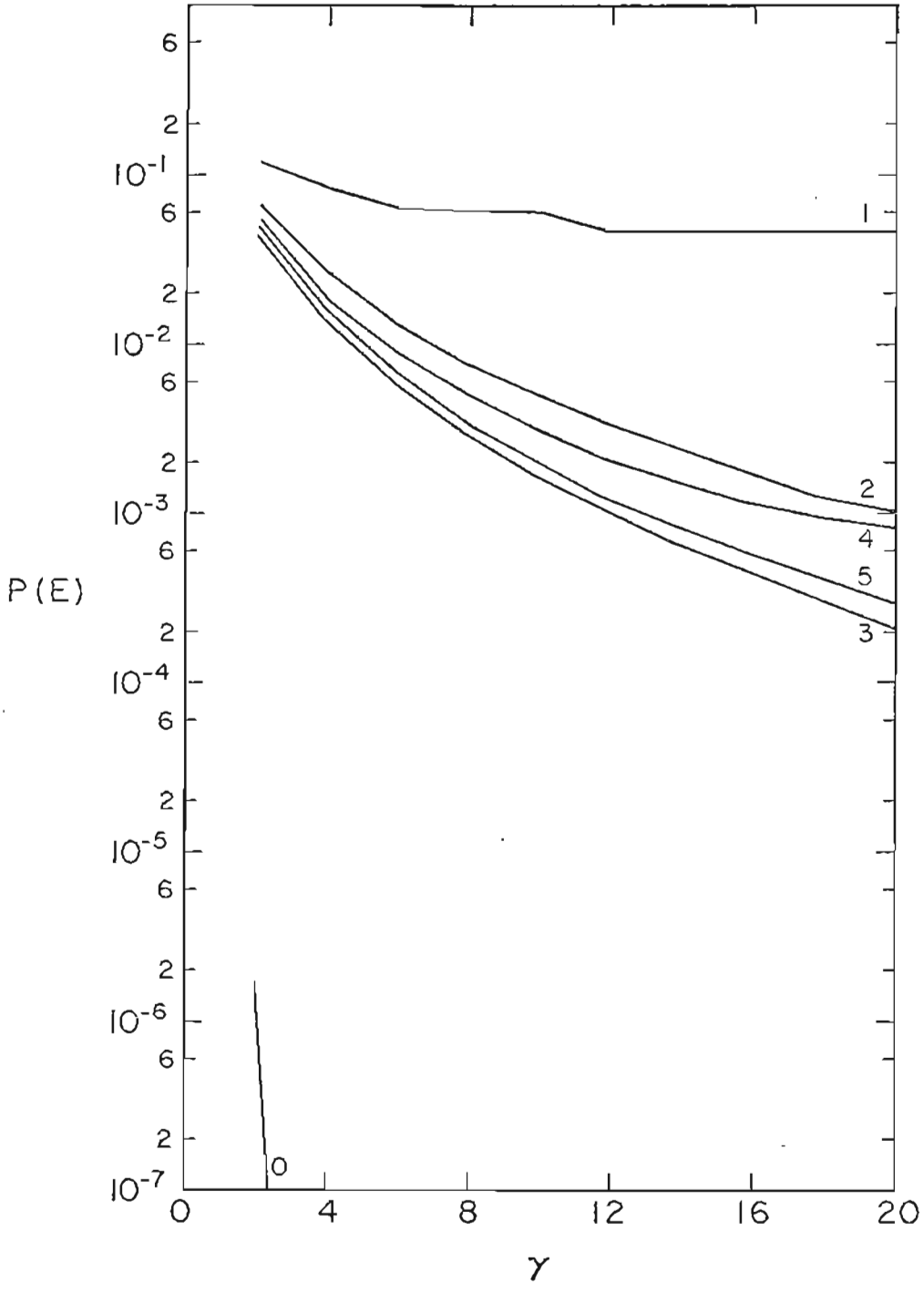

Fig. 2.14. N_B = 40, D = 1, σ = 1.0

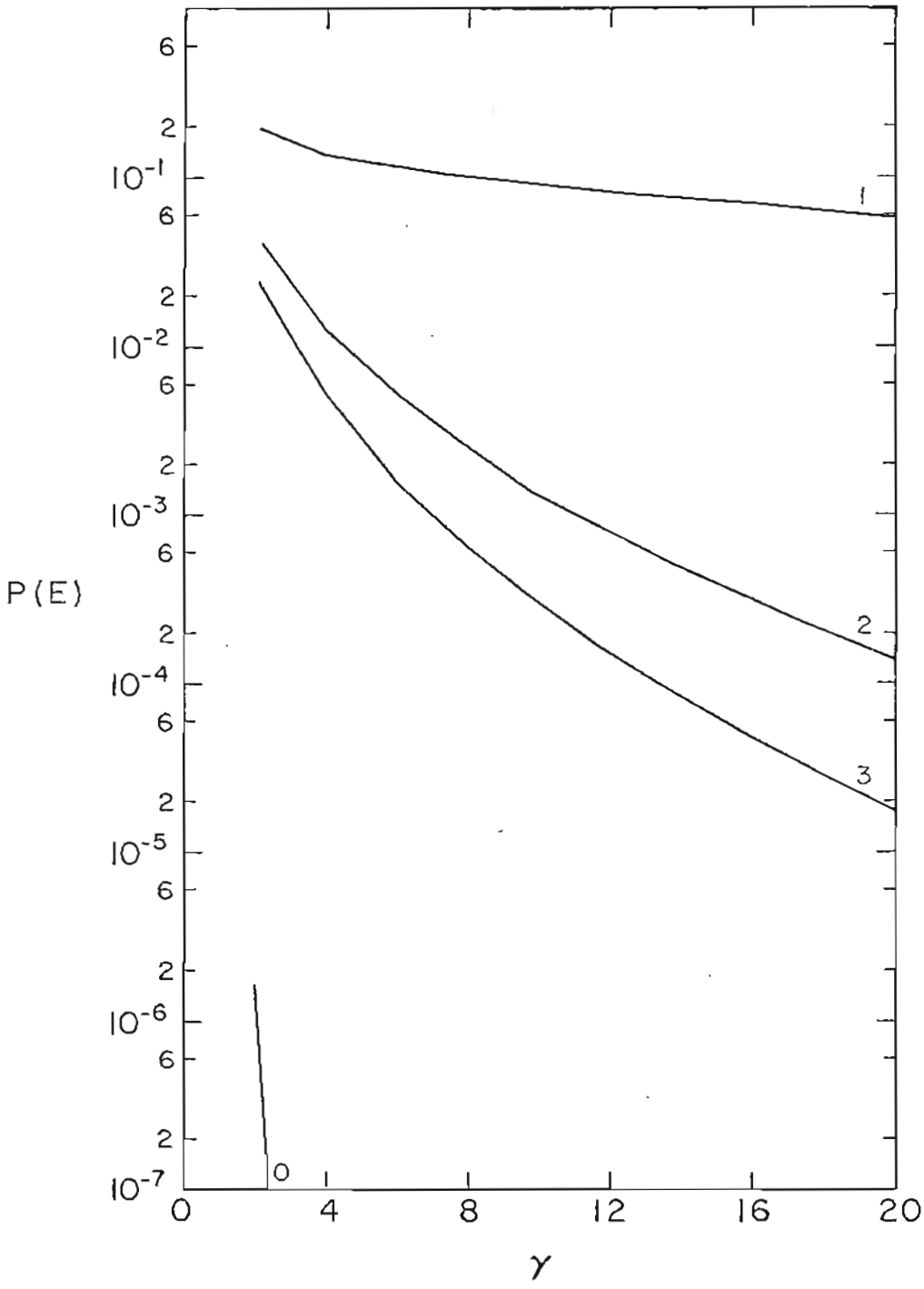

Fig. 2.15. $N_B = 10$, $D = 4$, $\sigma = 1.5$

3. PARTIAL TRACKING OPTICAL HETERODYNE ARRAYS

I. INTRODUCTION

The deleterious effects of atmospheric turbulence on optical heterodyne detection systems have been studied extensively using the average antenna gain, or SNR, as a measure of system performance.[18-20] In an attempt to improve the performance, a tracking receiver has been proposed, in which the average tilt of the incoming wavefront is effectively cancelled by the action of a servomechanism.[20-23] Another technique to increase the gain is to use an N-element array instead of a single collector aperture. This chapter concerns a hybridization of these two techniques; a partial tracking array, in which the average tilt across the entire array is cancelled using a single tracking system.

In Section 3.II, the gain is derived for a tracking heterodyne receiver whose aperture is contained within that of the tracking system. This will be called a partial tracking element to distinguish it from the case where the receiver aperture and the tracking system aperture are identical, called a full tracking element. Adding identical array elements then allows comparison of partial tracking arrays with those consisting of nontracking and of full tracking elements. It is shown that the most effective method of increasing the array gain is by increasing the array size in far field applications, and by adding either partial or full tracking in near field applications. Although full tracking results in a greater improvement, it may be difficult to implement for an

array. Partial tracking, on the other hand, can be accomplished by simply steering either the signal beam or the local oscillator.

Finally, the well-known similarities between optical heterodyne receiver gain and optical resolution[22,24] are recalled and applied to the partial tracking results. This is shown to give the explicit dependence of resolution and of the atmospheric modulation transfer function (MTF) on exposure time.

II. THEORETICAL BACKGROUND

The basic expression for the average antenna gain, $\langle G \rangle$, of a single circular receiver aperture can be obtained from Ref. 20, and is given by

$$\langle G \rangle = \langle \alpha\, D^{-2} \iint d\vec{x}_1\, d\vec{x}_2\, W(\vec{x}_1)\, W(\vec{x}_2)\, \exp[\ell(\vec{x}_1) + \ell(\vec{x}_2)] \times \cos\{[\phi(\vec{x}_1) - \vec{a} \cdot \vec{x}_1] - [\phi(\vec{x}_2) - \vec{a} \cdot \vec{x}_2]\} \rangle \qquad (1)$$

where D is the aperture diameter, $\vec{x}$ is a two-dimensional position vector in the receiver plane, W is the transmittance function of the receiver aperture (W = 1 therefore, inside a circle of diameter D and W = 0 elsewhere), ℓ is the logarithm of the turbulence induced singal amplitude perturbations (normalized by the mean signal amplitude), ϕ is the magnitude of the turbulence induced phase perturbations, and $\vec{a}$ is the corrective tilt introduced by the tracking system. The quantity α is a constant of proportionality that can be arbitrarily set in order to compare various receivers. In the results of Section 3.III, it will be set equal to $(4/\pi r_o)^2$ where r_o is a measure of the transverse coherence length of the

received field. Details of the calculation of r_o have been reported for plane wave propagation,[18] and these can be extended to spherical wave propagation by multiplying by $(8/3)^{3/5}$, (Ref. 23).

Since the distribution of $[\ell(\vec{x}_1) + \ell(\vec{x}_2)]$ is independent of the distribution of $\{[\phi(\vec{x}_1) - \vec{a} \cdot \vec{x}_1] - [\phi(\vec{x}_2) - \vec{a} \cdot \vec{x}_2]\}$ and since intergration commutes with ensemble averaging, Eq. (1) becomes[20]

$$\langle G \rangle = \alpha D^{-2} \iint d\vec{x}_1 \, d\vec{x}_2 \, W(\vec{x}_1) \, W(\vec{x}_2) \, \langle \exp[\ell(\vec{x}_1) + \ell(\vec{x}_2)] \rangle$$

$$\times \langle \cos\{[\phi(\vec{x}_1) - \vec{a} \cdot \vec{x}_1] - [\phi(\vec{x}_2) - \vec{a} \cdot \vec{x}_2]\} \rangle \qquad (2)$$

The assumption of Gaussian $\ell(\vec{x})$ and some manipulation allows the first ensemble average to be rewritten as[18]

$$\langle \exp[\ell(\vec{x}_1) + \ell(\vec{x}_2)] \rangle = \exp[-1/2 \, \mathcal{D}_\ell(\rho)] \qquad (3)$$

where $\rho = |\vec{x}_1 - \vec{x}_2|$ and the log-amplitude structure function $\mathcal{D}_\ell(\rho)$ is defined as $\langle [\ell(\vec{x}_1) - \ell(\vec{x}_2)]^2 \rangle$.

Evaluation of the second ensemble average depends on three Lemmas first presented in Ref. 23, and on using the exponential representation for the cosine function. Without duplicating this development, we will note the result that

$$\langle \cos\{[\phi(\vec{x}_1) - \vec{a} \cdot \vec{x}_1] - [\phi(\vec{x}_2) - \vec{a} \cdot \vec{x}_2]\} \rangle$$

$$= \exp\{-1/2 \, [\mathcal{D}_\phi(\rho) - 1/2 \, \langle \vec{a} \cdot \vec{a} \rangle \rho^2]\} \qquad (4)$$

where $\mathcal{D}_\phi(\rho)$, the phase structure function is defined as $\langle [\phi(\vec{x}_1) - \phi(\vec{x}_2)]^2 \rangle$.

The second of the three Lemmas used in Eq. (4), which states that the distribution of $\phi(\vec{x}) - \vec{a}\cdot\vec{x}$ is independent of the distribution of $\vec{a}$, must be viewed as an approximation. While it is an excellent approximation for the cases of spherical and plane wave propagation considered in this work, it should be noted that significant errors develop if it is applied to Gaussian beam wave propagation through strong turbulence.[25]

It has been shown that[22]

$$\langle \vec{a} \cdot \vec{a} \rangle = \frac{64}{D_T^2} \int_0^1 u\, du[(12u - 8u^3)\ (1 - u^2)^{1/2} - 4\cos^{-1}u]\ \mathcal{D}_\phi(D_T u) \tag{5}$$

where D_T is the diameter of the circular aperture over which the tracking system matches the signal wavefront and is not necessarily the same as the signal aperture diameter. The phase structure function, a rather complicated function of $D_T u$, reduces to manageable form in two limiting cases.[3] In the extreme far field, D_T, and therefore $D_T u$, is much less than the Fresnel zone size $\sqrt{\lambda L}$ and we have $\mathcal{D}_\phi(D_T u) \approx 3.44\ (D_T u/r_o)^{5/3}$. Where $D_T >> \sqrt{\lambda L}$, one can assume that $D_T u$ is also much larger than $\sqrt{\lambda L}$ over most of the range of integration so that $\mathcal{D}_\phi(D_T u) \approx 6.88\ (D_T u/r_o)^{5/3}$. Eq. (5) can then be evaluated for these two cases, resulting in

$$\langle \vec{a} \cdot \vec{a} \rangle \approx 6.88\ r_o^{-5/3}\ D_T^{-1/3} \qquad \text{(far field)} \tag{6a}$$

$$\langle \vec{a} \cdot \vec{a} \rangle \approx 2 \times 6.88\ r_o^{-5/3}\ D_T^{-1/3} \qquad \text{(near field)} \tag{6b}$$

Making use of the wave structure function $\mathcal{D}(\rho)$, which is equal to $\mathcal{D}_{\ell}(\rho) + \mathcal{D}_{\phi}(\rho)$ and is given by $\mathcal{D}(\rho) = 6.88\ (\rho/r_o)^{5/3}$ independent of near field/far field considerations,[18] we see that

$$\langle G\rangle = \alpha D^{-2} \iint d\vec{x}_1\ d\vec{x}_2\ W(\vec{x}_1)\ W(\vec{x}_2) \{\exp -3.44\ (\rho/r_o)^{5/3} \times [1 - C(\rho/D_T)^{1/3}]\} \tag{7}$$

where C = 1 in the near field and C = 1/2 in the far field. This can be simplified to[20]

$$\langle G\rangle = \frac{16}{\pi}\ (D/r_o)^2 \int_o^1 u\ du\ \left[\cos^{-1} u - u(1-u^2)^{1/2}\right] \times \exp\left[-3.44\ (D/r_o)^{5/3}\ u^{5/3}\ (1 - C(uD/D_T)^{1/3})\right] \tag{8}$$

which must be evaluated numerically.

The development of Eq. (8) is based on a circular tracking aperture, so that $\langle |a_x|^2\rangle = \langle |a_y|^2\rangle$ and

$$\langle |a_x|^2\rangle\ \rho_x^{\,2} + \langle |a_y|^2\rangle\ \rho_y^{\,2} = \frac{1}{2} \langle \vec{a} \cdot \vec{a}\rangle\ \rho^2 \tag{9}$$

which is used to arrive at Eq. (4). The result can be modified to include a rectangular tracking aperture of dimensions ℓ by h by expanding the phase front across the aperture and finding the rms fluctuations of the coefficients in the same manner as for circular apertures.[22] This results in

$$\langle |a_x|^2\rangle = -72\ (6.88\ C\ r_o^{-5/3})\ \ell^{-1/3} \times \int_{-1/2}^{1/2}\!\!\int\!\!\int\!\!\int\!\!\int dx_1 dx_2 dy_1 dy_2 x_1 x_2 \left[(x_1 - x_2)^2 + \frac{h^2}{\ell^2}\ (y_1 - y_2)^2\right]^{5/6} \tag{10a}$$

$$\langle |a_y|^2 \rangle = -72\ (6.88\ C\ r_o^{-5/3})(\ell^{5/3}/h^2)$$
$$\times \int_{-1/2}^{1/2}\int\int\int dx_1 dx_2 dy_1 dy_2 y_1 y_2 \left[(x_1 - x_2)^2 + \frac{h^2}{\ell^2}\ (y_1 - y_2)^2\right]^{5/6} \qquad (10a)$$

Numerical integration results in

$$\langle |a_x|^2 \rangle \approx 6.88\ C\ r_o^{-5/3}\ \ell^{-1/3} \left[1 + .107\ \left(1 - \frac{h}{\ell}\right)\right] \qquad (11a)$$

$$\langle |a_y|^2 \rangle \approx 6.88\ C\ r_o^{-5/3}\ \ell^{-1/3} \left[1 + .295\ \left(1 - \frac{h}{\ell}\right)\right] \qquad (11b)$$

where it has been assumed that $\ell \geq h$. The errors in Eq. (11) are on the order of 5% or less.

Comparison of Eq. (11) with Eq. (6) implies that $\langle \vec{a} \cdot \vec{a} \rangle$ is the same whether the tilt is averaged over an ℓ by h square or over a circle inscribed inside that square. This is not true however. A more precise analysis shows that one should multiply the right hand side of Eq. (6) by 1.026 and of Eq. (11) by .97 so that, as one would expect, a larger averaging area results in a smaller amount of fluctuations. Since the amount of smoothing added by the corners of the square is so small, however, both of these numerical coefficients were set equal to one for simplicity.

Note that for a square tracking aperture of dimension $\ell = h = D$, identical to the signal aperture, $\langle |a_x|^2 \rangle = \langle |a_y|^2 \rangle$, and the wavefront tilt is tracked exactly in both dimensions. For $\ell > h = D$, Eq. (11) shows that both $\langle |a_x|^2$ and $\langle |a_y|^2 \rangle$ are reduced and the wavefront tilt over the signal aperture is not tracked exactly in either axis. Although the y component of tilt is tracked better than the x component, the difference is relatively small, and the effectiveness

of tracking along both axes is primarily determined by the longest dimension, ℓ, which determines the amount of decorrelation in both tilt axes.

Using Eqs. (9) and (11) in the simplification of Eq. (2) results in

$$\langle G \rangle = \frac{16}{\pi} (D/r_o)^2 \int_0^1 u\, du \left[\cos^{-1} u - u (1 - u^2)^{1/2}\right] \times \exp\left\{-3.44 (D/r_o)^{5/3} u^{5/3}\left[1 - C(uD/\ell)^{1/3}\left(1 + .2\left(1 - \frac{h}{\ell}\right)\right)\right]\right\} \times I_o\left[.32\, C\, (D/r_o)^{5/3} (D/\ell)^{1/3} u^2 \left(1 - \frac{h}{\ell}\right)\right] \qquad (12)$$

where I_o is the modified Bessel function of order zero.

It should be mentioned at this point that the development above is based on a Kolmogorov spectrum of index-of-refraction fluctuations and ignores inner scale and outer scale effects. The results, therefore, should be suspect for both very short and very long propagation path lengths. The specific range of validity and the magnitude of the corresponding errors in $\mathcal{D}_\phi$ have been investigated by Lutomirski and Yura.[26]

III. RESULTS

The value of $\langle G \rangle$ from Eq. (8) has been plotted against the normalized aperture diameter D/r_o with the dependence on the ratio D_T/D shown parametrically. These curves are presented in Figs. 3.1 and 3.2 for near and far field conditions, respectively. Tracking over an infinite aperture is, as one might expect, equivalent to no tracking at all and this curve agrees with previously reported values.[18-20]

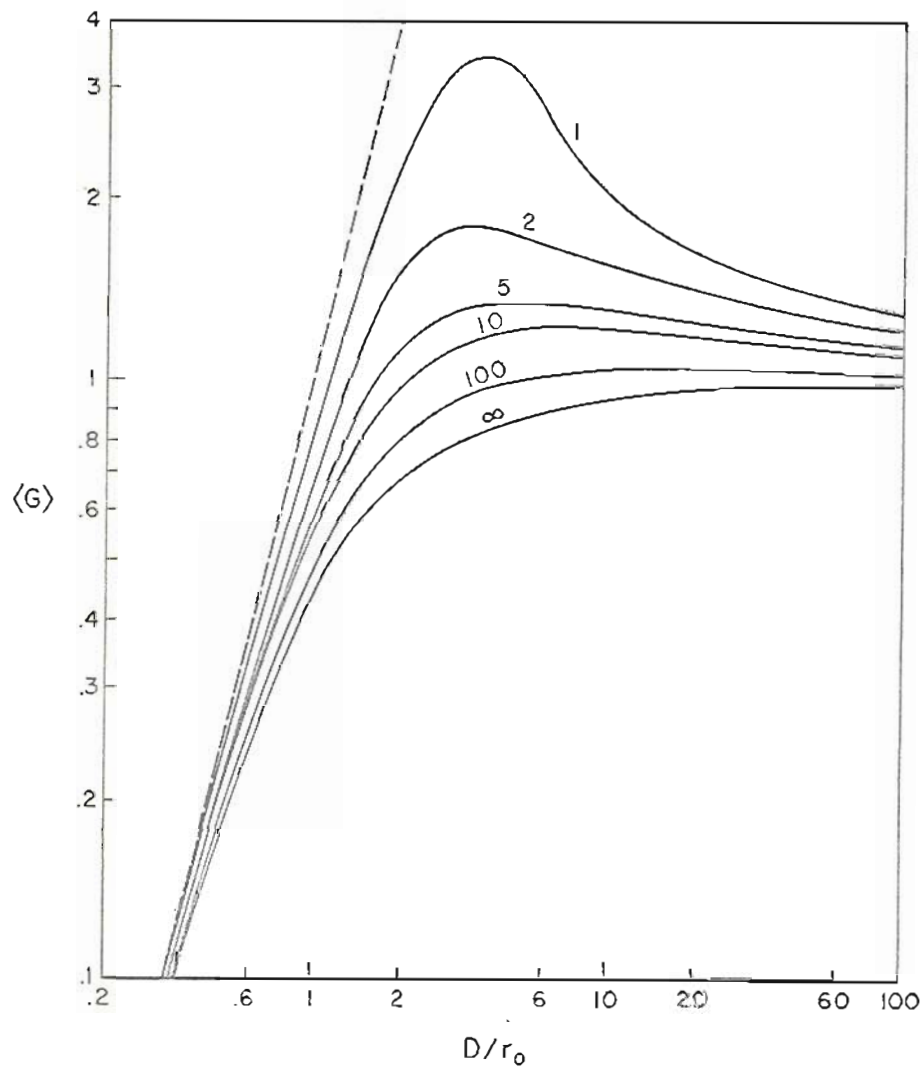

Fig. 3.1. Graph of average antenna gain <G> vs. normalized aperture D/r_o for near field applications. Dependence on normalized tracking diameter D_T/D is shown parametrically and the dashed line gives the free space value for reference.

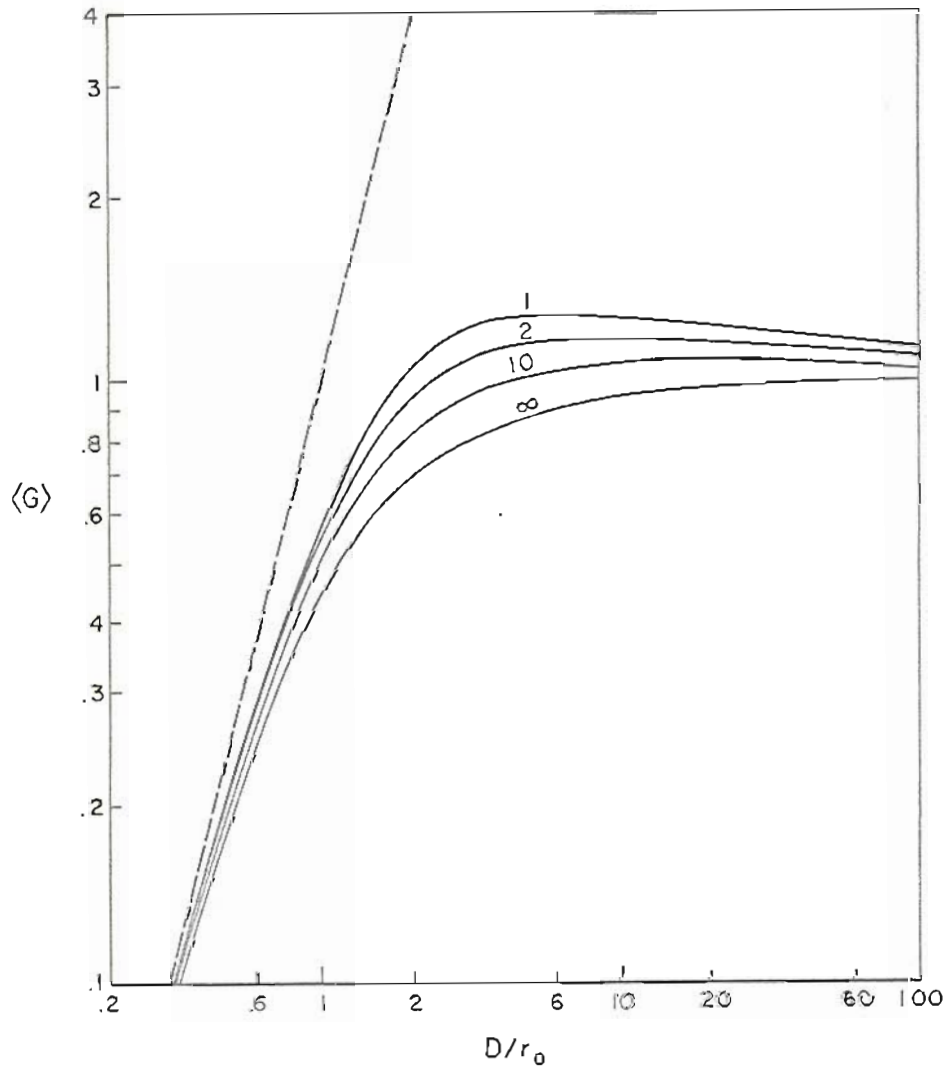

Fig. 3.2. Same as Fig. 3.1 for far field applications.

It is easily seen from these results, and in fact from Eq.(8) directly, that moving from the near field to the far field is equivalent to a factor of eight increase in the ratio of D_T to D. Partial tracking, therefore, more nearly approximates full tracking performance in the far field, even though tracking results in a greater improvement over non tracking in the near field.

Fig. 3.3 is a graph of <G> vs. number of diversity channels for an array consisting of N identical apertures, each with $D = 3.4\ r_o$. Using the well-known properties of the expected value operator, it is easy to see that

$$<G> \equiv \left< \sum_{i=1}^{N} G_i \right> = \sum_{i-1}^{N} <G_i> \qquad (13)$$

It should be noted that G is proportional to signal power so that Eq. (13) assumes that the IF currents are square-law demodulated and then added. In the partial tracking case, D_T was taken to be the diameter of the smallest circle that encloses N packed circles of diameter D. In the near field, the addition of partial tracking is roughly equivalent to doubling the array size, with full tracking equal to about a factor of four increase, and it is probably most reasonable to use small tracking arrays. In the far field, however, full tracking results in only about 2 dB improvement over non tracking and 1/2 dB or less over partial tracking. One would expect, then, to find larger arrays with non tracking elements. Even where tracking is desirable for some other reason (where one or both terminals of a communications link are in motion, for example), a full tracking antenna array can hardly be justified.

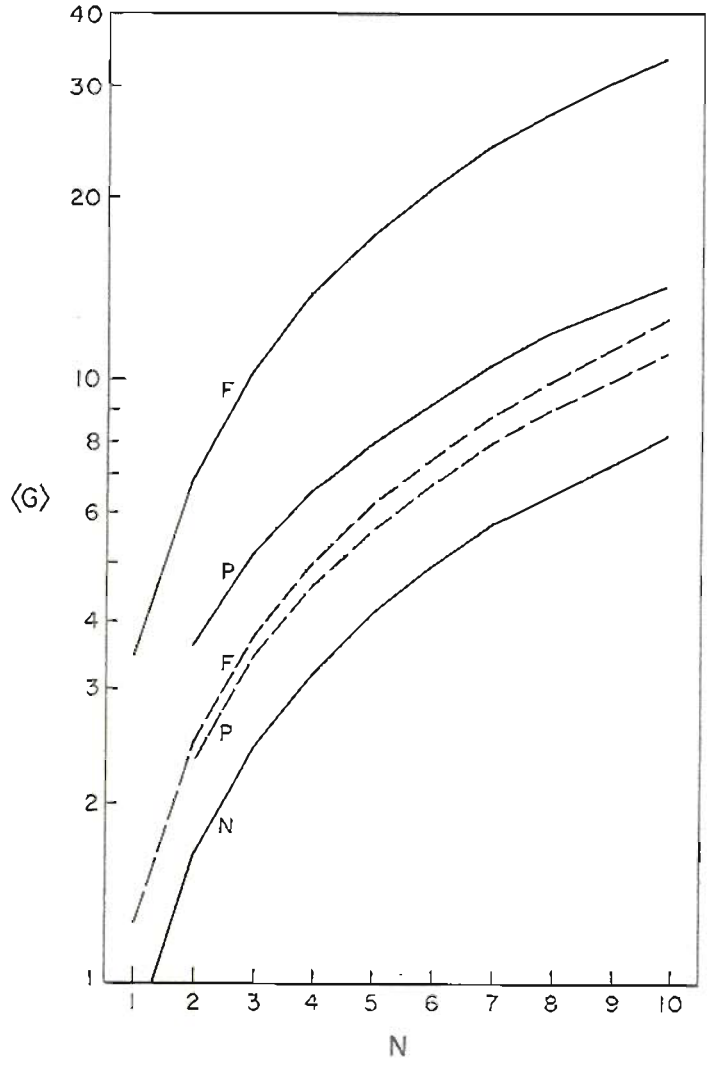

Fig. 3.3. Graph of average antenna gain <G> vs. number of array elements N for full (F), partial (P), and non (N) tracking antenna arrays. Solid lines give near field and dashed lines far field results. $D/r_o = 3.4$.

It is tempting to reinterpret Eq.(8) in terms of parameters pertinent to optical resolution studies. By comparison with the results of Ref. 23, it is seen that the resolution R, defined as the integral over all spatial frequencies of the system's ensemble-average MTF divided by the limit of this integral as $D \to \infty$, is given by Eq. (8) if D_T or Eq. (12) if ℓ and h can be interpreted in terms of the exposure time. Using Taylor's frozen turbulence hypothesis,[4] one can argue that an aperture of diameter D, exposed for a time τ, is sampling the tilt over an effective aperture of dimensions D by $D + V_\perp \tau$, where $V_\perp$ is the wind velocity component perpendicular to the path. Fig. 3.4, therefore, is a plot of Eq.(12) with $h = D$ and $\ell = D + V_\perp \tau$ for several values of $V_\perp \tau$ in the near field. The two limiting cases are identical to previously reported results.[23]

By analogy with Refs. 23 and 24, the exposure time dependent form of the atmospheric MTF is given by

$$\begin{aligned} MTF(f) = \exp \Bigg\{ & -3.44 \, (\lambda R f / r_o)^{5/3} \\ & \times \left[1 - C(\lambda R f)^{1/3} \left(D + V_\perp \tau \right)^{-1/3} \left(1 + .2 \, \frac{V_\perp \tau}{D + V_\perp \tau} \right) \right] \Bigg\} \\ & \times I_o \left[.32 \, C \, (\lambda R f)^2 \, r_o^{-5/3} \left(D + V_\perp \tau \right)^{-4/3} V_\perp \tau \right] \end{aligned} \tag{14}$$

where λ is the optical wavelength, R is the focal length of the imaging lens, and f is the spatial frequency of interest. Multiplying this equation by the MTF of the imaging optics results in the total system MTF.[23] For this reason, Eq.(14) was called the

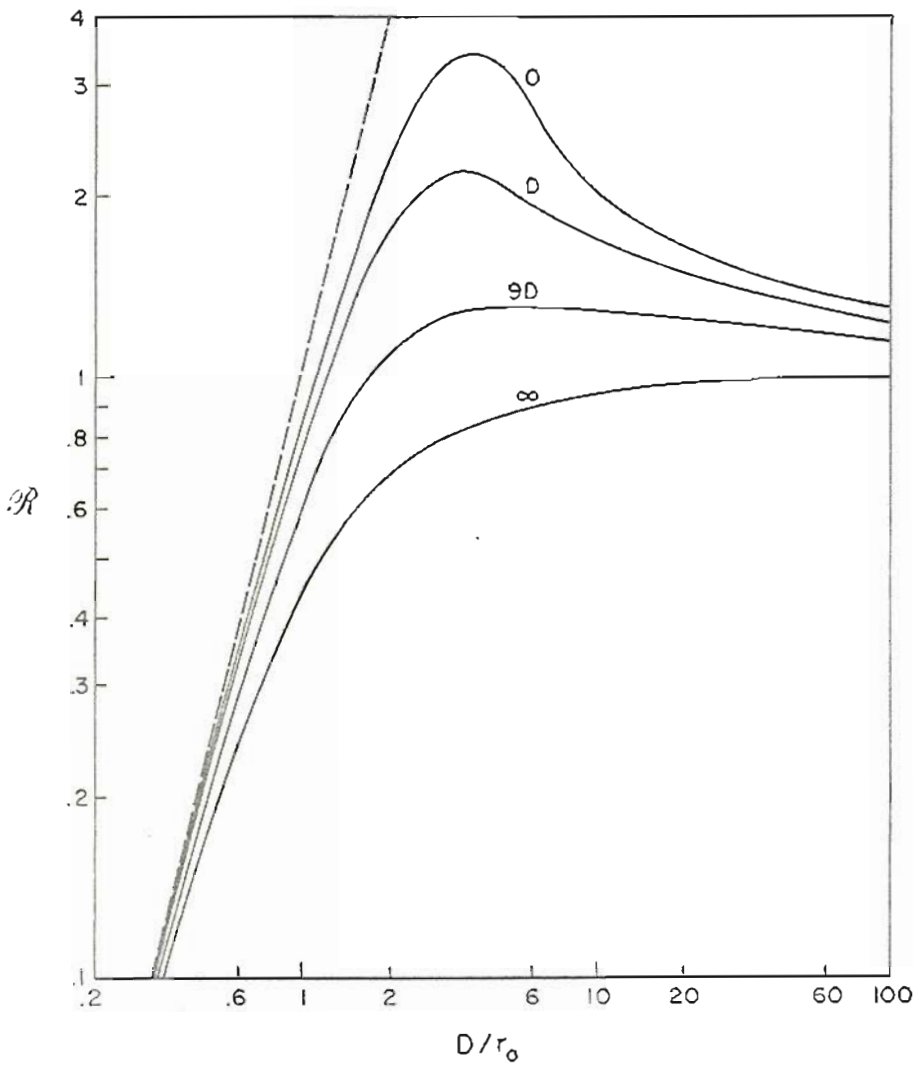

Fig. 3.4. Graph of resolution $\mathcal{R}$ vs. D/r_o for near field applications. Dependence on effective exposure time $V_\perp \tau$ is shown parametrically.

atmospheric MTF despite its dependence on the imaging lens parameters R and D.

4. SIGNAL CURRENT PROBABILITY DISTRIBUTION FOR OPTICAL HETERODYNE RECEIVERS IN THE TURBULENT ATMOSPHERE. 1: THEORY

I. INTRODUCTION

The performance of an optical heterodyne detection system can be severely degraded by the presence of atmospheric turbulence, which results in random fluctuations in the phase and amplitude of a coherent optical signal. For each optical wavelength and set of propagation conditions, these fluctuations limit the achievable average antenna gain (i.e., signal-to-noise ratio) to a value equal to the free space gain at some effective aperture diameter, r_o.[18,19,11] If the actual aperture diameter is less than r_o, the average antenna gain is only slightly less than the free space value for that aperture while, for diameters larger than r_o, the gain asymptotically approaches the limiting value.

Depending on the ratio of the actual aperture diameter to r_o, a significant fraction of the phase front distortion that causes reduction of the signal can be represented by an average tilt of the incoming wavefront across the aperture.[22] For this reason, a tracking heterodyne receiver has been proposed[21,22] in which the random tilts of the signal are eliminated by the action of a servomechanism. In extreme near-field applications (i.e., D >> the Fresnel zone size, $\sqrt{\lambda L}$), this results in an average antenna gain that is greater than that of the non-tracking (static) receiver at all diameters, and that increases with aperture size until the diameter reaches about 3.4 r_o,[20,21]

where the gain is about 4.3 times that of the static case.[23] In far-field applications, the increase in antenna gain with the addition of tracking is less dramatic, although it is still noticeable.

Because of this limitation on the total useful signal power that can be collected by a signal aperture, spatial diversity reception becomes an important technique for overcoming the deleterious effects of turbulence. A diversity receiver could either combine the IF signals from several collecting apertures directly, or combine the signals after demodulation. In order to find optimum combining procedures to most effectively utilize this technique, however, the pertinent density functions of the signal need to be known (as has been demonstrated in diversity reception by photon counting elements).[7] To optimize combination after demodulation, the density function of the magnitude of the IF signal is necessary and will be explored here. The statistics of the phase of the IF signal are important if combination is done before demodulation. This case will not be treated in this work.

As a first step toward the consideration of optimum diversity reception, approximate expressions are derived for the probability density functions of the IF signal magnitudes from both static and tracking optical heterodyne receivers operating in the far-field of the receiver. Following Ref. 22, the phase front is expanded in a finite series of orthonormal polynomials over the aperture area, and the mean signal currents are found as functions of the

instantaneous fading parameters. Then, in Sections 4.III and 4.IV the approximate density functions, considering shot noise, log-amplitude fluctuations, and phase front distortion, are developed using a steepest descents integration. In Section 4.V, numerical results are given for several combinations of log-amplitude variance and the ratio D/r_o. In the next chapter, experimental results are presented showing that, for the static receiver, the approximation is a reasonable one.

II. SIGNAL CURRENTS

The lensless optical heterodyne receiver diagrammed in Fig. 4.1 will be considered here since, from photocurrent considerations, this configuration is equivalent to the more practical one utilizing a converging lens and a smaller detector area.[18] The two-dimensional vector $\vec{x}$ denotes a position in the detector plane, where the orgin of the coordinate system is the center of the aperture, imaged on the photodetector surface. The aperture itself is assumed to be a circle of diameter D, so that its transmission function is given by

$$W(\vec{x}) = \begin{cases} 1, & \text{if } |\vec{x}| \leq 1/2\ D \\ 0, & \text{if } |\vec{x}| > 1/2\ D \end{cases} \tag{1}$$

The local oscillator wave will be assumed to be a uniform amplitude, plane wave, described by

$$E_o(\vec{x}) = E_o = A_o \exp\left[i\left(2\pi f_o t + \phi_o\right)\right] \tag{2}$$

where A_o, f_o, and ϕ_o are the oscillator amplitude, frequency, and phase. Similarly, the signal will be assumed to be an initially

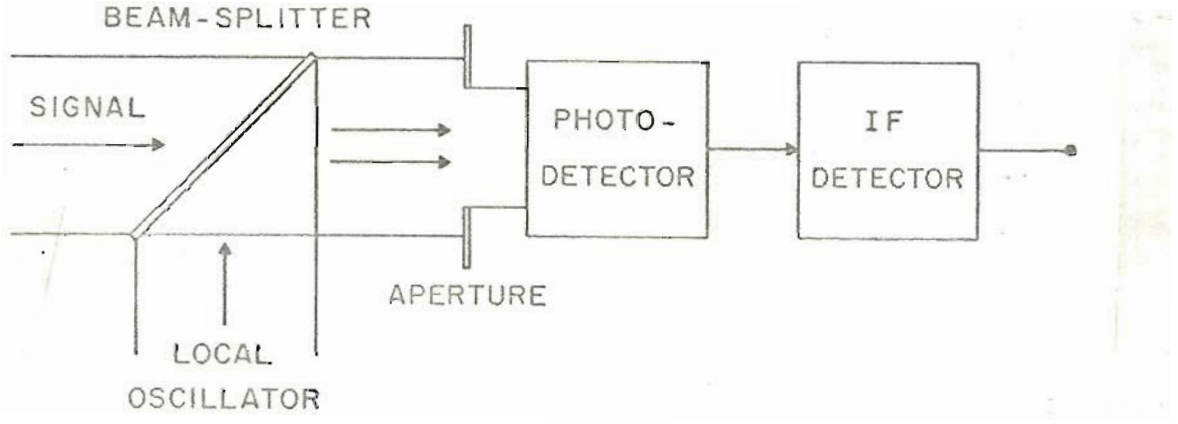

Fig. 4.1. Block diagram of a generalized optical heterodyne receiver.

uniform plane wave which is distorted by propagation through atmospheric turbulence resulting in a wave at the receiver that may be described by

$$E_s(\vec{x}) = A_s(\vec{x}) \exp\left[i\left(2\pi f_s t + \phi_s(\vec{x})\right)\right] \tag{3}$$

where $A_s(\vec{x})$, f_s, and $\phi_s(\vec{x})$ are the amplitude, frequency, and phase of the received signal wavefront. Both $A_s(\vec{x})$ and $\phi_s(\vec{x})$ are time varying statistical quantities. In the following development, the appropriate statistical description of relevant quantities related to $A_s(\vec{x})$ and $\phi_s(\vec{x})$ are introduced as required.

For a photodetector with quantum efficiency η, the total photocurrent is given by

$$i = \frac{1}{2}\int d\vec{x}\, W(\vec{x})\eta \left[E_s(\vec{x}) + E_o\right]^* \left[E_s(\vec{x}) + E_o\right] \tag{4}$$

In a well designed optical heterodyne system, the probability that A_o will be much larger than A_s will be high so that the A_s^2 term can be dropped, and Eq. (4) reduces to

$$i = \eta(\pi/8)D^2A_o^2 + \eta A_o \int d\vec{x}\, W(\vec{x})\, A_s(\vec{x}) \cos\left[2\pi\Delta f t + \phi_s(\vec{x}) - \phi_o\right] \tag{5}$$

Here, the second term, oscillating at the beat frequency, $\Delta f = f_s - f_o$, is the instantaneous signal current i_s.

In extreme far-field applications the normalized covariance function of the log-amplitude $b_\chi(D)$ is very nearly equal to one.[4] Therefore, $A_s(\vec{x})$ can be considered to be constant over the aperture area and can be replaced by $Z\,\bar{A}_s$, where $\bar{A}_s$ is the signal that would be present in the absence of turbulence and the normalized fading

parameter Z is defined by this substitution. The instantaneous signal current can then be represented by

$$i_s = \eta A_o \bar{A}_s Z \int d\vec{x}\, W(\vec{x}) \cos\left[2\pi\Delta f t - \phi_o + \phi_s(\vec{x})\right] \qquad (6)$$

Since most interesting applications will be in the far-field, this condition is not overly restrictive.

For large A_o, the first term in Eq. (5) is the average photocurrent, and the shot noise associated with this current is the only source of detector noise that needs to be considered.[10,11] The rms noise current, therefore, is given by

$$i_n = (2ieB)^{1/2} = (\pi\eta eB)^{1/2} \frac{1}{2} D A_o \qquad (7)$$

where e is the electronic charge and B is the system bandwidth. The development below will deal with the normalized signal, $i_s' \equiv i_s/i_n$, rather than the absolute value of i_s. This is given by

$$i_s' = \frac{\sqrt{2}\gamma Z}{\pi R^2} \int d\vec{x}\, W(\vec{x}) \cos\left[2\pi\Delta f t - \phi_o + \phi_s(\vec{x})\right] \qquad (8)$$

where $R = \frac{1}{2} D$ and γ, the rms current signal-to-noise ratio that would be present in the absence of turbulence,[18] is given by $(\pi\eta/8eB)^{1/2} D \bar{A}_s$.

Following Reference 22, the distorted wavefront of the signal will be represented by a finite series of orthonormal polynomials over the aperture area, so that

$$\phi_s(\vec{x}) \approx \sum_{k=1}^{6} a_k F_k(\vec{x}) \qquad (9)$$

with the polynomials $F_k(\vec{x})$ defined below:

$$F_1(\vec{x}) \equiv (\pi R^2)^{-1/2} \qquad (10a)$$

is a change in the average phase over the aperture.

$$F_2(\vec{x}) \equiv (\pi R^4/4)^{-1/2}\, x \tag{10b}$$

$$F_3(\vec{x}) \equiv (\pi R^4/4)^{-1/2}\, y \tag{10c}$$

are the average horizontal and vertical tilts.

$$F_4(\vec{x}) \equiv (\pi R^6/12)^{-1/2} \left(x^2 + y^2 - \frac{1}{2} R^2\right) \tag{10d}$$

is the spherical deformation, and finally,

$$F_5(\vec{x}) \equiv (\pi R^6/6)^{-1/2}\, (x^2 - y^2) \tag{10e}$$

$$F_6(\vec{x}) \equiv (\pi R^6/24)^{-1/2}\, xy \tag{10f}$$

represent a hyperbolic deformation.

These six polynomials are orthonormal over the aperture area and the coefficients are found, in the usual manner, by

$$a_k = \int d\vec{x}\; W(\vec{x})\; \phi_s(\vec{x})\; F_k(\vec{x}) \tag{11}$$

In order to justify truncating the series expansion of $\phi_s(\vec{x})$ after six terms, it is noted that, for $D \leq r_o$, the mean square error introduced by this truncation is less than or equal to about 0.06 rad^2.[22] The signal current then becomes

$$\begin{aligned} i_s' &= \sqrt{2}\gamma Z/\pi R^2 \int d\vec{x}\; W(\vec{x})\; \cos\left(2\pi\Delta f t - \phi_o + \sum_{k=1}^{6} a_k F_k(\vec{x})\right) \\ &= \sqrt{2}\gamma Z/\pi R^2 \left\{ \cos\left(2\pi\Delta f t - \phi_o + a_1 F_1\right) \int d\vec{x}\; W(\vec{x})\; \cos\left(\sum_{k=2}^{6} a_k F_k(\vec{x})\right) \right. \\ &\quad \left. - \sin\left(2\pi\Delta f t - \phi_o + a_1 F_1\right) \int d\vec{x}\; W(\vec{x})\; \sin\left(\sum_{k=2}^{6} a_k F_k(\vec{x})\right) \right\} \end{aligned} \tag{12}$$

A. Static Case

In order to facilitate evaluation of the integrals in Eq.(12), the assumption will be made that, in the static case, the second order terms in $\phi_s(\vec{x})$ can be neglected. This limits the usefulness of the results here to aperture diameters on the order of r_o or smaller,[22] a limitation which applies to practical static receivers anyway.[10] The substitution is made that

$$\Delta^2 = (4/\pi R^2)(a_2^2 + a_3^2) \tag{13}$$

and the integrals in Eq. (12) can easily be evaluated, resulting in

$$\int d\vec{x}\, W(\vec{x}) \cos\left(a_2 F_2(\vec{x}) + a_3 F_3(\vec{x})\right) = 2\pi R^2 J_1(\Delta)/\Delta \tag{14a}$$

and

$$\int d\vec{x}\, W(\vec{x}) \sin\left(a_2 F_2(\vec{x}) + a_3 F_3(\vec{x})\right) = 0 \tag{14b}$$

where $J_1(\Delta)$ is the first order Bessel function.

Putting Eq. (14) back into Eq.(12) and taking the time average of the beat frequency oscillations, the rms value of the normalized signal current is found to be

$$I = 2\gamma Z |J_1(\Delta)/\Delta| \tag{15}$$

where the vertical bars denote the absolute value. Under usual conditions, Δ will seldom exceed 3.83, and the absolute value of J_1 can be replaced by J_1. This assumption will be made in Section 4.III so that the integral over Δ can be evaluated by the method of steepest descents, and the resulting error will be discussed in Section 4.V.

B. Tracking Case

With angle-of-arrival tracking added, a_2 and a_3 are assumed to be held at zero by the action of a servo loop and the second order terms become important. The substitutions are made that

$$\alpha^2 = (12/\pi R^2)\, a_4^2 \tag{16a}$$

$$\beta^2 = (6/\pi R^2)(a_5^2 + a_6^2) \tag{16b}$$

and the angular integration becomes straightforward. For the radial integration, however, the following functions must be defined for numerical evaluation

$$C(\alpha,\beta) = \int_0^1 \cos(\alpha t)\, J_0(\beta t)\, dt \tag{17a}$$

$$S(\alpha,\beta) = \int_0^1 \sin(\alpha t)\, J_0(\beta t)\, dt \tag{17b}$$

where $J_0(\beta t)$ is the zero order Bessel function.

With these definitions

$$\int d\vec{x}\, W(\vec{x})\, \cos\left(\sum_{k=4}^{6} a_k F_k(\vec{x})\right) = \pi R^2 \left[\cos\left(\tfrac{1}{2}\alpha\right) C(\alpha,\beta) + \sin\left(\tfrac{1}{2}\alpha\right) S(\alpha,\beta)\right] \tag{18a}$$

$$\int d\vec{x}\, W(\vec{x})\, \sin\left(\sum_{k=4}^{6} a_k F_k(\vec{x})\right) = \pi R^2 \left[\sin\left(\tfrac{1}{2}\alpha\right) C(\alpha,\beta) - \cos\left(\tfrac{1}{2}\alpha\right) S(\alpha,\beta)\right] \tag{18b}$$

so that the rms value of the normalized signal current is given by

$$I = \gamma Z \left[C^2(\alpha,\beta) + S^2(\alpha,\beta)\right]^{1/2} \tag{19}$$

III. PROBABILITY DENSITY FUNCTION - STATIC RECEIVER

The probability density function of the normalized rms signal current in the static optical heterodyne receiver is given by

$$p(I) = \iint dX\, d\Delta\, p(I|X,\Delta)\, p(X)\, p(\Delta) \tag{20}$$

where X, the normalized log-amplitude, is equal to $\ln(Z)$, and the independence of X and Δ has been assumed.

In a well designed system, shot noise associated with the local oscillator intensity will completely mask all other sources of detector noise. While shot noise is a Poisson process, the local oscillator photocurrent will generally be large enough to be considered Gaussian.[10] If X and Δ are known, therefore, and after filtering, the IF signal consists of the signal current i_s plus a zero mean Gaussian noise current with standard deviation i_n. The normalized rms signal current, then, is a Gaussian random variable with standard deviation of one and mean given by Eq.(15) so that

$$p(I|X,\Delta) = \frac{1}{\sqrt{2\pi}} \exp\left[-\frac{1}{2}(I - 2\gamma Z\, J_1(\Delta)/\Delta)^2\right] \qquad (21)$$

The normalized log-amplitude X will be considered to be a Gaussian random variable[3,4] with variance σ_X^2. It should be mentioned at this point that under conditions of very high path integrated turbulence, the actual distribution of amplitude fluctuations deviates from the assumed log-normal form.[27] It can easily be seen from conservation of energy considerations that the mean of X must be equal to $-\sigma_X^2$,[18] so that

$$p(X) = \frac{1}{\sqrt{2\pi}\,\sigma_X} \exp\left\{-\frac{\left(X + \sigma_X^2\right)^2}{2\sigma_X^2}\right\} \qquad (22)$$

The quantities $(2/\sqrt{\pi}R)\, a_2$ and $(2/\sqrt{\pi}R)\, a_3$ are proportional to the x and y components of the angle of arrival of the signal, respectively. They are, therefore, like the angle of arrival components, independent,

zero mean, Gaussian random variables, each with the same variance, which will be denoted by σ_Δ^2. From this it follows that the parameter Δ must have the Rayleigh density function

$$p(\Delta) = \frac{\Delta}{\sigma_\Delta^2} \exp\left\{-\frac{\Delta^2}{2\sigma_\Delta^2}\right\} \tag{23}$$

An approximation, using the method of steepest descents, was used to evaluate the integral in Eq.(20). This method has also been used to evaluate analogous expressions in cases of direct detection[5,28] and is found to give excellent agreement to numerical evaluations in both cases. First, Eq.(20) is rewritten as

$$p(I) = \frac{1}{2\pi\, \sigma_\Delta^2\, \sigma_X} \iint dX\, d\Delta\, \exp[f(X,\Delta)] \tag{24a}$$

where (24b)

$$f(X,\Delta) = -\frac{1}{2}(I - 2\gamma J_1(\Delta)/\Delta)^2 - \frac{1}{2\sigma_X^2}(X + \sigma_X^2)^2 - \frac{\Delta^2}{2\sigma_\Delta^2} + \ln\Delta$$

The stationary point (X_o, Δ_o) is found from the pair of coupled equations

$$\left(\frac{\partial f}{\partial X}\right)\Big|_{X_o,\Delta_o} = (I - 2\gamma Z_o J_1(\Delta_o)/\Delta_o)\, 2\gamma Z_o J_1(\Delta_o)/\Delta_o + \frac{1}{\sigma_X^2}(X_o + \sigma_X^2) = 0 \tag{25a}$$

$$\left(\frac{\partial f}{\partial \Delta}\right)\Big|_{X_o,\Delta_o} = (I - 2\gamma Z_o J_1(\Delta_o)/\Delta_o)\, 2\gamma Z_o J_1(\Delta_o)/\Delta_o$$
$$(J_o(\Delta_o)/\Delta_o - 2J_1(\Delta_o)/\Delta_o^2) - \frac{\Delta_o}{\sigma_\Delta^2} + \frac{1}{\Delta_o} = 0 \tag{25b}$$

where $Z_o = \ln X_o$. The determinant B is defined by

$$B = \left| \begin{matrix} \frac{\partial^2 f}{\partial X^2} & \frac{\partial^2 f}{\partial X \partial \Delta} \\ \frac{\partial^2 f}{\partial X \partial \Delta} & \frac{\partial^2 f}{\partial \Delta^2} \end{matrix} \right|_{(X_o, \Delta_o)} \tag{26}$$

with

$$\frac{\partial^2 f}{\partial X^2} = (I - 4\gamma Z J_1(\Delta)/\Delta)\ 2\gamma Z J_1(\Delta)/\Delta - \frac{1}{\sigma_X^2} \tag{27a}$$

$$\frac{\partial^2 f}{\partial X \partial \Delta} = (I - 4\gamma Z J_1(\Delta)/\Delta)\ 2\gamma Z (J_o(\Delta)/\Delta - 2J_1(\Delta)/\Delta^2) \tag{27b}$$

$$\frac{\partial^2 f}{\partial \Delta^2} = (I - 2\gamma Z J_1(\Delta)/\Delta)\ 2\gamma Z\ (6J_1(\Delta)/\Delta^3 - J_1(\Delta)/\Delta - 3J_o(\Delta)/\Delta^2)$$

$$- 4\gamma^2 Z^2 (J_o(\Delta)/\Delta - 2J_1(\Delta)/\Delta^2)^2 - \frac{1}{\sigma_\Delta^2} - \frac{1}{\Delta^2} \tag{27c}$$

The signal current density function, then, is given by

$$p(I) = \frac{\Delta_o}{\sqrt{B}\ \sigma_\Delta^2\ \sigma_X} \exp\left[- \frac{1}{2} (I - 2\gamma Z_o J_1(\Delta_o)/\Delta_o)^2 \right.$$

$$\left. - \frac{1}{2\sigma_X^2} \left(X_o + \sigma_X^2\right)^2 - \frac{\Delta_o^2}{2\sigma_\Delta^2} \right] \tag{28}$$

IV. PROBABILITY DENSITY FUNCTION - TRACKING RECEIVER

The probability density function of the normalized rms signal current in the tracking optical heterodyne receiver is given by

$$p(I) = \iiint dX\ d\alpha\ d\beta\ p(I|X, \alpha, \beta)\ p(X)\ p(\alpha)\ p(\beta) \tag{29}$$

As in the static case, the normalized rms signal current is a Gaussian random variable with standard deviation of one and mean given by Eq.(19), so that

$$p(I|X, \alpha, \beta) = \frac{1}{\sqrt{2\pi}} \exp\left\{-\frac{1}{2}\left[I - \gamma 2(C^2 + S^2)^{1/2}\right]^2\right\} \qquad (30)$$

Note that the functional dependence of C and S on α and β has been suppressed for convenience, rather than stated explicitly.

The density function of the log-amplitude fluctuations is the same as for the static case, but the phase terms are a little more complex. Assuming, from symmetry considerations, that $\langle\phi^2(\vec{x})\rangle$ has a constant value at any point around the edge of the aperture (i.e., $|\vec{x}| = R$), it can easily be shown that a_4, a_5, and a_6 are independent random variables, and $\langle a_4^2\rangle = \langle a_5^2\rangle = \langle a_6^2\rangle$. This last statement is consistent with the statement in Ref. 4 that $\langle a_4^2\rangle = 1/3\left[\langle a_4^2\rangle + \langle a_4^2\rangle + \langle a_5^2\rangle\right]$. It is also obvious from symmetry that $\langle a_4\rangle = \langle a_5\rangle = \langle a_6\rangle = 0$.

That a_4, a_5, and a_6 are Gaussian random variables follows directly from the fact that each is obtained from the Gaussian variable $\phi(\vec{x})$ by the action of a linear operator. The variables α and β, then, have Gaussian and Rayleigh statistics, respectively, with density functions given by

$$p(\alpha) = \frac{1}{\sqrt{2\pi}\,\sigma_\alpha} \exp - \frac{\alpha^2}{2\sigma_\alpha^2} \qquad (31a)$$

$$p(\beta) = \frac{2\beta}{\sigma_\alpha^2} \exp - \frac{\beta^2}{\sigma_\alpha^2} \qquad (31b)$$

where $\sigma_\alpha^2 = \left\langle \frac{12\, a_4^2}{\pi R^6} \right\rangle$

The signal current density function, therefore, is given by

$$p(I) = \frac{2\ (2\pi)^{-3/2}}{\sigma_X\ \sigma_\alpha^{\,3}} \iiint dX\ d\alpha\ d\beta\ \exp[f(X,\ \alpha,\ \beta)] \tag{32a}$$

where

$$f(X,\ \alpha,\ \beta) = -\frac{1}{2}\left(I - \gamma Z\sqrt{C^2 + S^2}\right)^2 - \frac{1}{2\sigma_X^{\,2}}\left(X + \sigma_X^{\,2}\right)^2 - \frac{\alpha^2}{2\sigma_\alpha^{\,2}} - \frac{\beta^2}{\sigma_\alpha^{\,2}} + \ln \beta \tag{32b}$$

Applying the method of steepest descents once more, the stationary point is now found from the three coupled equations

$$\left(\frac{\partial f}{\partial X}\right)\Bigg|_{(X_o,\ \alpha_o,\ \beta_o)} = \left(I - \gamma Z_o\sqrt{C^2 + S^2}\right)\gamma Z_o\sqrt{C^2 + S^2} - \frac{1}{\sigma_X^{\,2}}\left(X_o + \sigma_X^{\,2}\right) = 0 \tag{33a}$$

$$\left(\frac{\partial f}{\partial \alpha}\right)\Bigg|_{(X_o,\ \alpha_o,\ \beta_o)} = \left(I - \gamma Z_o\sqrt{C^2 + S^2}\right)\gamma Z_o\frac{C\frac{\partial C}{\partial \alpha} + S\frac{\partial S}{\partial \alpha}}{\sqrt{C^2 + S^2}} - \frac{\alpha_o}{\sigma_\alpha^{\,2}} = 0 \tag{33b}$$

$$\left(\frac{\partial f}{\partial \beta}\right)\Bigg|_{(X_o,\ \alpha_o,\ \beta_o)} = \left(I - \gamma Z_o\sqrt{C^2 + S^2}\right)\gamma Z_o\frac{C\frac{\partial C}{\partial \beta} + S\frac{\partial S}{\partial \beta}}{\sqrt{C^2 + S^2}} - \frac{2\beta_o}{\sigma_\alpha^{\,2}} + \frac{1}{\beta_o} = 0 \tag{33c}$$

It turned out in all cases that $\alpha_o = 0$ so that $\left(\frac{\partial f}{\partial \alpha}\right)\Big|_{(X_o,\ 0,\ \beta_o)} = 0$

and X_o and β_o can be found from the simplified equations

$$\left(I - \gamma Z_o C(0,\ \beta_o)\right)\ \gamma Z_o C(0,\ \beta_o) - \frac{1}{\sigma_X^{\,2}}\left(X_o + \sigma_X^{\,2}\right) = 0 \qquad (34a)$$

$$\left(I - \gamma Z_o C(0,\ \beta_o)\right)\ \gamma Z_o \left(\frac{\partial C}{\partial \beta}\right)_{(0,\ \beta_o)} - \frac{2\beta_o}{\sigma_\alpha^{\,2}} + \frac{1}{\beta_o} = 0 \qquad (34b)$$

The determinant B is here given by

$$B = \left| \begin{array}{ccc} \frac{\partial^2 f}{\partial X^2} & 0 & \frac{\partial^2 f}{\partial X \partial \beta} \\ 0 & \frac{\partial^2 f}{\partial \alpha^2} & 0 \\ \frac{\partial^2 f}{\partial X \partial \beta} & 0 & \frac{\partial^2 f}{\partial \beta^2} \end{array} \right|_{(X_o,\ 0,\ \beta_o)} \qquad (35)$$

where

$$\left(\frac{\partial^2 f}{\partial X^2}\right) = (I - 2\gamma Z\ C)\ \gamma Z\ C - \frac{1}{\sigma_X^{\,2}} \qquad (36a)$$

$$\left(\frac{\partial^2 f}{\partial X \partial \beta}\right) = (I - 2\gamma Z\ C)\ \gamma Z \left(\frac{\partial C}{\partial \beta}\right) \qquad (36b)$$

$$\left(\frac{\partial^2 f}{\partial \alpha^2}\right) = (I - \gamma Z\ C)\ \gamma Z \left[\frac{\partial^2 C}{\partial \alpha^2} + \frac{\left(\frac{\partial S}{\partial \alpha}\right)^2}{C}\right] - \frac{1}{\sigma_\alpha^{\,2}} \qquad (36c)$$

$$\left(\frac{\partial^2 f}{\partial \beta^2}\right) = (I - \gamma Z\ C)\ \gamma Z \left(\frac{\partial^2 C}{\partial \beta^2}\right) - \gamma^2 Z^2 \frac{\left(\frac{\partial^2 C}{\partial \beta^2}\right)}{C} - \frac{2}{\sigma_\alpha^{\,2}} - \frac{1}{\beta_o^{\,2}} \qquad (36d)$$

and the probability density function of the signal is given by

$$p(I) = \frac{2\beta_o}{\sigma_\chi \sigma_\alpha^3 \sqrt{-B}} \exp\left[-\frac{1}{2}\left[I - \gamma Z_o C(0, \beta_o)\right]^2 - \frac{1}{2\sigma_\chi^2}\left(\chi_o + \sigma_\chi^2\right)^2 - \frac{\alpha_o^2}{2\sigma_\alpha^2} - \frac{\beta_o^2}{\sigma_\alpha^2}\right] \tag{37}$$

V. DISCUSSION

The final probability density functions for the static and tracking cases have been plotted as functions of the normalized rms signal current and are presented in Figs. 4.2 through 4.5 for several parameter values. In each graph, the density function in the absence of turbulence ($\sigma_\chi = \sigma_\Delta = \sigma_\alpha = 0$) is present for comparison, and is denoted by 0. The curves labeled by S and T are for the static and tracking receivers respectively, in the presence of turbulence.

In all cases presented, the mean current SNR, γ, has a value of ten. Values shown for the log-amplitude standard deviation are 0.3, corresponding to relatively low turbulence levels, and 0.8, which is the maximum value under saturated conditions.

The phase fluctuations in the static case are described by σ_Δ^2, which has been defined as $\langle (4/\pi R^2)\, a_2^2 \rangle$. It can easily be seen geometrically that this must be equal to $\langle k^2 \frac{D^2}{4} \theta^2 \rangle$ where k is the wavenumber of the optical signal, Θ is the angle between the receiver aperture plane and the average phase front along the x axis, and the assumption has been made that $\tan \theta = \theta$.

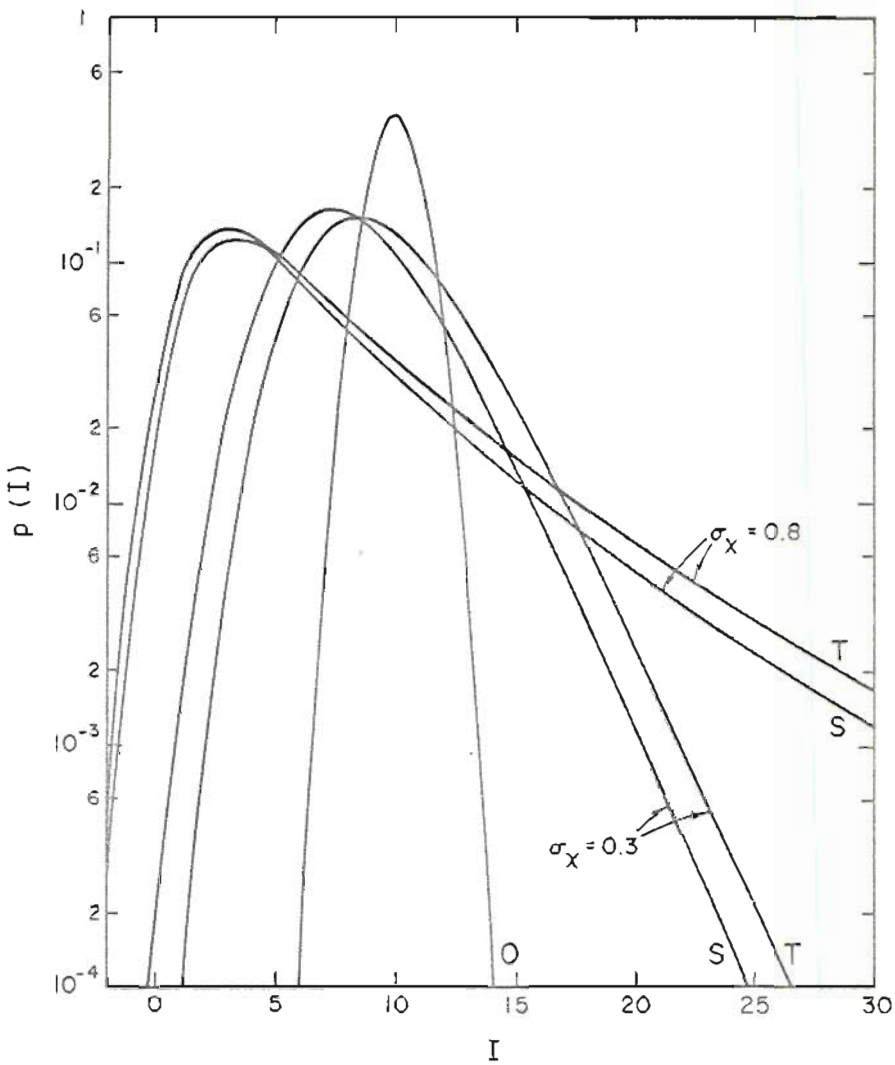

Fig. 4.2. Probability density function p(I) vs. normalized rms signal current I for static receiver (S), tracking receiver (T), and quiescent atmosphere (0) cases. $D/r_o = 0.5$.

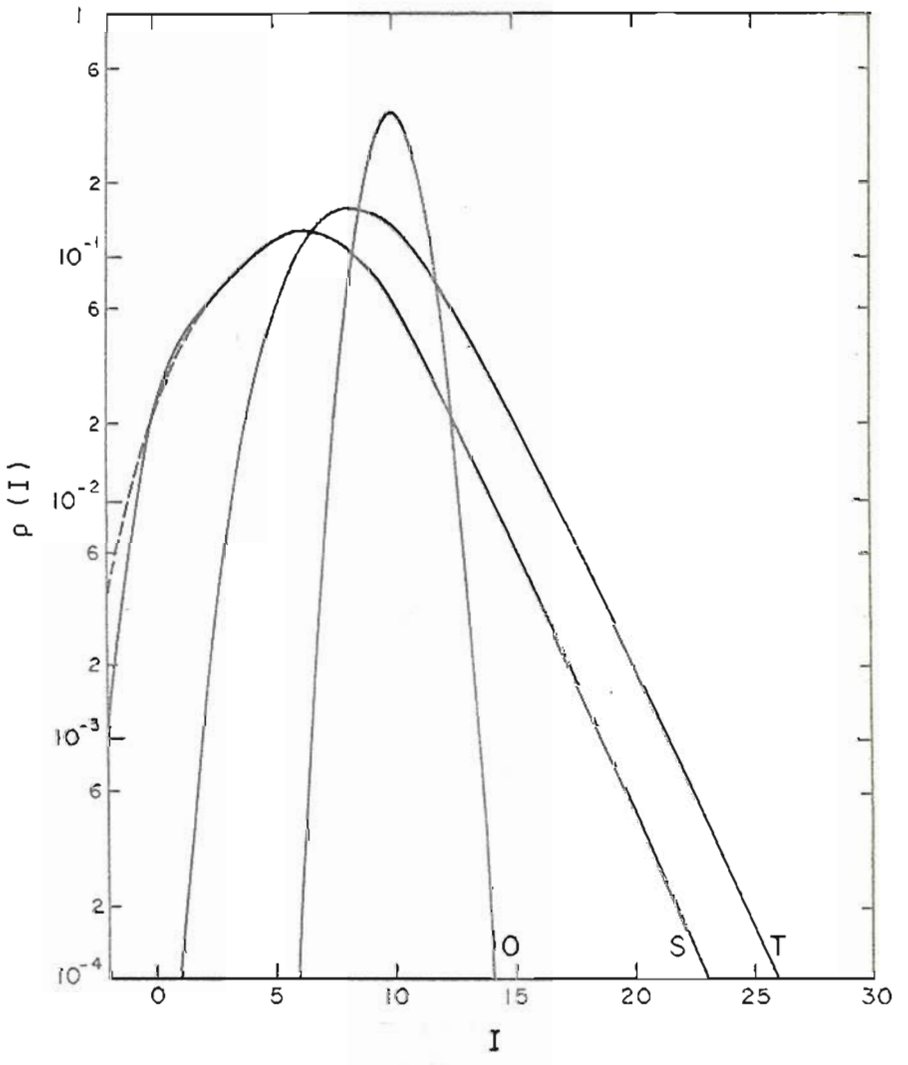

Fig. 4.3. Same as Fig. 4.2 with $D/r_o = 1.0$ and $\sigma_\chi = 0.3$. Dashed line neglects first order correction term.

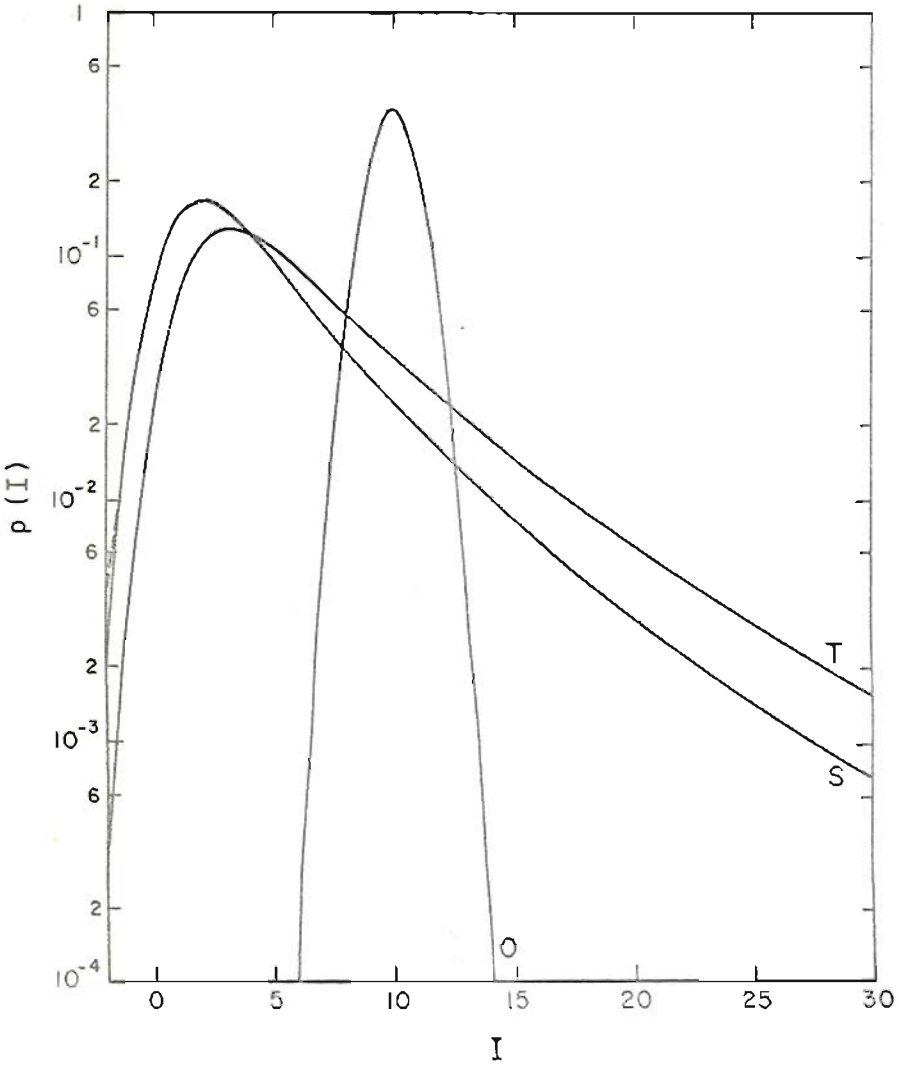

Fig. 4.4. Same as Fig. 4.2 with $D/r_o = 1.0$ and $\sigma_\chi = 0.8$.

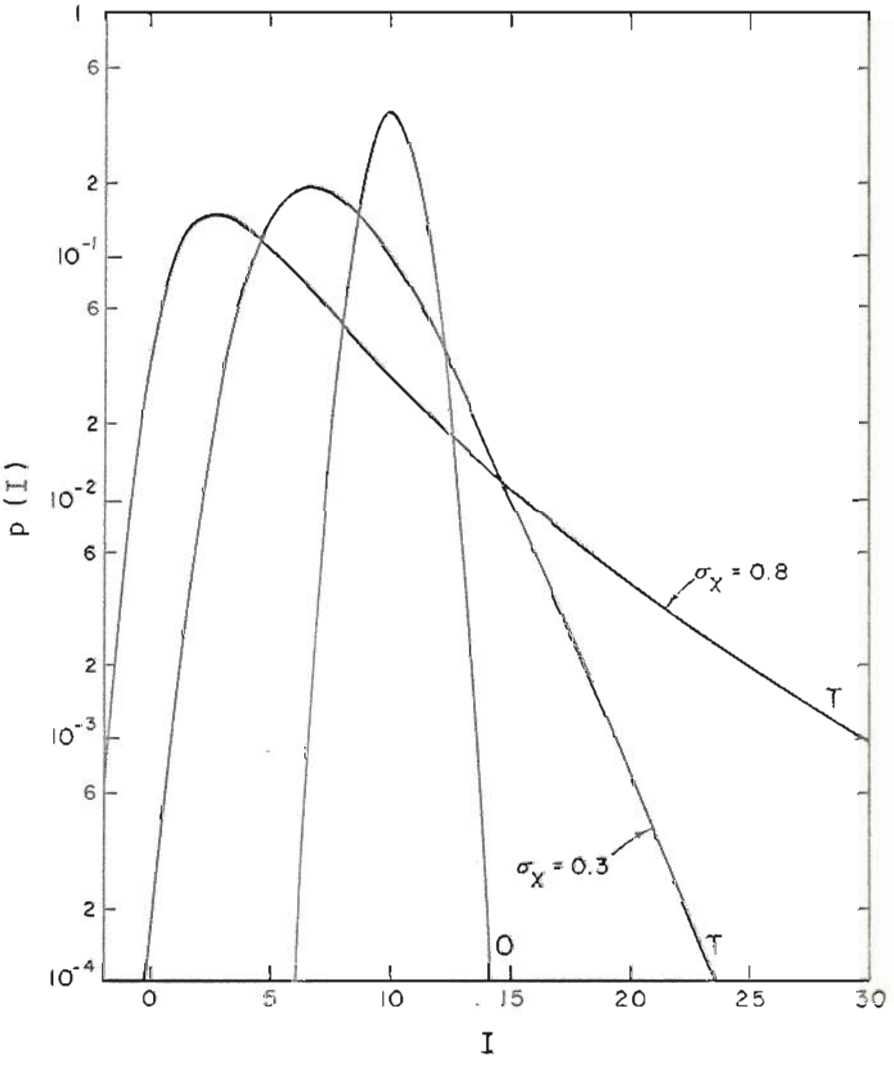

Fig. 4.5. Same as Figure 4.2 with D/r_o = 3.4.

It can be seen that

$$\sigma_\Delta^2 = \langle k^2 \frac{D^2}{4} \theta^2 \rangle = \frac{D_s(D)}{4} = 0.73\, k^2 C_n^2 L\, D^{5/3} = 1.72\, (D/r_o)^{5/3} \tag{38}$$

where $D_s(D)$ is the structure function of phase, C_n^2 is the refractive index structure constant, and L is the path length. Implicit in Eq.(38) is the assumption that the phase structure function is very nearly equal to the total wave structure function, which is a very good approximation in the near field[3] or under conditions of saturated amplitude fluctuations.[29] Even where these conditions are not satisfied, the phase fluctuations are overestimated by no more than a factor of two. The coefficient of $(D/r_o)^{5/3}$ is calculated in Ref. 18 by a different method and found to be 1.77, which is in excellent agreement with the results here. Accepting the results of Ref. 18, then

$$\sigma_\alpha^2 = \langle (1.2/\pi R^2)\, a_4^2 \rangle = 0.253\, (D/r_o)^{5/3} \tag{39}$$

Both density functions were calculated for $(D/r_o) = 1$ and $(D/r_o) = \frac{1}{2}$.

In Section 4.III, it was assumed that the absolute value bars around $J_1(\Delta)$ could be dropped. To find the effects of this assumption, it is seen that, to first order

$$p(I) = \int_0^\infty \int_{-\infty}^\infty dX\, d\Delta\, \frac{1}{\sqrt{2\pi}} \exp\left[-\frac{1}{2}\left(I - 2\gamma Z \left|J_1(\Delta)\right|/\Delta\right)^2\right] p(X)\, p(\Delta)$$

$$\approx \int_0^\infty \int_{-\infty}^\infty dX\, d\Delta\, \frac{1}{\sqrt{2\pi}} \exp\left[-\frac{1}{2}\left(I - 2\gamma Z\, J_1(\Delta)/\Delta\right)^2\right] p(X)\, p(\Delta)$$

$$- \int_{3.83}^{7.02} \int_{-\infty}^\infty dX\, d\Delta\, p(X)\, p(\Delta)\, \frac{1}{\sqrt{2\pi}} \left\{ \exp\left[-\frac{1}{2}\left(I - 2\gamma Z J_1(\Delta)/\Delta\right)^2\right] \right.$$

$$\left. - \exp\left[-\frac{1}{2}\left(I + 2\gamma Z J_1(\Delta)/\Delta\right)^2\right] \right\} \tag{40}$$

since the first negative portion of $J_1(\Delta)$ lies in the region where $3.83 < \Delta < 7.02$. In Figs. 4.3 and 4.4, the curves for the static receiver are double valued for very small signal currents. The dashed line in each case is the uncorrected value, while the solid curve takes into consideration the first order correction term, which was negligible in all cases for which $D/r_o = \frac{1}{2}$.

The curves in the tracking case are essentially the same for $D/r_o = 1$ or $D/r_o = \frac{1}{2}$ and, in fact, change very little in the limit as D/r_o goes to zero. Where D/r_o is on the order of one or less, therefore, amplitude fluctuations are the major effect of turbulence on signal current, so that the density function can be approximated by

$$p(I) = \frac{\frac{1}{\sqrt{2\pi}\,\sigma_X} \exp\left[-\frac{1}{2}\left(I - \gamma Z_o\right)^2\right] \exp\left[-\frac{\left(X_o + \sigma_X^2\right)^2}{2\sigma_X^2}\right]}{\left(\frac{1}{\sigma_X^2} - \left(I - 2\gamma Z_o\right)\gamma Z_o\right)^{1/2}} \tag{41a}$$

where

$$\left(I - \gamma Z_o\right)\gamma Z_o + \frac{1}{\sigma_X^2}\left(X_o + \sigma_X^2\right) = 0 \tag{41b}$$

This fact also confirms that second order phase terms can be neglected in the static receiver.

In the limit as D/r_o goes to zero, the static receiver is identical to the tracking. As D/r_o takes on larger values, however, the peak probability shifts to lower signal currents and the curves broaden. The general shape (i.e., skewness) of the curves, however, still depends to a large degree on the log-amplitude variance.

5. SIGNAL CURRENT PROBABILITY DISTRIBUTION FOR OPTICAL HETERODYNE RECEIVERS IN THE TURBULENT ATMOSPHERE. 2: EXPERIMENT

I. INTRODUCTION

In the previous chapter approximate expressions were developed for the probability density functions describing the magnitudes of the IF signals from optical heterodyne receivers operating in the presence of clear air turbulence, both with and without active tilt-tracking systems. In this chapter the theoretical predictions for the non-tracking, or static, receiver are compared with measurements of the signal distribution from a static receiver that was used to detect a 632.8 nm signal propagating through 1.6 km of the open atmosphere.

In the derivation of the predicted density, given in Eqs.(25) through (28) of the last chapter, several assumptions and idealizations have been made. For example, both the transmitter and the local oscillator were considered to be perfectly monochromatic and to have constant amplitude and frequency. In designing the experimental apparatus, the emphasis was not on duplicating these idealizations but rather on reproducing, insofar as possible, conditions under which optical heterodyne detection might be practically used. This chapter is, therefore, not a rigorous test of the theoretical model but is instead an investigation into the accuracy with which that model can be used to predict the performance of a typical system. As an example, instead of trying to amplitude- and frequency-stabilize the transmitter, every attempt was made to keep the transmitter package small, lightweight, and simple. It consists, therefore, of an inexpensive two milliwatt Helium-Neon

laser, two converging lenses comprising a two power transmitting telescope, and a hand operated steering mirror. The intensity that would be present at the receiver under diffraction limited conditions is estimated to be on the order of 0.5 $\mu W/cm^2$, which is divided between two major longitudinal modes so that only about one-half of this contributes to the IF signal.

From the transmitter, the signal propagates across 1.6 km of flat, featureless farmland at a height of about two meters. Because of the uniformity of the range, the measurement of temperature, atmospheric pressure, and temperature structure constant C_T^2 is made at one point and assumed to be constant along the path. From these measurements, along with the mean signal and the mean and variance of the local oscillator signal alone, estimates were made of the parameters necessary to calculate the predicted curve for each data run. In parameter estimation, as in hardware design, the emphasis was on the simple, practical application of the theory, rather than on trying to optimize agreement between theory and experiment through complex curve fitting. The next section is a description of the receiver that was used, and this is followed by a discussion of the method used to fit the theoretical parameters to operating conditions. The results presented in Section 5.IV show that the results of Chapter 4, at least in the static case, comprise a good approximation to the operation of an actual receiver, even for cases where the normalized aperture diameter, D/r_o, is larger than one.

II. RECEIVER DESCRIPTION

An optical heterodyne receiver, which is diagrammed in Fig. 5.1 and described in detail in Appendix E, has been built and installed

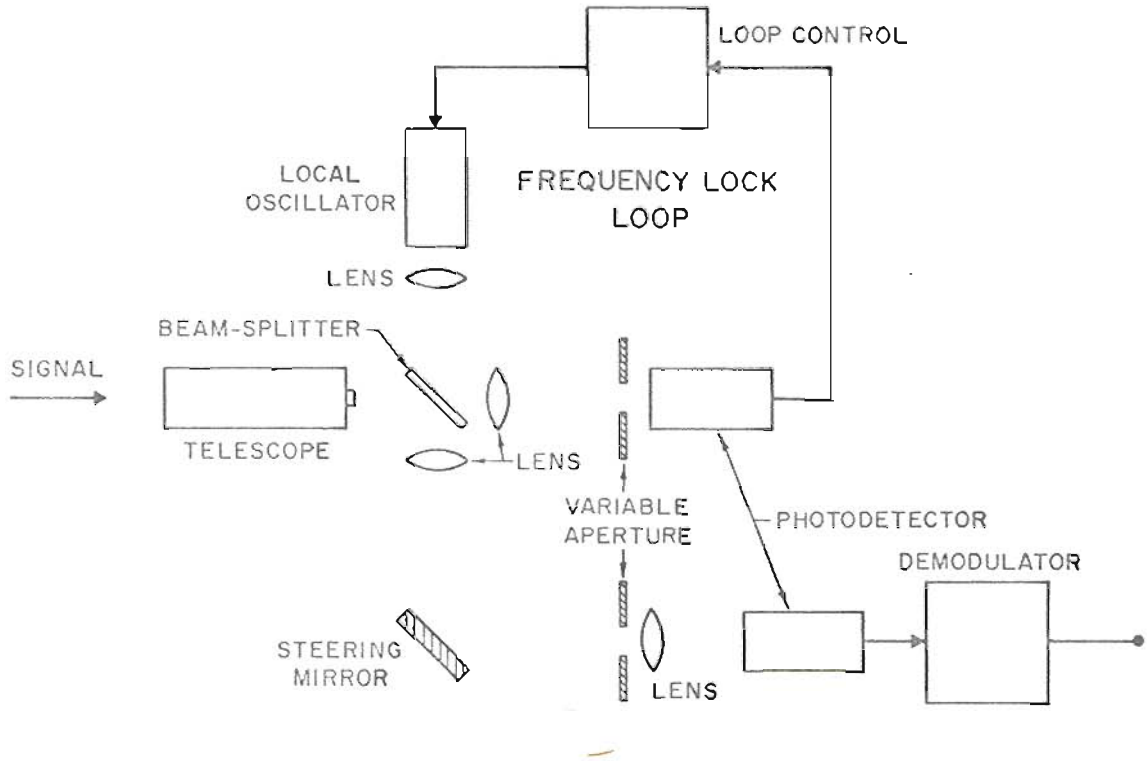

Fig. 5.1. Block diagram of static optical heterodyne receiver with frequency tracking.

at the end of the 1.6 km propagation range. The receiver optics collect the signal, mix it with the local oscillator beam, and deliver it to an optical detector. The IF signal from this detector is fed into an amplitude demodulator. In addition, the mixed optical signal also goes to a separate optical detector, from which the IF signal is frequency demodulated and used as the error signal in a frequency lock loop. Any frequency changes in the received signal are then tracked by the local oscillator.

The receiver antenna consists of a 200 mm Tinsley-Cassegrain telescope which is focused at infinity to collimate the signal and project it onto the surface of a ten percent reflecting beamsplitter, where it is mixed with the beam from the local oscillator. Following the beamsplitter there are two optical paths. In one path, the reflected local oscillator beam and the transmitted signal are projected onto a variable aperture directly in front of the photomultiplier tube that drives the loop. In the other path, the transmitted local oscillator beam, combined with the reflected signal, is reflected from a front surface steering mirror and projected onto another variable aperture. The optical reduction between the front of the collecting telescope and this, the signal aperture, is a factor of 5.3 and the effective telescope aperture is variable from .21 cm to 5.1 cm. Immediately behind the signal aperture is a collecting lens to focus the signal onto the photomultiplier tube from which the signal is demodulated.

The IF signal from the loop photomultiplier tube goes into an amplifier-limiter and from there into a discriminator with center frequency at the desired IF. For this receiver the center frequency

is 29.5 MHz. The output of the discriminator goes into a high voltage amplifier which drives the frequency control of a Spectra-Physics 119 He-Ne laser. The rear mirror of the 119 is mounted on a piezoelectric element so that the cavity length of the laser is a function of the voltage across the element, and the laser functions as a voltage controlled oscillator, closing the loop. The bandwidth of the loop response is about one kilohertz, which is sufficient to track thermally induced frequency shifts. To minimize the effects of higher frequency acoustic vibrations, therefore, the entire receiver is rigidly mounted on a concrete slab.

The IF signal from the receiver signal photomultiplier tube is filtered, mixed down to one megahertz electronically, and fed into a full wave rectifying envelope detector. In the theoretical work, an idealized demodulator was assumed which allows the magnitude of the IF signal to be found with no distortion of signal or noise characteristics. Envelope demodulation, although a very good approximation to this ideal whenever the signal is much larger than the noise envelope, introduces distortion when the magnitude of the signal is small. Synchronous demodulation introduces less distortion, and in all probability would have provided better agreement. However, it was not used in this experiment due to the added complexity.

III. PARAMETER ESTIMATION

In each data run, the output signal from the above receiver was directly recorded on an F.M. tape recorder both with the optical signal present and with it blocked to obtain reference levels for normalization. In addition, instantaneous point measurements were made of the temperature, T, atmospheric pressure, P, and temperature structure constant,

C_T^2, the last being measured with a pair of balanced microthermal probes at ten cm. separation and employing 100 second time averaging. The tape recorded data was converted to digital format and processed on a digital computer. Knowledge of the meteorological conditions allowed estimates to be made of the theoretical parameters.

The refractive index structure constant is found from the relationship[3]

$$C_n^2 = \left(77.6 \times 10^{-6}\ P/T^2\right)^2\ C_T^2 \qquad (1)$$

and is used, along with physical dimensions of the system, for parameter estimation. From the optical carrier wavelength in microns, λ_μ, the path length, L, and the structure constant of turbulence strength, C_n^2, the characteristic coherence length r_o for each turbulence level can be found from the equation[18] (2)

$$r_o = 1.2 \times 10^{-8}\ \lambda_\mu^{6/5}\ L^{-3/5}\ C_n^{-6/5} = 8.22 \times 10^{-11}\ C_n^{-6/5}$$

From this, the tilt fading parameter σ_Δ^2 can be found from the relationship given in the last chapter

$$\sigma_\Delta^2 = 1.72\ (D/r_o)^{5/3} \qquad (3)$$

Here D is the effective aperture diameter at the front end of the collecting telescope and is equal to 5.3 times the diameter of the variable aperture in front of the signal photomultiplier tube.

The derivation of Eq.(2), however, is based on the propagation of an infinite plane wave while the experiment was made with a finite beam wave. The mutual coherence function of a finite beam, and hence the second order moments of the received field, is essentially the same as that for a point source provided that[30]

$$L >> \frac{1}{4} k w_o \left[1/\rho_o^2 + 1/w_o^2\right]^{-1/2} \qquad (4)$$

where w_o is the diameter of the beam at the transmitter, k is its wavenumber, and ρ_o, the 1/e diameter of the spherical wave MCF, is equal to 0.83 times the plane wave r_o given by Eq.(2). Since w_o was about 2.5 mm, this inequality holds at all turbulence levels. Also, the largest effective aperture diameter used, 8.5 mm, is significantly less than the Fresnel zone size, and the second order moments of the received field can be found from the spherical wave theory in the far-field regime. Thus, the structure function of phase differs from the plane wave case by a constant factor,[4] so that

$$r_{o\ (sph)} = 1.8\ r_{o\ (plane)} = 1.48 \times 10^{-10}\ C_n^{-6/5} \qquad (5)$$

This value was used in Eq.(3) to find σ_Δ^2.

Since the inner scale of turbulence, generally on the order of a few millimeters,[4] is also much less than the Fresnel zone size, the spherical wave theory predicts that the log-amplitude variance will be given by[3]

$$\sigma_\chi^2 = 0.124\ k^{7/6}\ L^{11/6}\ C_n^2 = 1.38 \times 10^{13}\ C_n^2 \qquad (6)$$

as long as this is small enough that saturation of the scintillation does not occur. In this experiment, however, where predicted values of σ_Δ^2 range from 0.6 to 7.0, the phenomenon of saturation must be considered. A number of experimental investigations of saturation in spherical wave propagation have been made[4,31,32] showing that σ_χ generally follows the value predicted by Eq.(6) until it reaches a value of about 0.8. It then remains fairly constant at this level with

increasing turbulence. This simple formulation agrees well with experimental evidence over the range of interest here, and will be used to estimate the log-amplitude standard deviation.

The third and final parameter needed to calculate the theoretical curves is γ, the current signal-to-noise ratio that would be present in the absence of turbulence. Since it is not possible to turn off the turbulent atmosphere in order to make this measurement, an estimate based on the expected value of the normalized signal, $\langle I \rangle$, has been used. From Eq.(24) of the last chapter, it is easy to find an expression for the mean signal predicted by the theory, which can then be solved for γ, resulting in

$$\gamma = \langle I \rangle \frac{\sigma_\Delta^2}{4} \exp\left(\frac{\sigma_\Delta^2}{4} + \frac{\sigma_\chi^2}{2}\right) \Big/ \sinh \frac{\sigma_\Delta^2}{4} \tag{7}$$

which was calculated for each data run.

Normalization of the signal was accomplished by letting

$$I = (S + N - \langle N \rangle)/\sigma_N \tag{8}$$

where $S + N$ is the recorded signal value, σ_N is the standard deviation of the shot noise, and $\langle N \rangle$, the mean value of the shot noise, is not zero due to rectification. With signal present, however, I', will be less than that given by Eq.(8), falling in fact, within the range

$$(S + N - \langle N \rangle)/\sigma_N \leq I' \leq (S + N)/\sigma_N \tag{9}$$

For I' very small, it will be very close to the left hand side of the possible range while, for large values, it will approach the right hand side. Since the total width of the allowed region, $\langle N \rangle/\sigma_N$, becomes less significant as $S + N$ becomes large, the estimate given by Eq.(8) is more

reasonable than the other obvious possibility. It was also seen to provide consistently better agreement with experimental results.

IV. RESULTS

For each data run the value of the signal plus noise was recorded, generally for a period of one or two minutes. The transmitted beam was then blocked and the local oscillator shot noise alone was recorded for a similar period of time. At the same time the meteorological measurements were made. After normalization, the probability density function of the recorded signal, p(I), was plotted against the normalized signal, I. The results are given for several typical data runs in Figs. 5.2 through 5.5. Theoretical curves (solid lines), including the first order correction (dashed lines) in cases where it is significant, were calculated for comparison with the experimental points (X's). In each case the calculated value of the quiescent atmosphere signal-to-noise ratio, γ, is indicated.

The agreement is generally very good, although there are two major factors that introduce consistent inaccuracies. The first of these is the assumption that the absolute value bars in Eq. (15) of the last chapter may be dropped, which is an increasingly bad assumption with increasing values of D/r_o. The second major source of disagreement seems to result from making a single point measurement of C_T^2 and using this to infer all three of the theoretical parameters.

The magnitude of the first effect is clearly seen in Figs. 5.2 through 5.4. The first of these is a case where D/r_o is less than one and the correction term is negligible. In the next case, where D/r_o equals one, dropping the absolute value bars introduces a noticeable

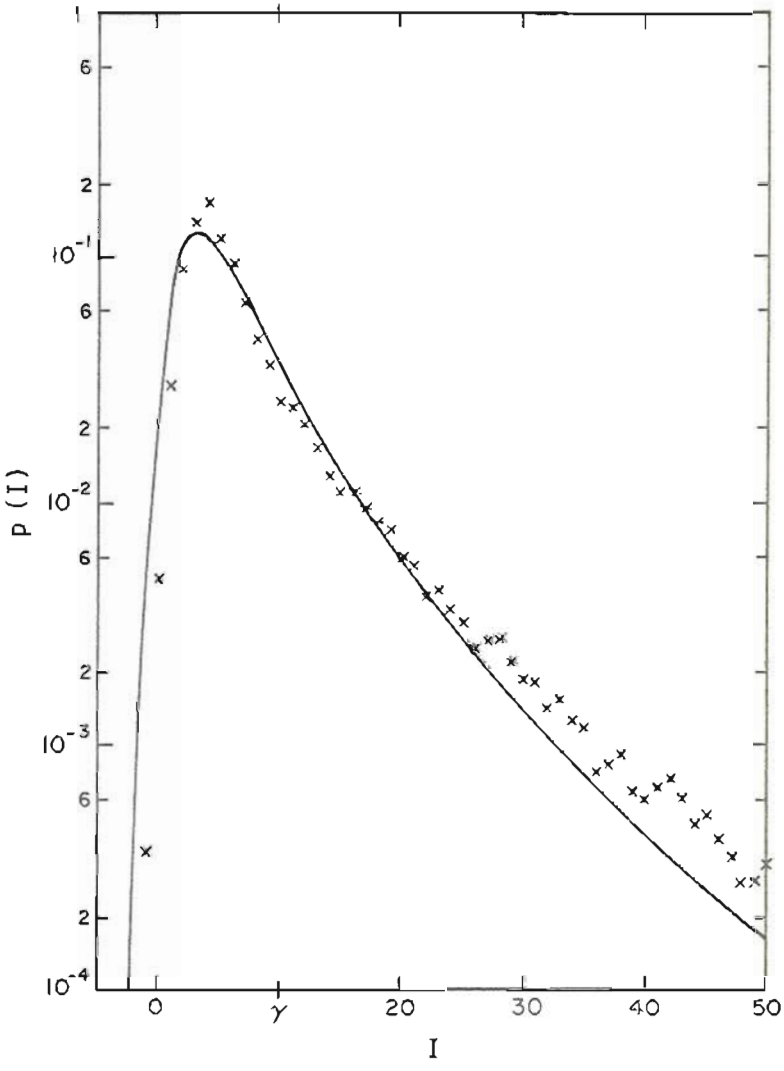

Fig. 5.2. Signal current probability density function, p(I) vs. normalized signal current amplitude, I; experimental results (X) and theoretical curve with $\sigma_\chi = 0.8$, $D/r_o = 0.15$, and quiescent atmosphere SNR, $\gamma = 10$.

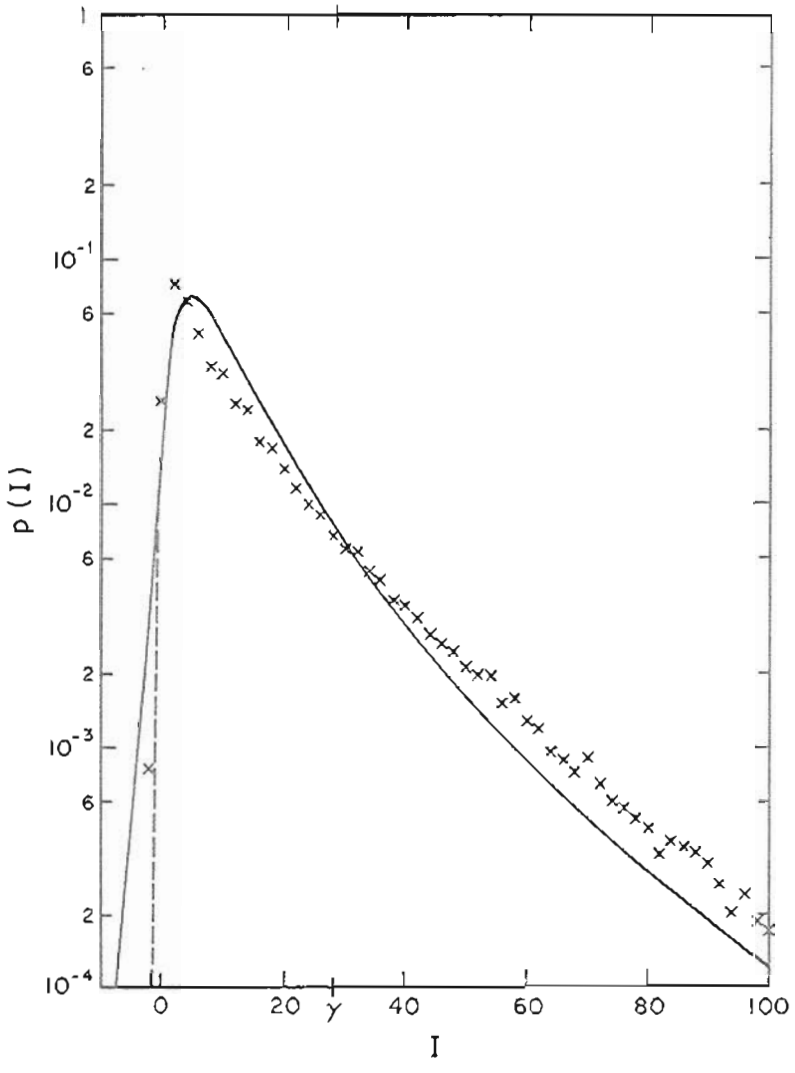

Fig. 5.3. Same as Fig. 5.2 with $\sigma_\chi = 0.8$, $D/r_o = 1.0$, and $\gamma = 28$. Dashed line is theoretical curve including effects of first order correction term.

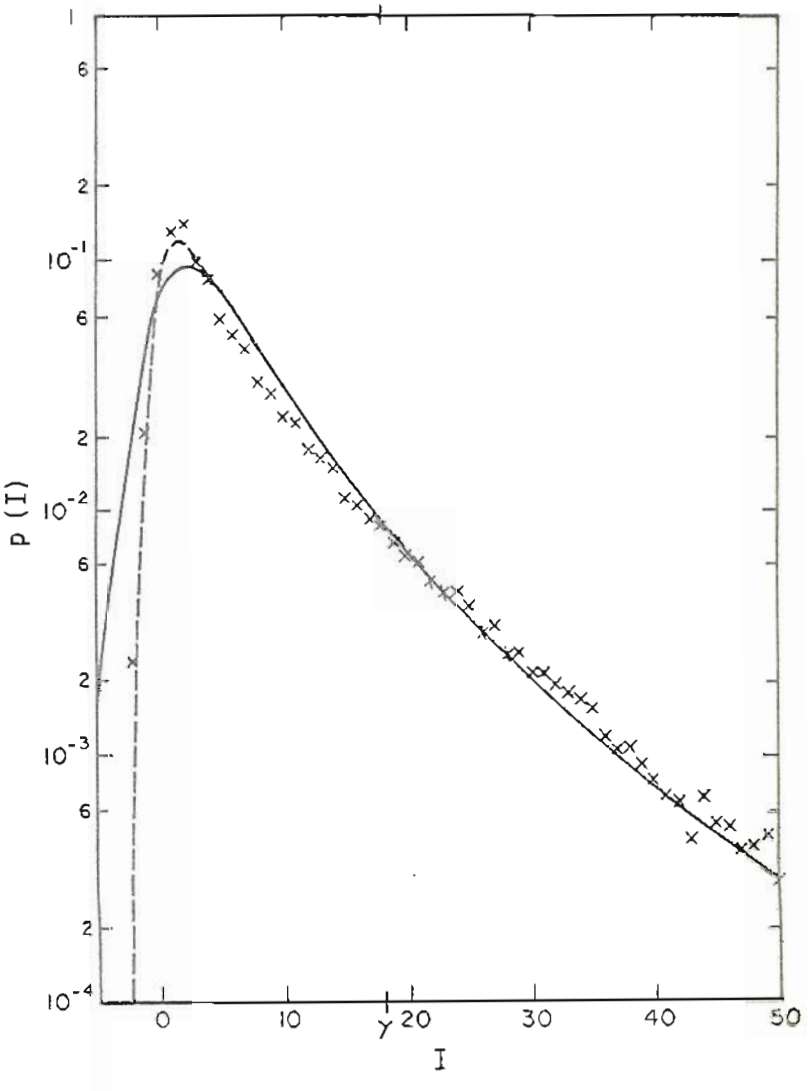

Figure 5.4. Same as Fig. 5.3 with $\sigma_\chi = 0.8$, $D/r_o = 1.5$, and $\gamma = 18$.

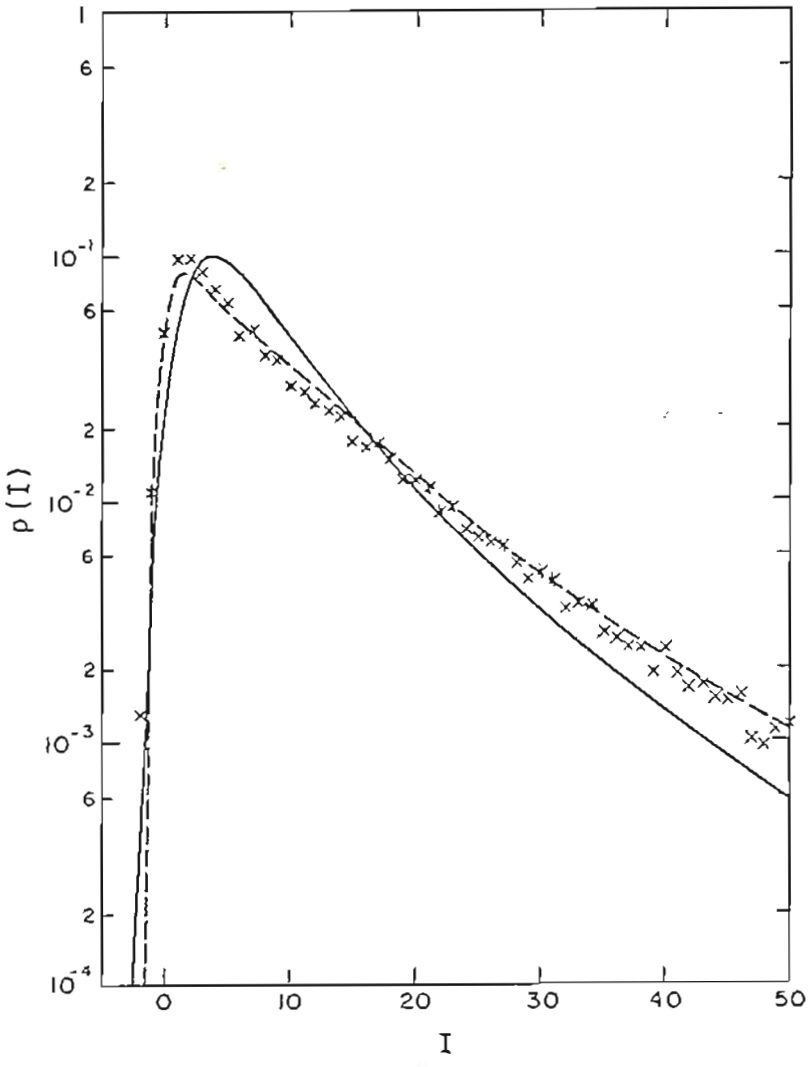

Fig. 5.5. Solid line is theoretical distribution at measured value of C_n and has parameters $\sigma_\chi = 0.8$, $D/r_o = 0.75$, and $\gamma = 17$. Dashed line is corrected theory for C_n 1.8 times larger, resulting in $\sigma_\chi = 0.8$, $D/r_o = 1.5$, and $\gamma = 29$.

error at very small signal levels. For signals greater than zero, however, the distribution is still very well approximated by the uncorrected theory. In Fig. 5.4, D/r_o is greater than one and, although this violates a condition of the theoretical derivation, excellent agreement is obtained. The correction term in this case has a greater influence and also must be applied at larger signal levels.

In Figs. 5.2 and 5.3, the theoretical curve drops off more rapidly than experimental points with increasing signal levels. This feature, in varying degrees, is common to a large number of data runs and can probably best be explained by considering the measurement of C_n^2 that was used in parameter estimation. Several comparisons have been made of optically and thermally measured C_n values.[33,34] These experiments have shown the thermally measured values to be consistently lower and to exhibit large fluctuations. With this in mind, a number of the worst cases were plotted and C_n^2 was increased until good qualitative agreement was obtained. Figure 5.5 is a typical result. The solid line is based on the thermally measured value of C_n, and the dashed line gives the corrected theory with C_n higher by a factor of 1.8. This difference is within the spread between optically and thermally measured values of C_n as reported by Pearson and by Dowling and Livingston. The better fit to a theoretical curve using an increased value of C_n, as seen in Fig. 5.5, suggests that use of a point thermal measurement of C_n to determine the value of the theoretical paramenters for comparison with the experimental data may account for a major portion of the small discrepancy between theory and experiment. The increase in C_n required to account for this difference agrees both in magnitude and

direction with the discrepancies between optically and thermally measured C_n found previously.[33,34]

The development of Chapter 4 for the case of the static optical heterodyne receiver, therefore, is felt to be an excellent approximation to the performance of practical systems. With the addition of the first order correction term, agreement is seen to extend to D/r_o values larger than one and seems to be limited primarily by inaccuracies inherent in thermal C_n^2 measurements. Additional data, presented in Figs. 5.6 through 5.19, supports these conclusions, although it should be mentioned that only conditions of saturated log-amplitude fluctuations were available.

In the last chapter it was noted that the general shape of the density functions depends strongly on amplitude fluctuations. Since these fluctuations are log-normal, this effect can be seen in a comparison of the data with a log-normal probability density function. A fit of the data to a distribution of the form

$$p(I) = \frac{1}{\sqrt{2\pi}\sigma_{\ln I}\, I} \exp\left[-(\ln I - \mu_{\ln I})^2 / 2\sigma_{\ln I}^2\right] \qquad (10)$$

is easily accomplished by setting

$$\sigma_{\ln I}^2 = \ln(\sigma_I^2/\mu_I^2 + 1) \qquad (11a)$$

$$\mu_{\ln I} = \ln \mu_1 - \frac{1}{2}\sigma_{\ln I}^2 \qquad (11b)$$

Where μ_I and σ_I^2 are the measured mean and variance of the data.

Typical results of this investigation are presented in Figs. 5.20 through 5.24. In all cases the discrepancies between the curve and the data are larger than statistical fluctuations of the data, which implies

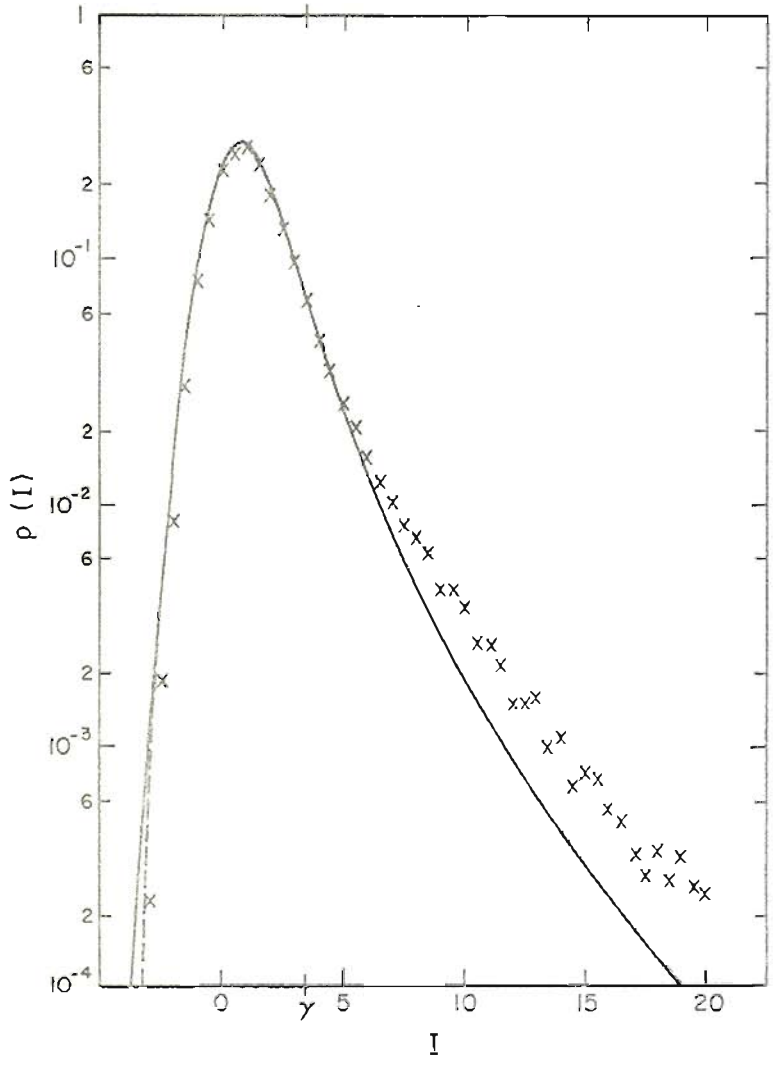

Fig. 5.6. Same as Fig. 5.3 with σ_χ = 0.8, D/r_o = 1.2, and γ = 3.4.

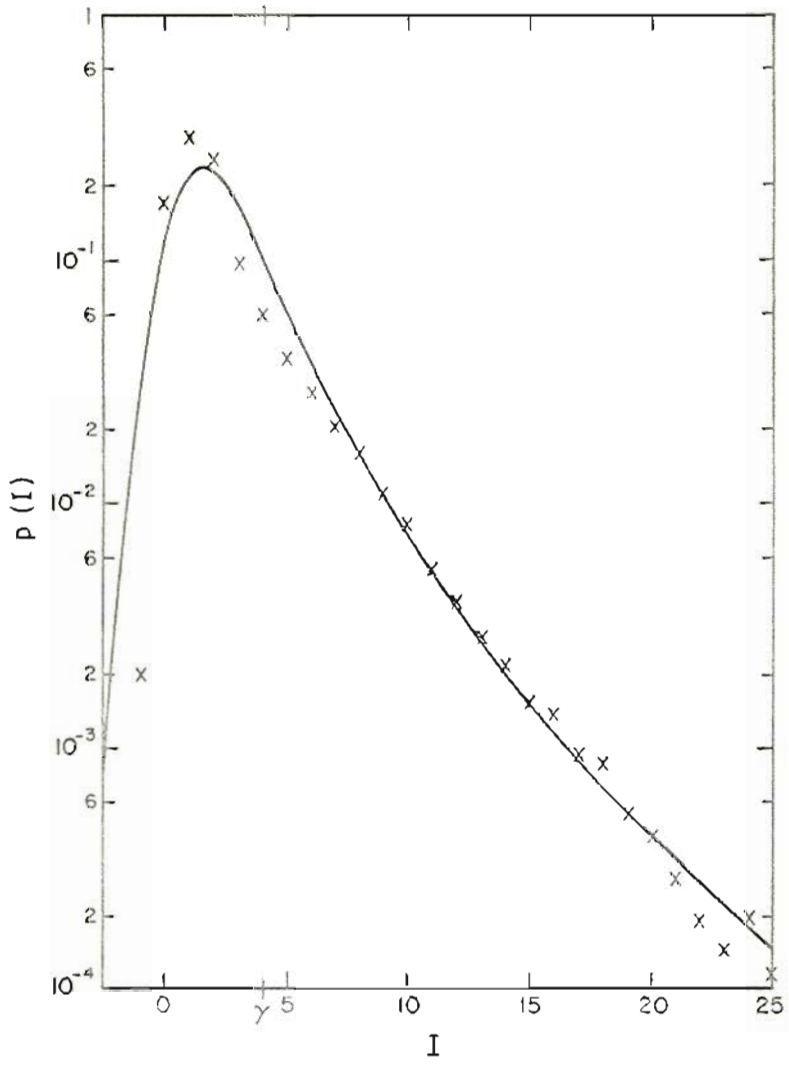

Fig. 5.7. Same as Fig. 5.3 with σ_χ = 0.8, D/r_o = 0.4, and γ = 4.1.

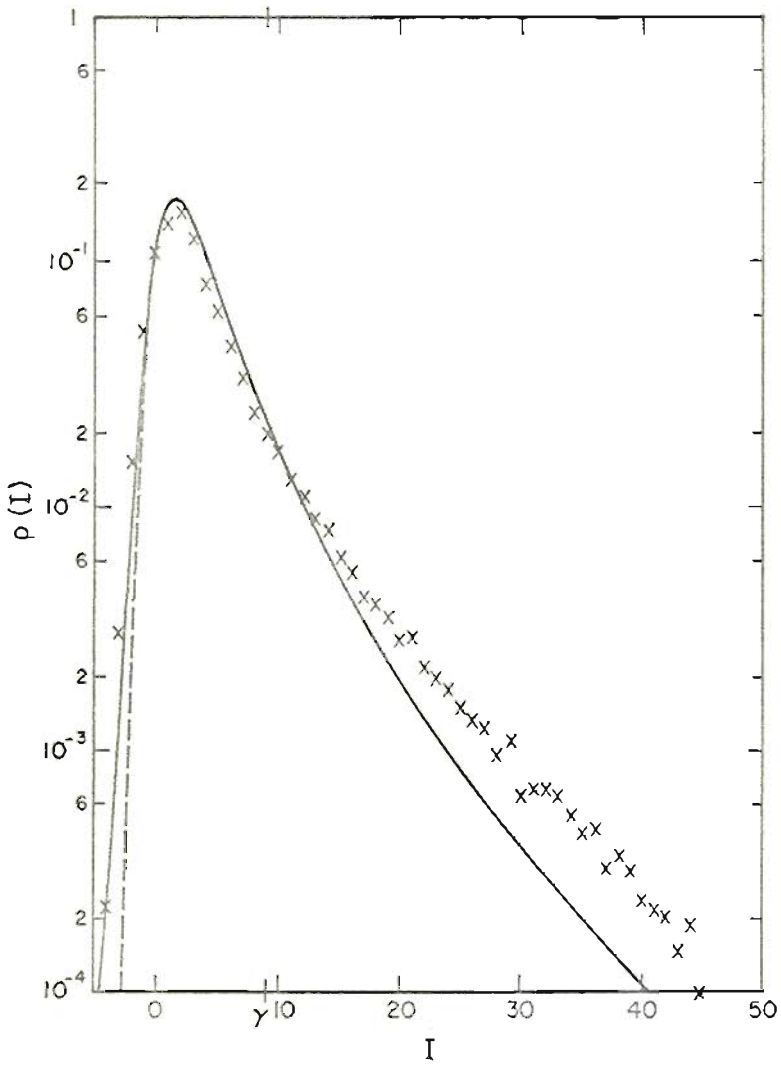

Fig. 5.8. Same as Fig. 5.3 with σ_χ = 0.8, D/r_o = 1.2, and γ = 8.8.

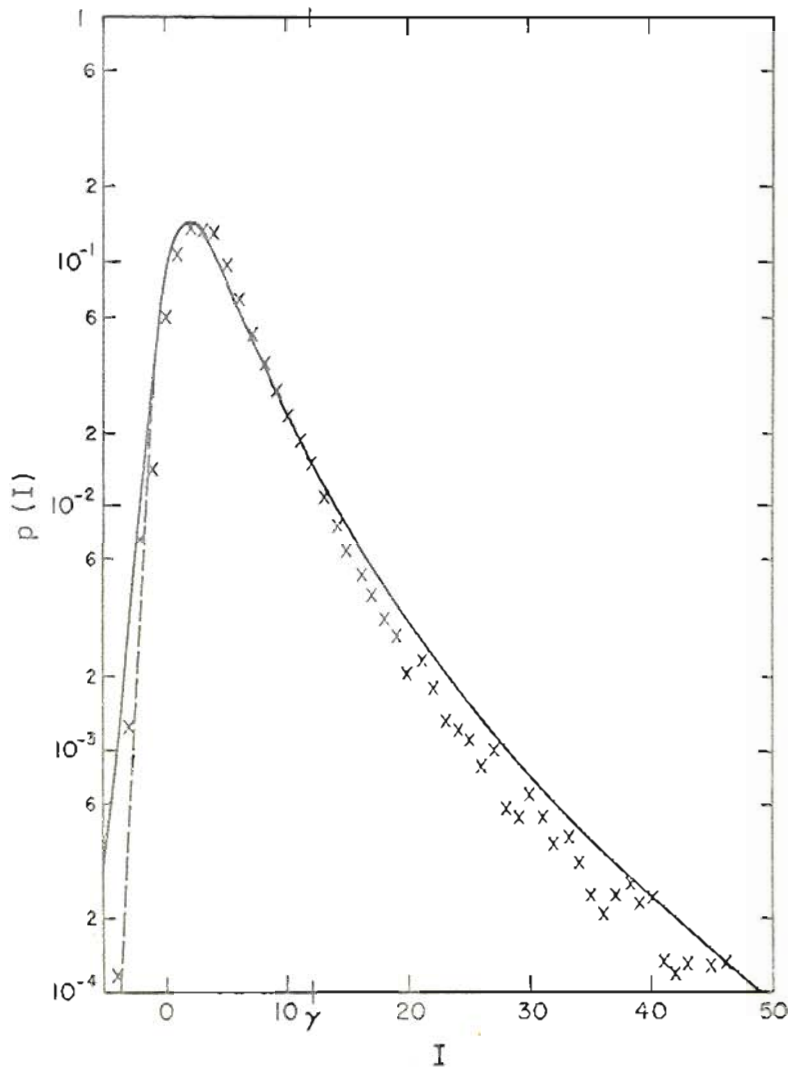

Fig. 5.9. Same as Fig. 5.3 with $\sigma_\chi = 0.8$, $D/r_o = 1.3$, and $\gamma = 12$.

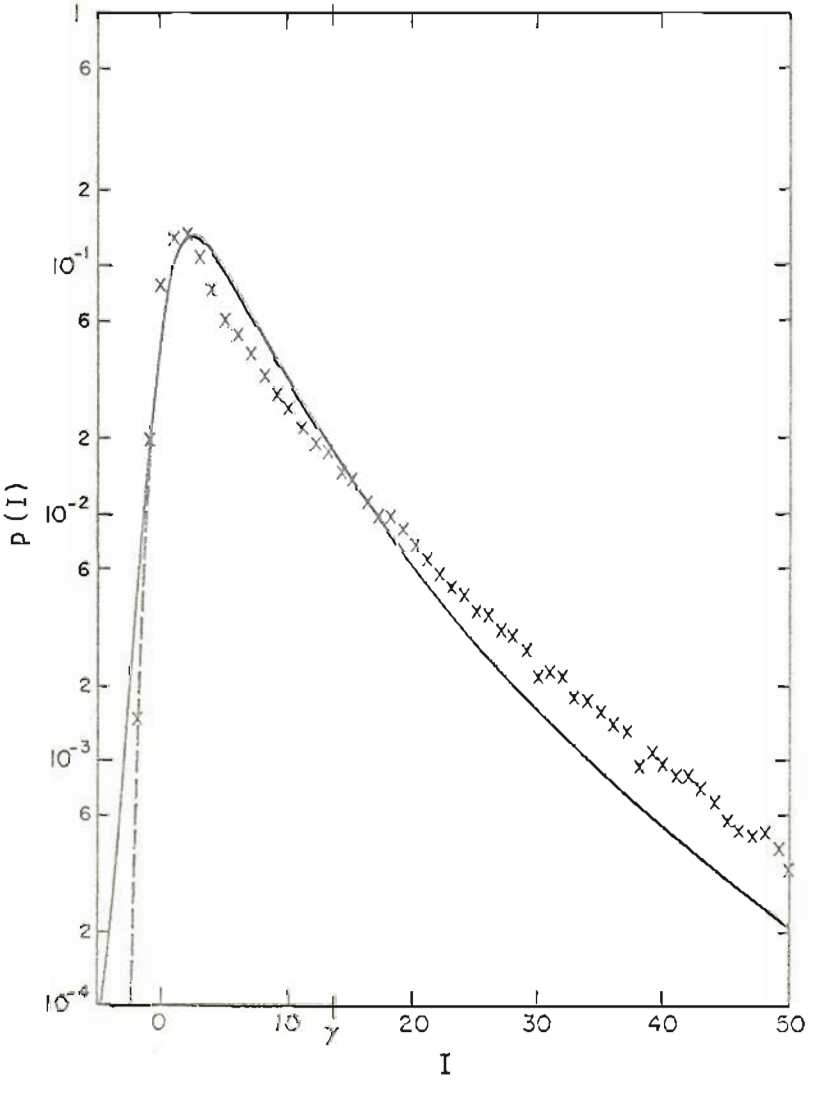

Fig. 5.10. Same as Fig. 5.3 with $\sigma_\chi = 0.8$, $D/r_o = 1.0$, and $\gamma = 13$.

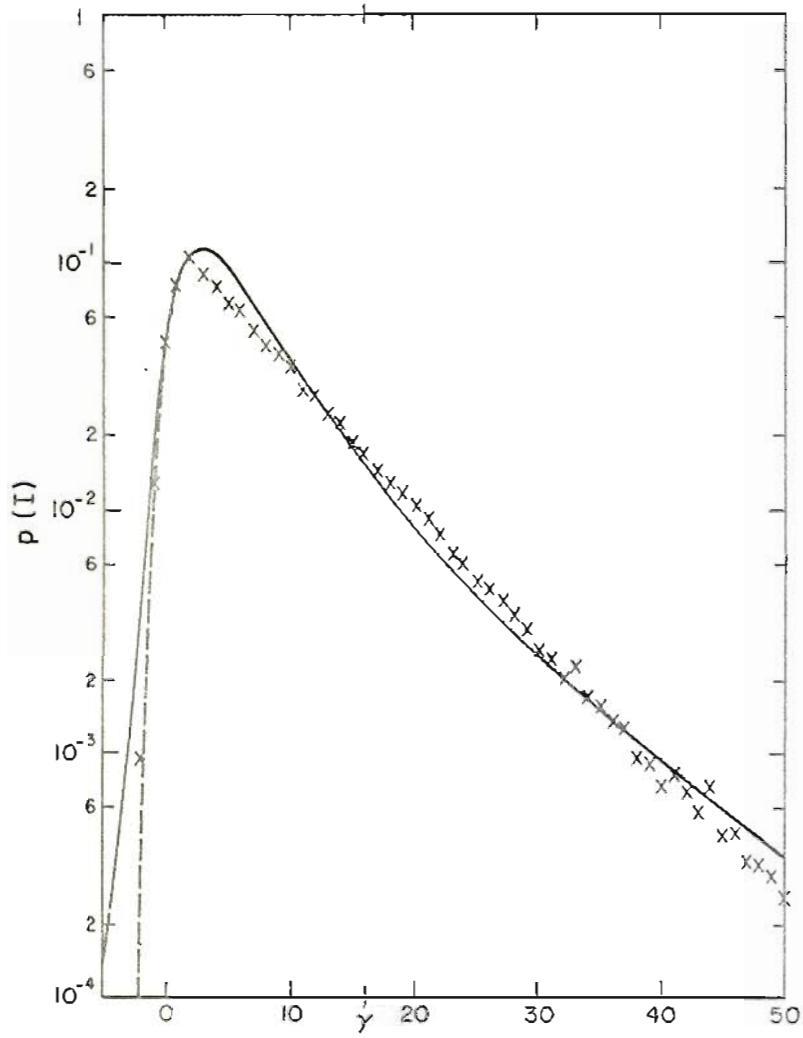

Fig. 5.11. Same as Fig. 5.3 with $\sigma_\chi = 0.8$, $D/r_o = 1.0$, and $\gamma = 16$.

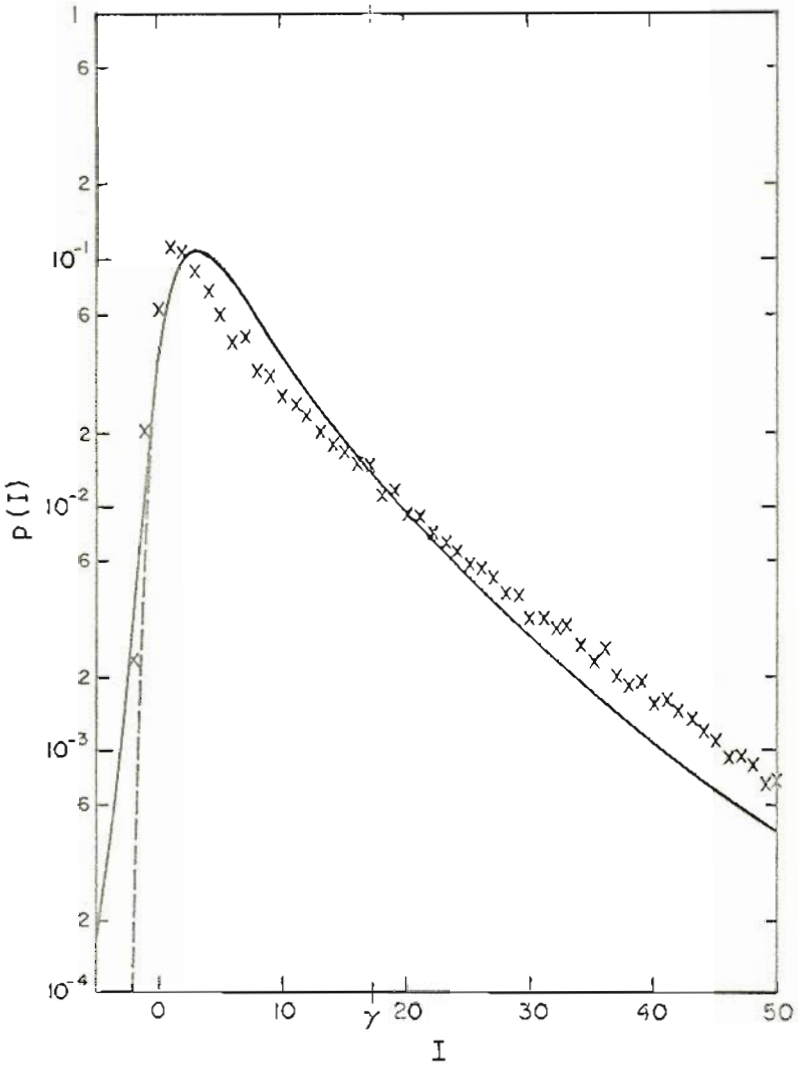

Fig. 5.12. Same as Fig. 5.3 with σ_χ = 0.8, D/r_o = 1.0, and γ = 17.

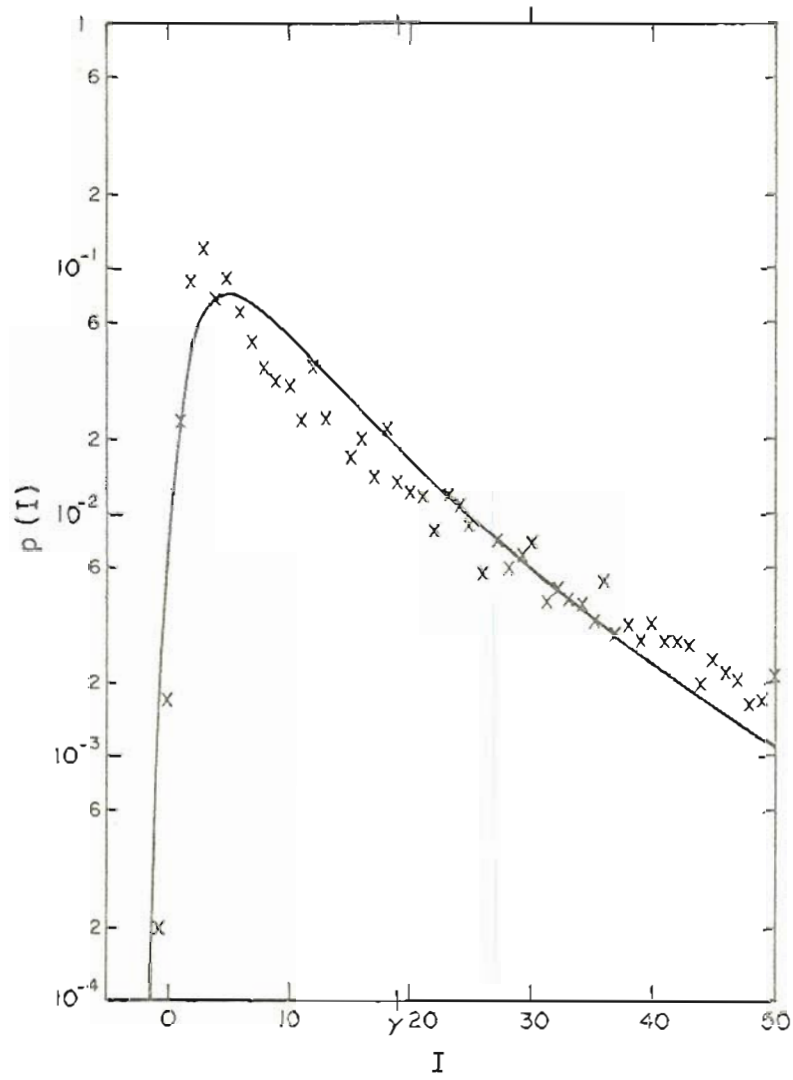

Fig. 5.13. Same as Fig. 5.3 with $\sigma_\chi = 0.8$, $D/r_o = 0.5$, and $\gamma = 19$.

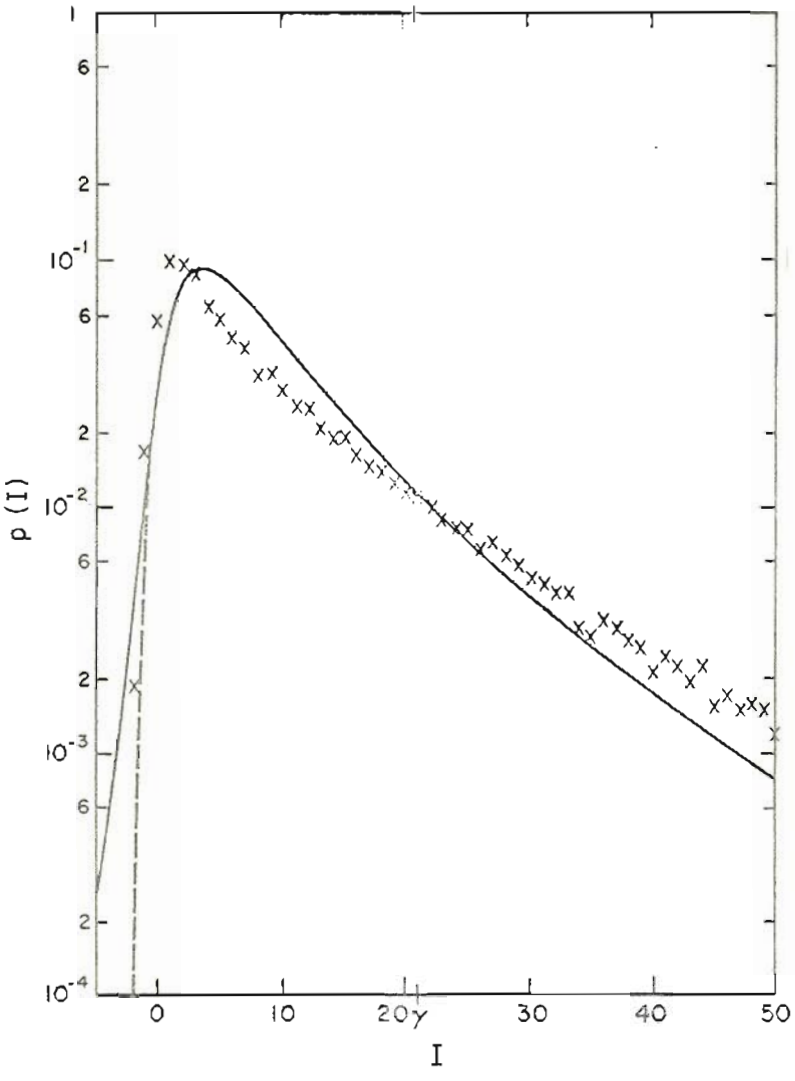

Fig. 5.14. Same as Fig. 5.3 with σ_χ = 0.8, D/r_o = 1.0, and γ = 21.

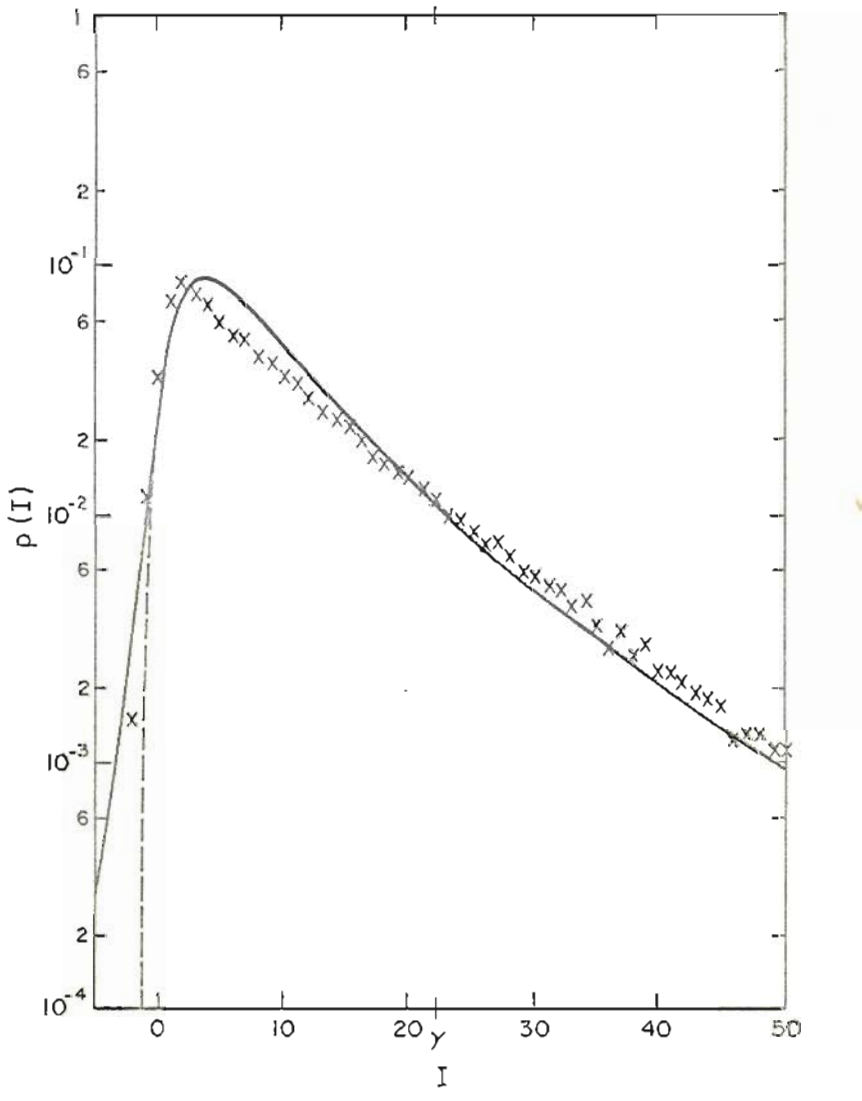

Fig. 5.15. Same as Fig. 5.3 with $\sigma_\chi = 0.8$, $D/r_o = 1.0$, and $\gamma = 22$.

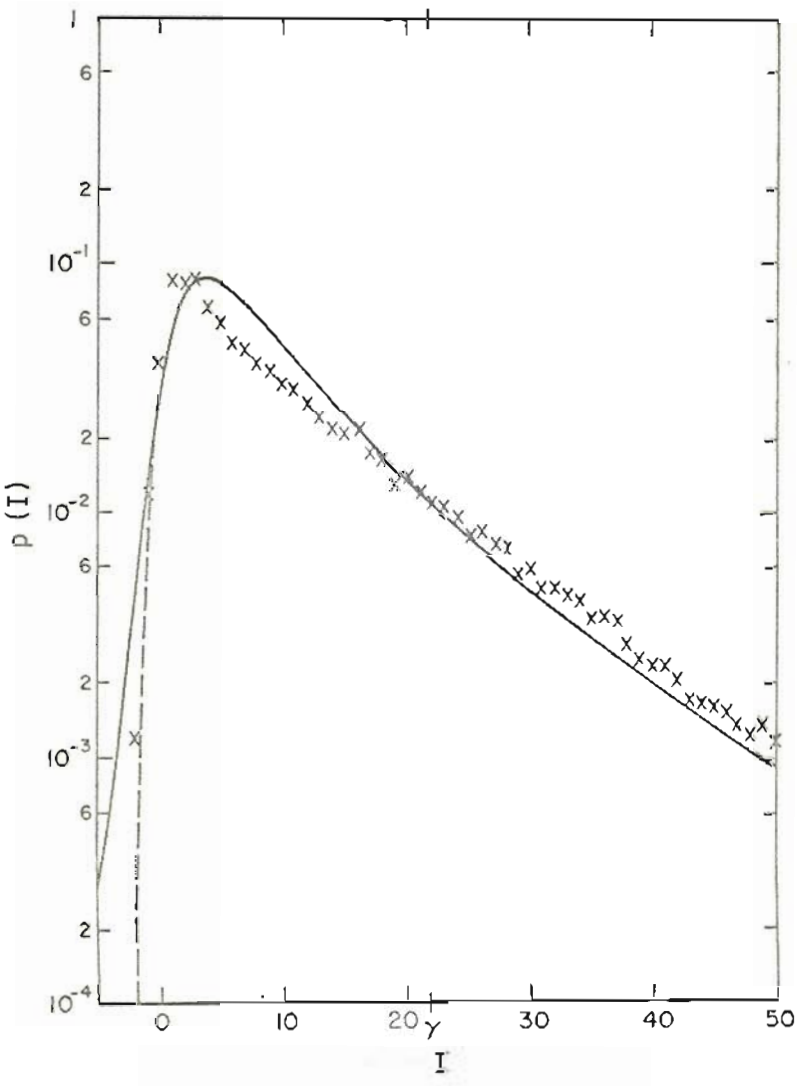

Fig. 5.16. Same as Fig. 5.3 with $\sigma_\chi = 0.8$, $D/r_o = 1.0$, and $\gamma = 22$.

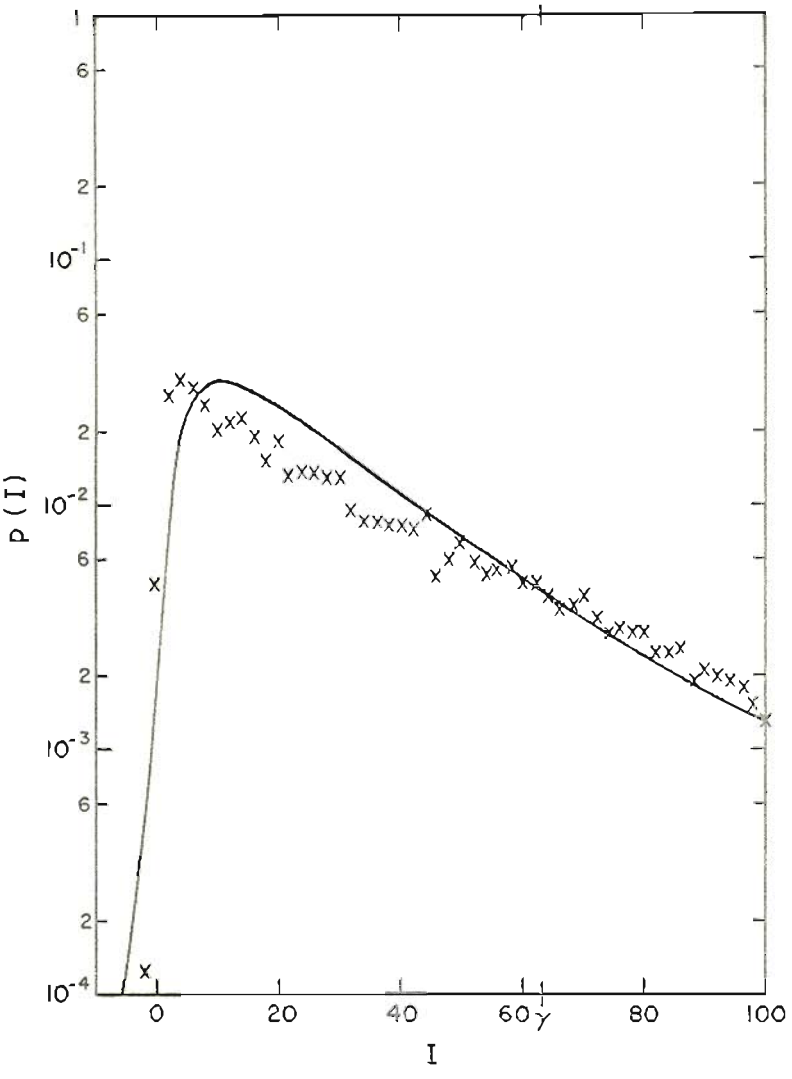

Fig. 5.17. Same as Fig. 5.3 with σ_χ = 0.8, D/r_o = 0.8, and γ = 63.

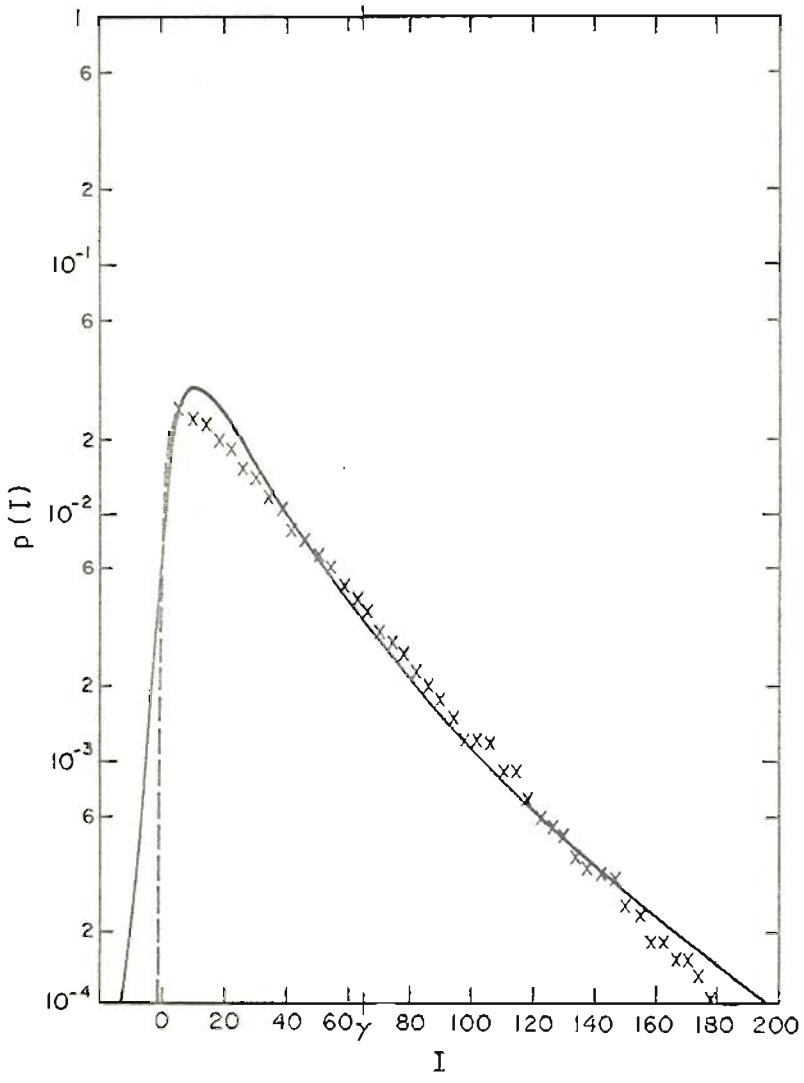

Fig. 5.18. Same as Fig. 5.3 with σ_χ = .08, D/r_o = 1.0, and γ = 65.

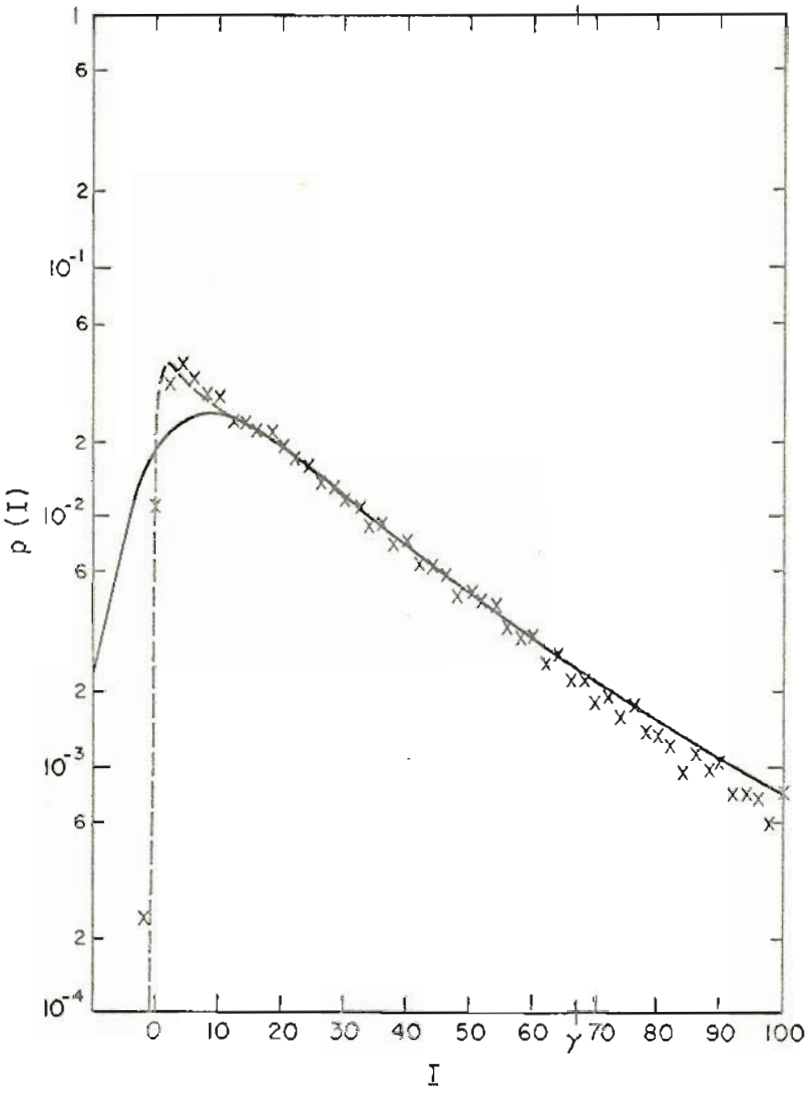

Fig. 5.19. Same as Fig. 5.3 with $\sigma_\chi = 0.8$, $D/r_o = 1.5$, and $\gamma = 67$.

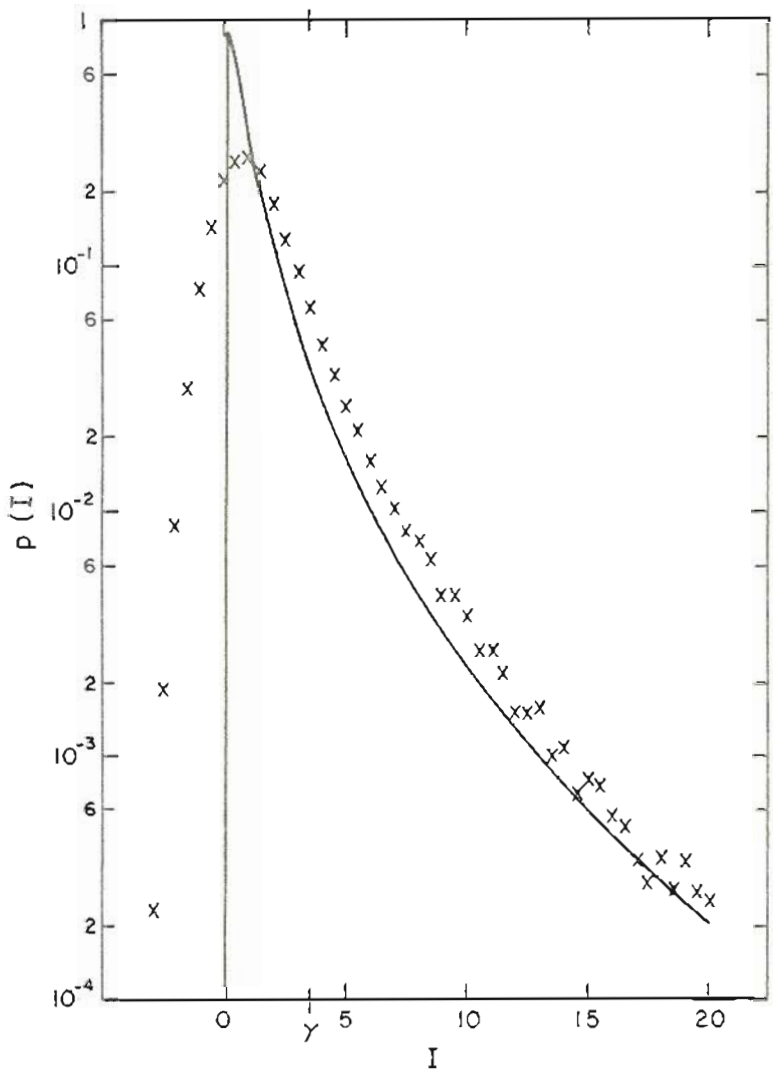

Fig. 5.20. Plot of probability density function p(I) vs. signal current I. Experimental points (X) for case with σ_χ = 0.8, D/r_o = 1.2, and γ = 3.4 are compared to log-normal distribution (line) with $\mu_{\ln I}$ = 0.26 and $\sigma_{\ln I}^2$ = 1.2.

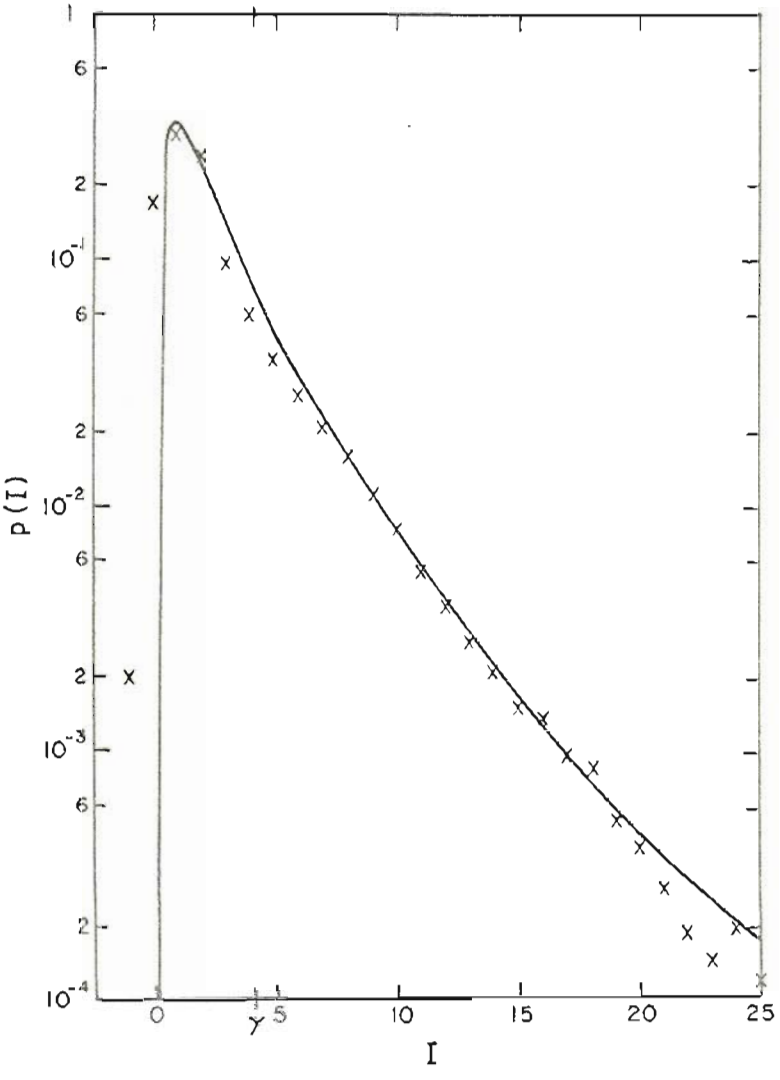

Fig. 5.21. Same as Fig. 5.20 with $\sigma_\chi = 0.8$, $D/r_o = 0.4$. $\gamma = 4.1$, $\mu_{\ln I} = 0.64$, and $\sigma^2_{\ln I} = 0.71$.

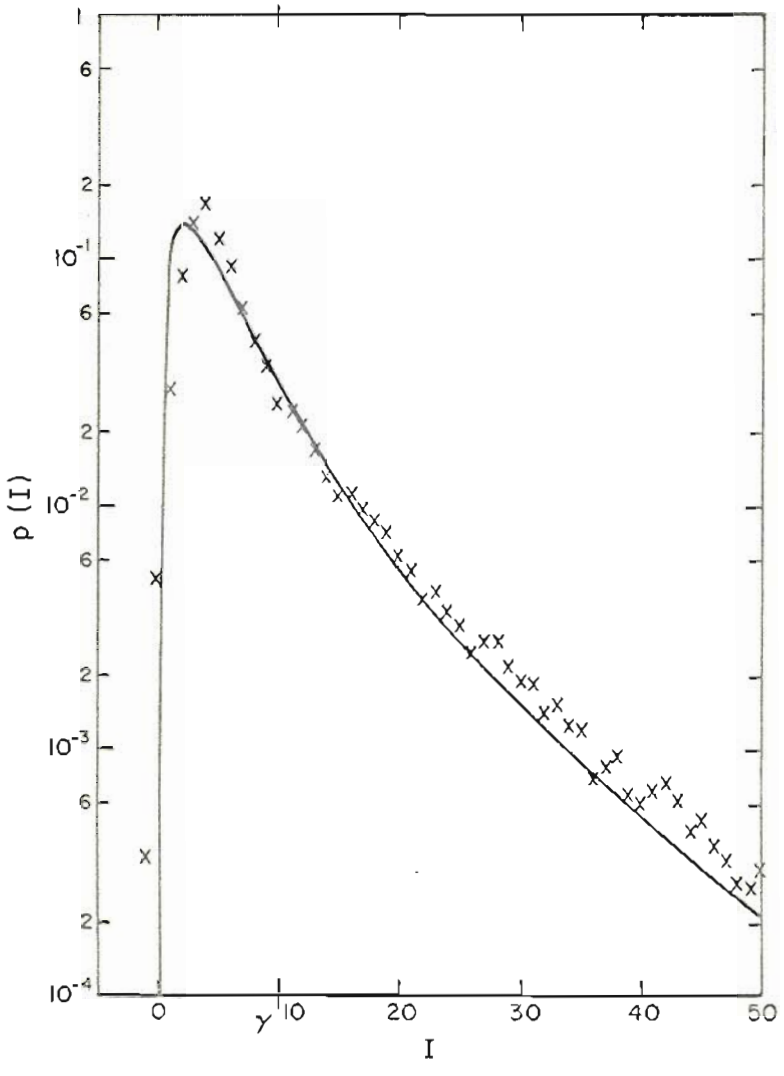

Fig. 5.22. Same as Fig. 5.20 with $\sigma_\chi = 0.8$, $D/r_o = 0.15$, $\gamma = 10$, $\mu_{\ln I} = 1.5$, and $\sigma_{\ln I}^2 = 0.74$.

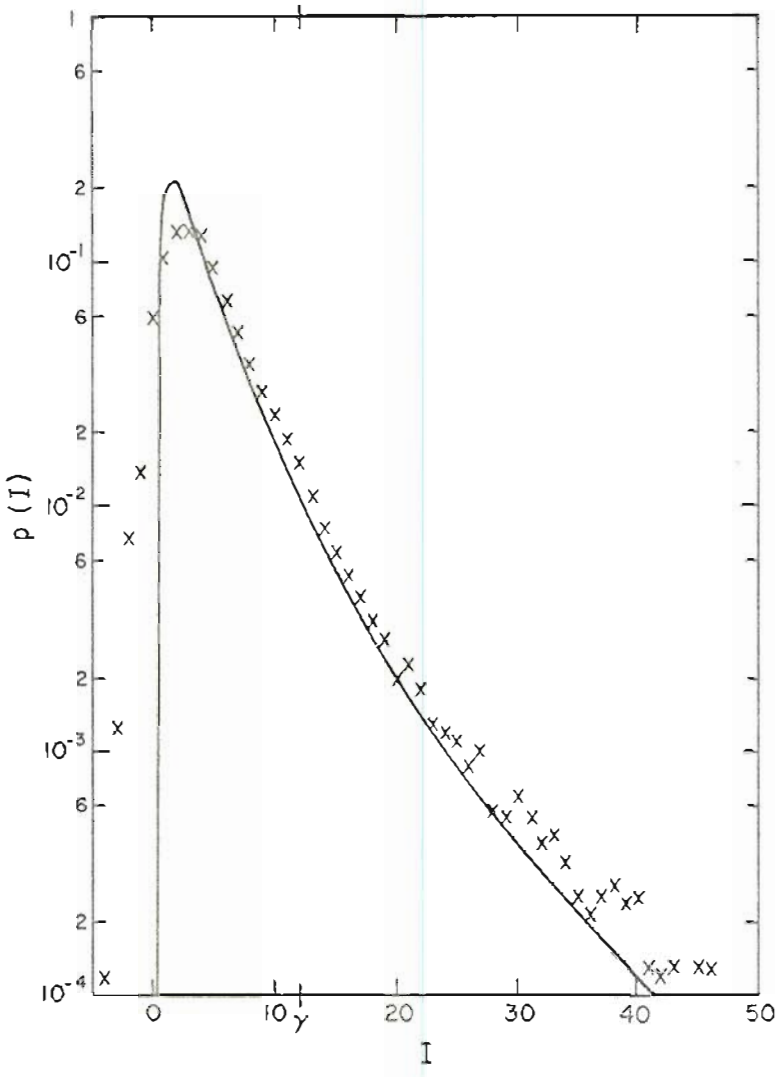

Fig. 5.23. Same as Fig. 5.20 with $\sigma_\chi = 0.8$, $D/r_o = 1.3$, $\gamma = 12$, $\mu_{\ln I} = 1.1$, and $\sigma_{\ln I}^2 = 0.71$.

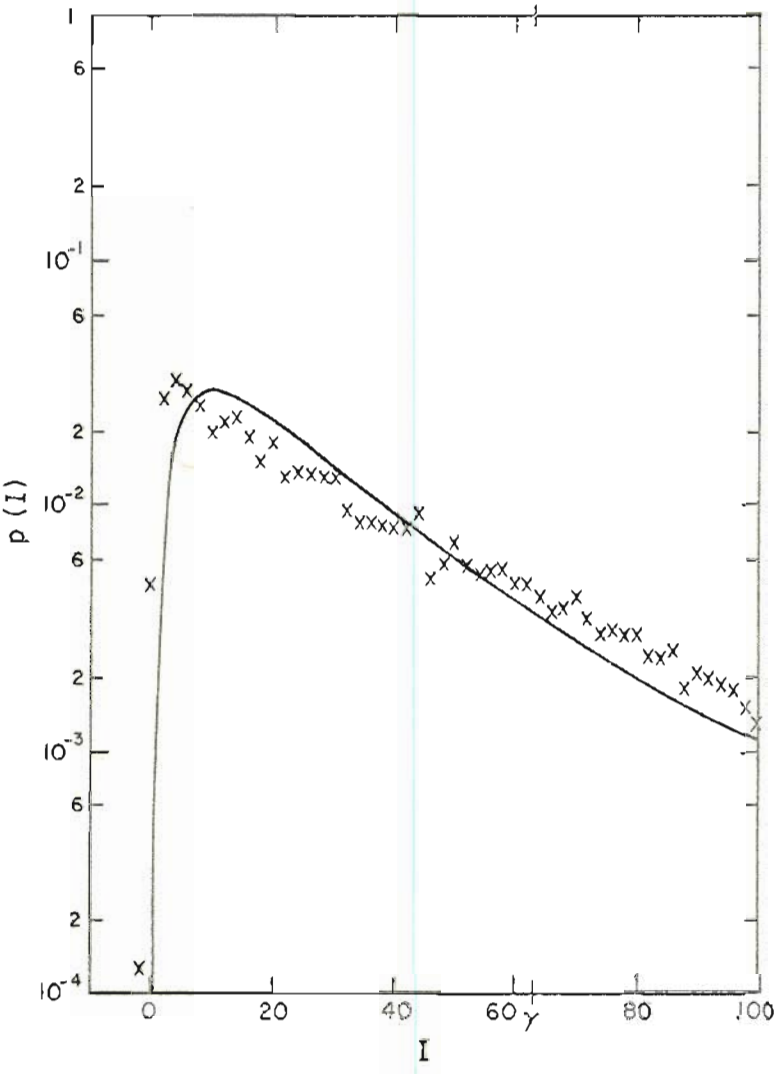

Fig. 5.24. Same as Fig. 5.20 with $\sigma_\chi = 0.8$, $D/r_o = 0.8$, $\gamma = 63$, $\mu_{\ln I} = 3.1$, and $\sigma_{\ln I}^2 = 0.82$.

that the data does not have a pure log-normal distribution. In addition, σ_I^2 is always larger than the saturation value of 0.64 that one would expect for amplitude fading only. One can conclude, therefore, that log-normal amplitude fading is not the only source of signal fluctuations.

At the same time one finds that the log-normal approximation is instructive qualitatively. For small γ and large D/r_o, as in Fig. 5.20, the data is obviously not log-normal. In the other cases, however, and especially in Figs. 5.21 and 5.22 where D/r_o is small, the fit is much better. This suggests that, at least in saturation, amplitude fluctuations are the major source of total signal fluctuations. Care should be exercised in drawing this conclusion, however, since the angle-of-arrival fluctuations are Rayleigh distributed and, qualitatively at least, the Rayleigh and log-normal distributions can be very similar.

6. N-FOLD PROBABILITY DISTRIBUTION OF AN OPTICAL HETERODYNE RECEIVER ARRAY IN THE TURBULENT ATMOSPHERE

I. INTRODUCTION

In Chapter 4 an approximate expression was derived for the probability density function of the IF signal magnitude from an optical heterodyne detector operating in the clear air turbulent atmosphere. The effects of local oscillator intensity induced shot noise, log-normal amplitude fluctuations, and Gaussian phase front perturbations were considered. Using a steepest descents approximation to the convolution integral containing these three processes, expressions were derived for heterodyne receivers incorporating active tracking systems to negate the effects of random tilting of the incoming signal wavefront and also for receivers without this feature.

In Chapter 5 experimental results were presented for the case of the non-tracking, or static, receiver. The amplitude demodulated signal was recorded from a receiver that was used to detect a .633 μ signal after propagation through 1.6 km of the open atmosphere. Simultaneous measurement of meteorological parameters allowed comparison of theory and experiment.

In this chapter the results of the last two chapters are extended to include the joint probability density function of the IF signal magnitudes from an array of N detectors with arbitrarily correlated amplitude fading and phase front perturbations. Both theoretical and experimental results are presented for the static receiver case. The tracking receiver is not treated in this work. The channel model and experimental

configuration are essentially extensions of those used in the previous work, and the necessary modifications are presented as needed.

The general N-fold probability density function is presented in Section 6.II and one finds that for arrays of more than a few elements the result is a rather complex expression. Section 6.III treats the specific case of a two element array in some detail. It is seen here that the distribution of large signals is influenced primarily by the amount of amplitude correlation, while small signal levels are more sensitive to the amount of correlation between the phase front tilts. Experimental results, discussed in Section 6.IV demonstrate the applicability of the theoretical approximation to actual system performance for N equal to two.

II. GENERAL THEORY

The first effect to consider is atmospheric fading of the received signal amplitude. Let Z_i, the normalized fading parameter for the i'th detector, be defined as the instantaneous signal amplitude at that detector divided by the amplitude that would be present in the absence of turbulence. This can then be used to define X_i as $\ln Z_i + C_{\chi ii}$, where $C_{\chi ii}$ is the i'th diagonal element of the log-amplitude covariance matrix C_χ, and is, therefore, the log-amplitude variance at the i'th detector. The N-dimensional column vector $\vec{X}$, then, is a jointly Gaussian random vector[3, 6, 35] with probability density function.

$$p(\vec{X}) = (2\pi)^{-N/2} |C_\chi|^{-\frac{1}{2}} \exp(-\frac{1}{2} \vec{X}^t C_\chi^{-1} \vec{X}) \qquad (1)$$

The second atmospheric effect is a random perturbation of the incoming signal wavefront. If the aperture diameter D is on the order of r_o or less, where r_o is a measure of the coherence diameter of the received signal, this perturbation is well approximated by considering the average tilt of the incoming wavefront across D.[3] A random vector $\vec{\Delta}$ is, therefore, defined with Δ_i proportional to the magnitude of the tilt at the i'th detector. Because of this relationship to the angle-of-arrival of the signal, resolving each Δ_i into its x- and y-direction components in the detector plane yields two jointly Gaussian random vectors[3,4] with density functions

$$p(\vec{\Delta}_x) = (2\pi)^{-N/2} |C_{\Delta x}|^{-\frac{1}{2}} \exp(-\tfrac{1}{2} \vec{\Delta}_x^{\dagger} C_{\Delta x}^{-1} \vec{\Delta}_x) \tag{2a}$$

$$p(\vec{\Delta}_y) = (2\pi)^{-N/2} |C_{\Delta y}|^{-\frac{1}{2}} \exp(-\tfrac{1}{2} \vec{\Delta}_y^{\dagger} C_{\Delta y}^{-1} \vec{\Delta}_y) \tag{2b}$$

where the column vectors $\vec{\Delta}_x$ and $\vec{\Delta}_y$ have covariance matrices $C_{\Delta x}$ and $C_{\Delta y}$, respectively. Since $\Delta_i^2 = \Delta_{xi}^2 + \Delta_{yi}^2$ and since, assuming an isotropic atmosphere, $C_{\Delta xii}^{-1} = C_{\Delta yii}^{-1}$, this leads to

$$p(\vec{\Delta}) = |C_{\Delta x}|^{-\frac{1}{2}} |C_{\Delta y}|^{-\frac{1}{2}} \prod_{i=1}^{N} \left[\Delta_i \exp(-\tfrac{1}{2} C_{\Delta xii}^{-1} \Delta_i^2) \right] G_N(\vec{\Delta}) \tag{3}$$

where the effects of non-zero correlation coefficients are contained in the function $G_N(\vec{\Delta})$. The derivation and properties of this function are left to Appendix F.

The final source of signal current fluctuations is in the detection process itself. In a well designed system the local oscillator intensity will be large enough that the shot noise associated with it is the predominate source of detector noise[10,11,18] and is, moreover, approximately

Gaussian. For simplicity, the variance of the shot noise will be assumed to be one; all signal currents are scaled accordingly. To the shot noise at each detector is added the rms current due to the optical signal at that detector. At the i'th detector, this is given by $2\gamma_i Z_i |J_1(\Delta_i)/\Delta_i|$, where γ_i is the rms signal current that would be present in the absence of turbulence and J_1 is the first order Bessel function. In the development that follows, however, the absolute value bars around $J_1(\Delta_i)$ will be dropped. The range of validity of this approximation and an estimate of the magnitude of the resulting error outside of that range have been discussed in Chapters 4 and 5. The signal current vector $\vec{I}$, then has the conditional density function approximately given by

$$p(\vec{I}|\vec{X}, \vec{\Delta}) = (2\pi)^{-N/2} \exp\left[-\tfrac{1}{2} \sum_{i=1}^{N} (I_i - 2\gamma_i Z_i J_1(\Delta_i)/\Delta_i)\right]^2 \tag{4}$$

Using the independence of $\vec{X}$ and $\vec{\Delta}$, $p(\vec{I})$ can be expressed as the following 2N-fold integral:

$$p(\vec{I}) = \int d\vec{X} \int d\vec{\Delta}\; p(\vec{I}|\vec{X},\vec{\Delta})\; p(\vec{X})\; p(\vec{\Delta}) \tag{5}$$

which can be approximated using the method of steepest descents.

First the function $f(\vec{X},\vec{\Delta})$ is defined by

$$f(\vec{X},\vec{\Delta}) = -\tfrac{1}{2} \sum_{i=1}^{N} (I_i - 2\gamma_i Z_i J_1(\Delta_i)/\Delta_i)^2 - \tfrac{1}{2} \vec{X}^{\dagger} C_X^{-1} \vec{X} \tag{6}$$

$$+ \sum_{i=1}^{N} (\ln\Delta_i - \tfrac{1}{2} C_{\Delta xii}^{-1} \Delta_i^2) + \ln G_N(\vec{\Delta})$$

The stationary points $\vec{X}_o$ and $\vec{\Delta}_o$ are then found from the 2N coupled equations

$$\left(\frac{\partial f}{\partial X_i}\right)\Big|_{\vec{X}_o,\ \vec{\Delta}_o} = 0$$

$$\left(\frac{\partial f}{\partial \Delta_i}\right)\Big|_{\vec{X}_o,\ \vec{\Delta}_o} = 0 \qquad i = 1, 2, \ldots N \tag{7}$$

and the matrix B is defined by

$$B = \left(\begin{array}{ccccccc} \frac{\partial^2 f}{\partial X_1^2} & \cdots & \frac{\partial^2 f}{\partial X_1 \partial X_N} & \frac{\partial^2 f}{\partial X_1 \partial \Delta_1} & \cdots & \frac{\partial^2 f}{\partial X_1 \partial \Delta_N} \\ \vdots & & \vdots & \vdots & & \vdots \\ \frac{\partial^2 f}{\partial X_1 \partial X_N} & \cdots & \frac{\partial^2 f}{\partial X_N^2} & \frac{\partial^2 f}{\partial X_N \partial \Delta_1} & \cdots & \frac{\partial^2 f}{\partial X_N \partial \Delta_N} \\ \frac{\partial^2 f}{\partial X_1 \partial \Delta_1} & \cdots & \frac{\partial^2 f}{\partial X_N \partial \Delta_1} & \frac{\partial^2 f}{\partial \Delta_1^2} & \cdots & \frac{\partial^2 f}{\partial \Delta_1 \partial \Delta_N} \\ \vdots & & \vdots & \vdots & & \vdots \\ \frac{\partial^2 f}{\partial X_1 \partial \Delta_N} & \cdots & \frac{\partial^2 f}{\partial X_N \partial \Delta_N} & \frac{\partial^2 f}{\partial \Delta_1 \partial \Delta_N} & \cdots & \frac{\partial^2 f}{\partial \Delta_N^2} \end{array} \right)_{\substack{\vec{X} = \vec{X}_o \\ \vec{\Delta} = \vec{\Delta}_o}} \tag{8}$$

These definitions lead directly to the result[36] that

$$p(\vec{I}) \approx |C_X|^{-\frac{1}{2}} \, |C_{\Delta_x}|^{-\frac{1}{2}} \, |C_{\Delta_y}|^{-\frac{1}{2}} \, |-B|^{-\frac{1}{2}} \exp[f(\vec{X}_o, \vec{\Delta}_o)] \tag{9}$$

III. N = 2

In the special case of a two detector array, an analytical expression can be found for $p(\vec{\Delta})$. Since, in addition, this case lends itself to graphical presentation, it is worth considering in some detail.

Note first that the log-amplitude covariance matrix matrix can be expressed as

$$C_\chi = \sigma_\chi^2 \begin{pmatrix} 1 & r_\chi \\ r_\chi & 1 \end{pmatrix} \tag{10}$$

Details of the calculation of the normalized log-amplitude variance, σ_χ^2, and correlation coefficient, r_χ, have been presented elsewhere,[3,4,32] and will not be repeated here. In a similar manner the assumptions leading to Eq. (F5) allow the substitution

$$C_{\Delta_\chi} = C_{\Delta_y} = \sigma_\Delta^2 \begin{pmatrix} 1 & r_\Delta \\ r_\Delta & 1 \end{pmatrix} \tag{11}$$

where expressions for the phase parameter variance, σ_Δ^2, and correlation coefficient, r_Δ, are presented in Appendix G.

Using these substitutions and Eq. (G5), the function f becomes

$$f(\vec{X},\vec{\Delta}) = -\tfrac{1}{2}\,(I_1 - 2\gamma_1 Z_1 J_1(\Delta_1)/\Delta_1)^2 - \tfrac{1}{2}\,(I_2 - 2\gamma_2 Z_2 J_1(\Delta_2)/\Delta_2)^2$$

$$- \frac{1}{2\sigma_\chi^2 (1-r_\chi^2)} (X_1^2 - 2r_\chi X_1 X_2 + X_2^2) - \frac{1}{2\sigma_\Delta^2 (1-r_\Delta^2)} (\Delta_1^2 + \Delta_2^2)$$

$$+ \ln \left[\Delta_1 \Delta_2 I_o\left(\frac{r_\Delta \Delta_1 \Delta_2}{\sigma_\Delta^2 (1-r_\Delta^2)}\right)\right] \tag{12}$$

The stationary points $(\vec{X}_o, \vec{\Delta}_o)$ are found from the four coupled equations

$$\left(\frac{\partial f}{\partial X_1}\right) \Big| (\vec{X}_o, \vec{\Delta}_o) = \left(\frac{\partial f}{\partial X_2}\right) \Big| (\vec{X}_o, \vec{\Delta}_o) = \left(\frac{\partial f}{\partial \Delta_1}\right) \Big| (\vec{X}_o, \vec{\Delta}_o)$$

$$= \left(\frac{\partial f}{\partial \Delta_2}\right) \Big| (\vec{X}_o, \vec{\Delta}_o) = 0 \tag{13}$$

where

$$\frac{\partial f}{\partial X_i} = (I_i - 2\gamma_i Z_i J_1(\Delta_i)/\Delta_i)\, 2\gamma_i Z_i J_1(\Delta_i)/\Delta_i$$

$$- \frac{1}{\sigma_\chi^2 (1-r_\chi^2)} (X_i - r_\chi X_j)$$

$$\frac{\partial f}{\partial \Delta_i} = (I_i - 2\gamma_i Z_i J_1(\Delta_i)/\Delta_i)\, 2\gamma_i Z_i (J_o(\Delta_i) - 2 J_1(\Delta_i)/\Delta_i)/\Delta_i$$

$$- \frac{\Delta_i}{\sigma\Delta^2 (1-r_\Delta^2)} + \frac{1}{\Delta_i} + \frac{r_\Delta \Delta_j}{\sigma\Delta^2 (1-r_\Delta^2)} I_1\left[\frac{r_\Delta \Delta_i \Delta_j}{\sigma\Delta^2 (1-r_\Delta^2)}\right] / I_o\left[\frac{r_\Delta \Delta_i \Delta_j}{\sigma\Delta^2 (1-r_\Delta^2)}\right]$$

$$(i,j) = (1,2),\ (2,1) \tag{14}$$

where J_o and I_1 are the zero order Bessel function and first order modified Bessel function, respectively. With the solutions of Eq. (13), it is straightforward to find

$$p(I_1, I_2) = \exp\left[f(\vec{X}_o, \vec{\Delta}_o)\right] / \sigma_\Delta^4 (1-r_\Delta^2) \sigma_\chi^2 (1-r_\chi^2)^{\frac{1}{2}} |-B|^{\frac{1}{2}} \tag{15}$$

The results of Eq. (15) are presented graphically in Figures 6.1 through 6.4. In order to show the effects of varying the correlation coefficients, all other parameters are constant from figure to figure; in particular, $\gamma_1 = \gamma_2 = 10$, $\sigma_\chi = 0.8$, and $D/r_o = 1$. Another feature of the graphs that should be mentioned is that any calculated value that turned out to be less than 10^{-6} was arbitrarily set equal to 10^{-6}. This was

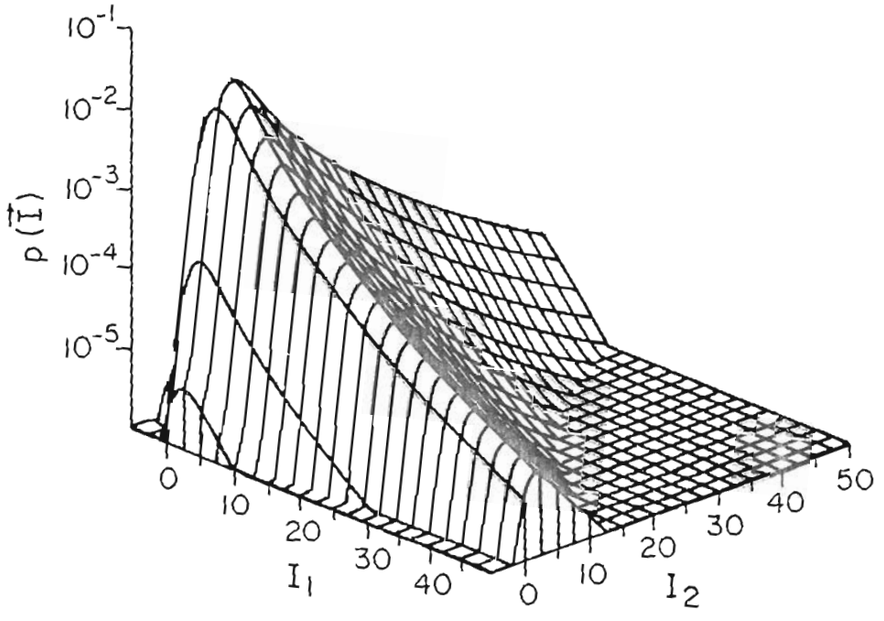

Fig. 6.1a: Plot of probability distribution $p(\vec{I})$ vs. signal current vector (I_1, I_2) for $\gamma_1 = \gamma_2 = 10$, $\sigma_\chi = 0.8$, $D/r_o = 1$, and $r_\chi = r_\Delta = 0$. Curve is truncated at $p(\vec{I}) = 10^{-6}$ for clarity.

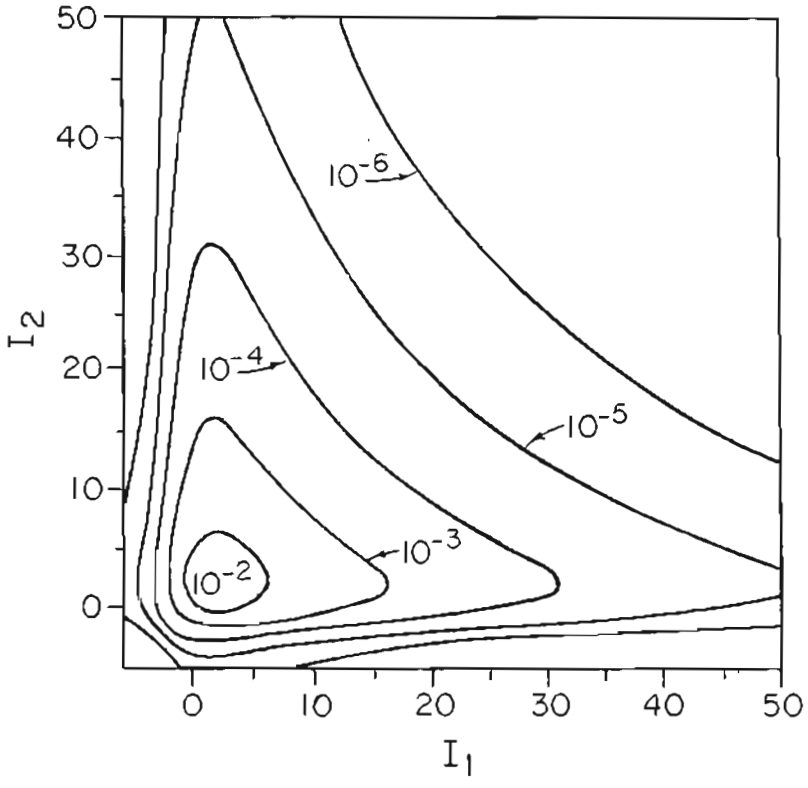

Fig. 6.1b: Contour plot of 1a.

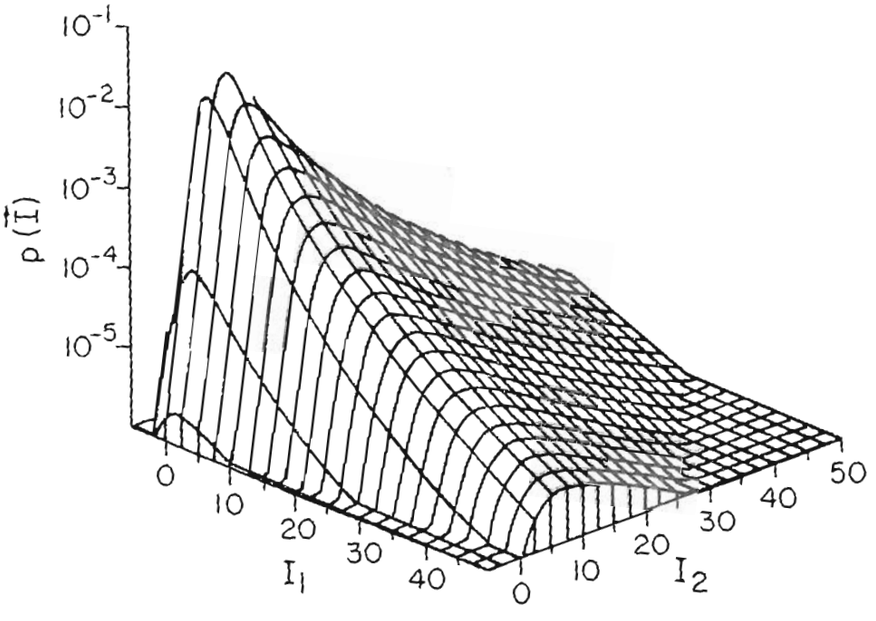

Fig. 6.2a: Same as Fig. 6.1 except that $r_\chi = r_\Delta = 0.5$.

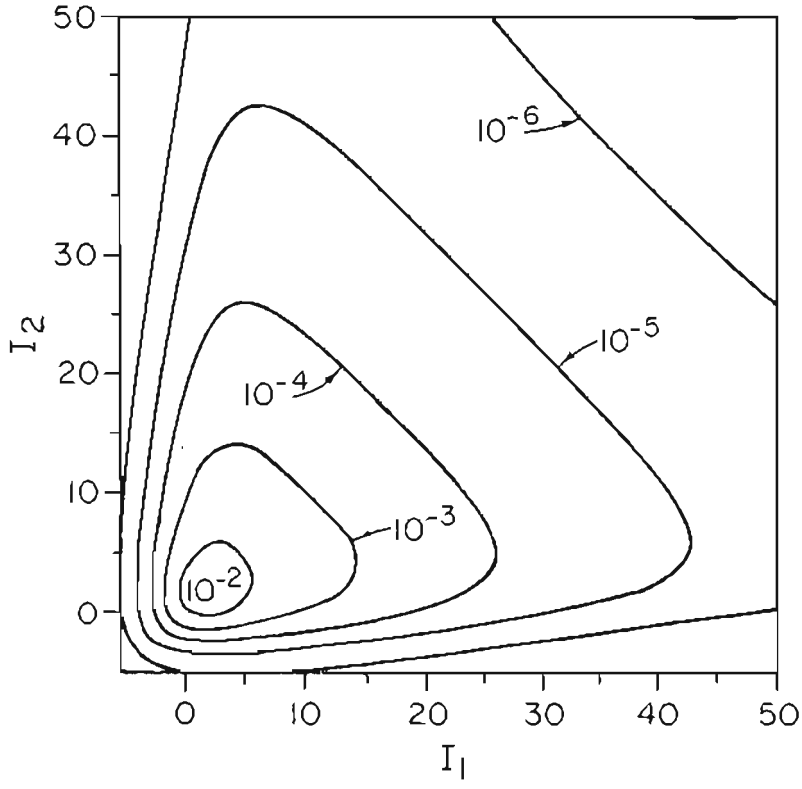

Fig. 6.2b: Contour plot of 2a.

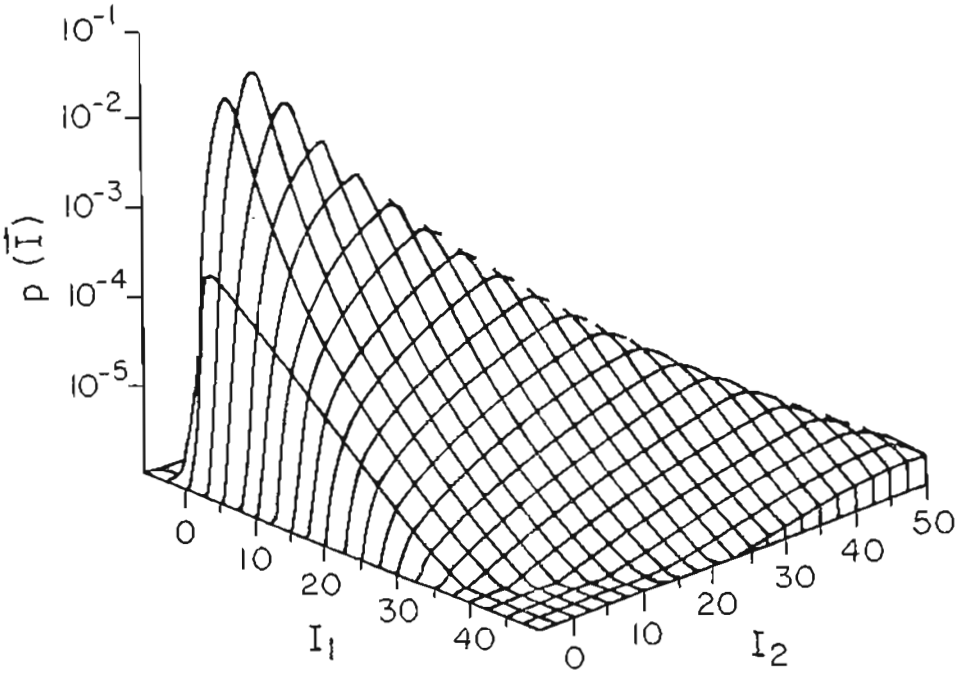

Fig. 6.3a: Same as Fig. 6.1 except that $r_\chi = 1$ and $r_\Delta = 0$.

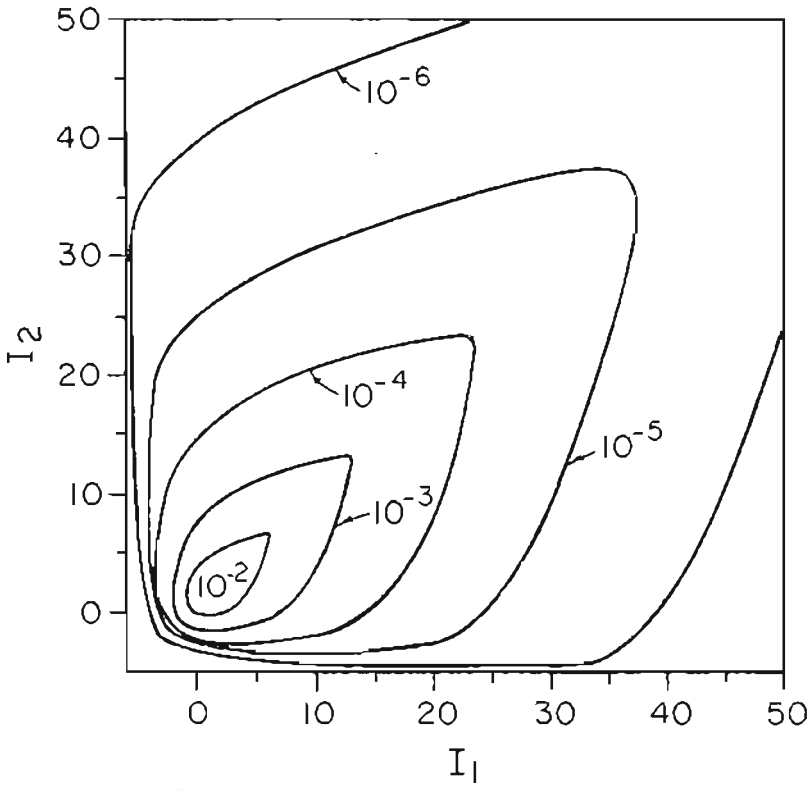

Fig. 6.3b: Contour plot of 3a.

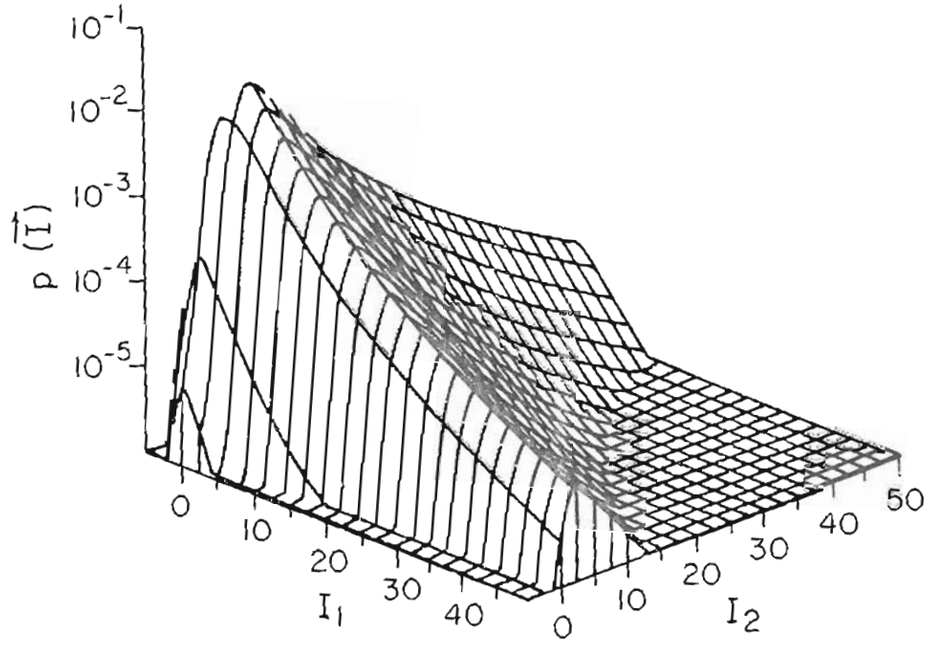

Fig. 6.4a: Same as Fig. 6.1 except that $r_\chi = 0$ and $r_\Delta = 0.711$.

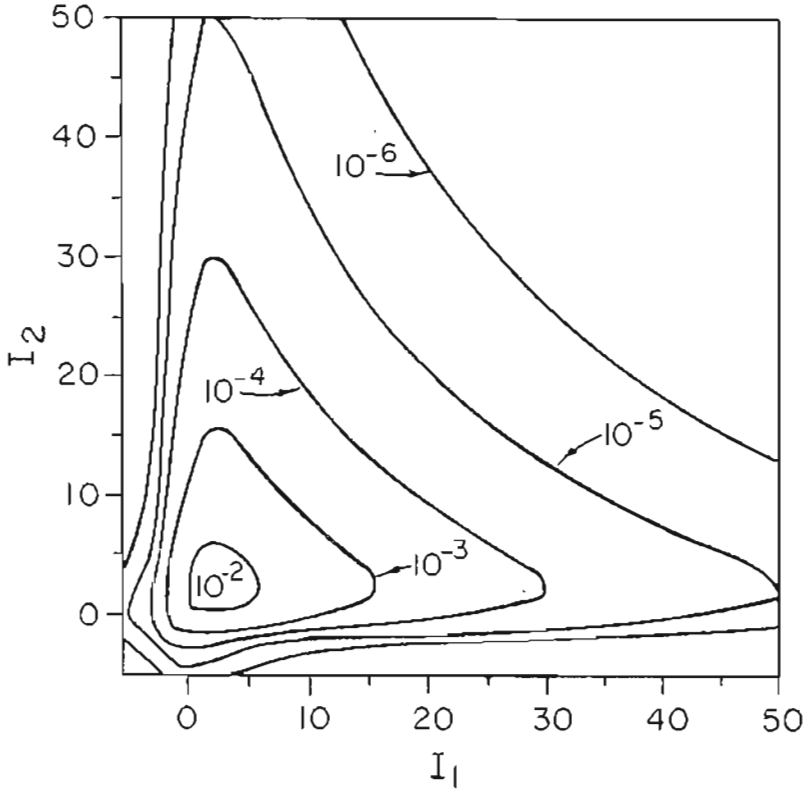

Fig. 6.4b: Contour plot of 4a.

done in order to obtain a clearer graphical representation of the function over the remaining probability range.

First, Figure 6.1 is a plot of the above case with independent fading at the two detectors ($r_\chi = r_\Delta = 0$). As one would expect from Chapter 4, this function exhibits ridges along the lines $I_1 \approx 2$ and $I_2 \approx 2$, falling off sharply from the peak along the line $I_1 = I_2$. Figure 6.2 displays partial correlation with $r_\chi = r_\Delta = \frac{1}{2}$ causing the peak probability to be shifted to a slightly lower value, and the distribution to be more tightly grouped along the line $I_1 = I_2$.

In Figures 6.3 and 6.4, the relative effects of correlated amplitude and phase fluctuations are demonstrated. The first case is for $r_\chi = 1$ and $r_\Delta = 0$, in which the distribution has a fairly sharp ridge along $I_1 = I_2$, especially where I_1 and I_2 are greater than about two. The second case is for $r_\chi = 0$ and $r_\Delta = 0.711$ which corresponds to a separation ρ equal to D and is, therefore, the maximum value allowable. While this looks at first glance very much like the case of independent fading, it actually introduces more distortion than the previous case over the range where I_1 and I_2 are less than about two. Correlated phase and amplitude fluctuations, therefore, influence the distribution of currents primarily at small and large current levels, respectively.

IV. EXPERIMENTAL RESULTS

The experimental configuration for this work is the same as that described in Chapter 5 with two basic modifications. First, three additional signal detectors were added, allowing simultaneous recording of four identical channels. The aperture centers form a square approximately 10 cm. on a side. As in Chapter 5, this is not the separation of

the physical apertures, but of their images at the front of the collecting telescope. The second modification was the addition of a chopping wheel at the transmitter and of a radio link to allow recording of the transmitter state along with the data. This was done in anticipation of bit error rate measurements and has no effect on the results presented here.

Typical experimental results are presented in Figures 6.5 and 6.7. The corresponding theoretical curves are given in Figures 6.6 and 6.8, where the parameters necessary to the theory were inferred from meteorological measurements using the same relationships as in Chapter 5. Of the two additional parameters, r_Δ was found from the results of Appendix G and r_χ was taken from the results of Clifford, et. al..[32] For the fixed detector spacing used here, r_χ was found to be esentially zero in all cases.

Agreement between theory and experiment was found to be generally very good, as demonstrated by the figures. The predicted probability peaks, however, tend to be lower, broader, and to occur at slightly higher current levels than the measured peaks. These same qualitative features are also observed for single detector cases where they are thought to arise from inaccuracies inherent in single point, thermal measurements of turbulence strength. Because of this, the major source of discrepancies between the two-dimensional theory and experiment is probably due to a consistant underestimation of turbulence strength.

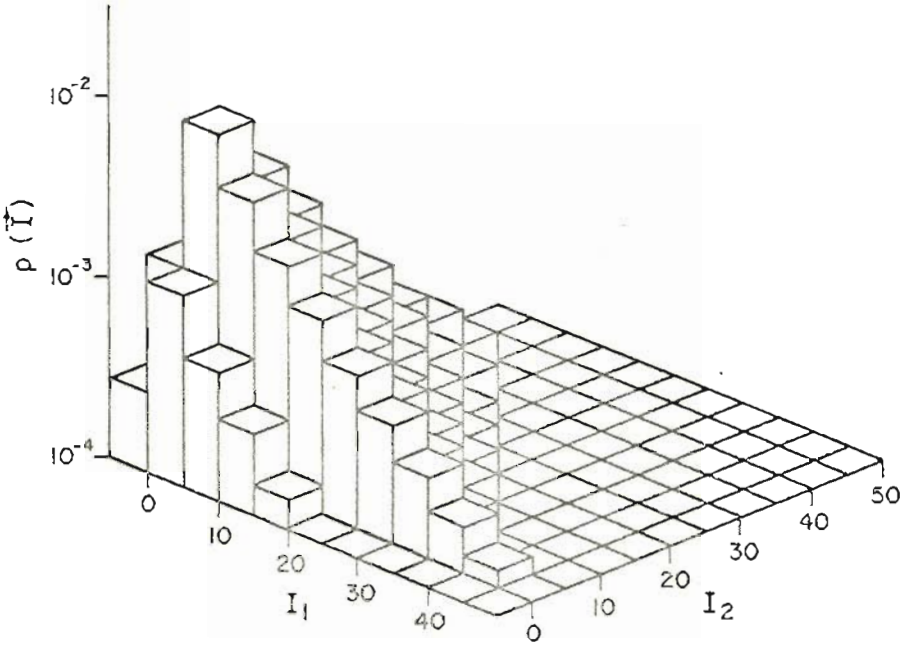

Fig. 6.5 a: Plot of experimental probability distribution $p(\vec{I})$ vs. signal current vector (I_1, I_2) for case with estimated parameters $\gamma_1 = 17$, $\gamma_2 = 16$, $\sigma_\chi = 0.8$, $D/r_o = 0.75$, $r_\chi = 0$, and $r_\Delta = 0.24$. Graph is truncated at $p(\vec{I}) = 10^{-4}$ for clarity.

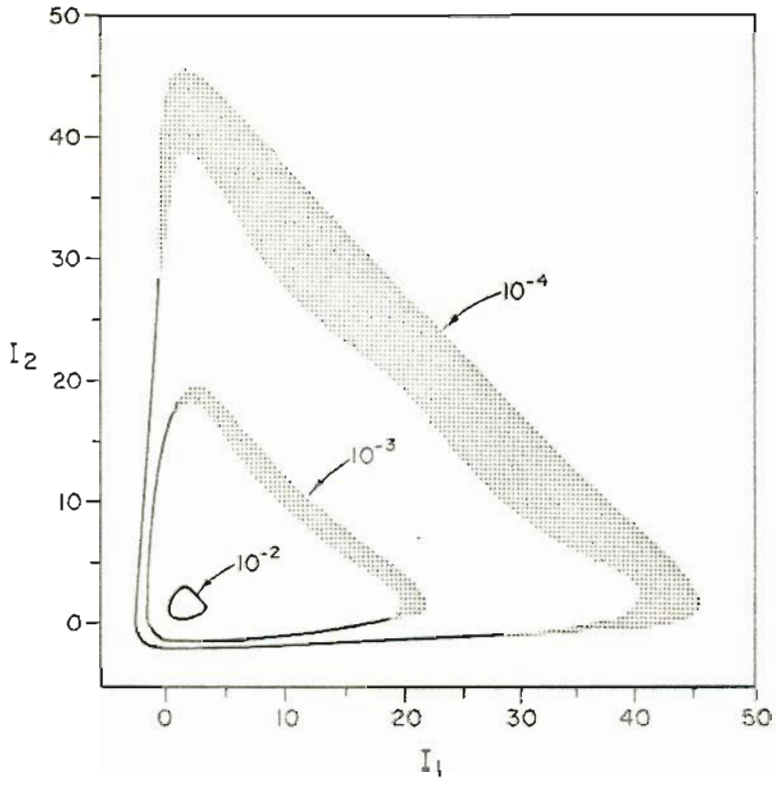

Fig. 6.5b: Contour plot of data used for 5a.

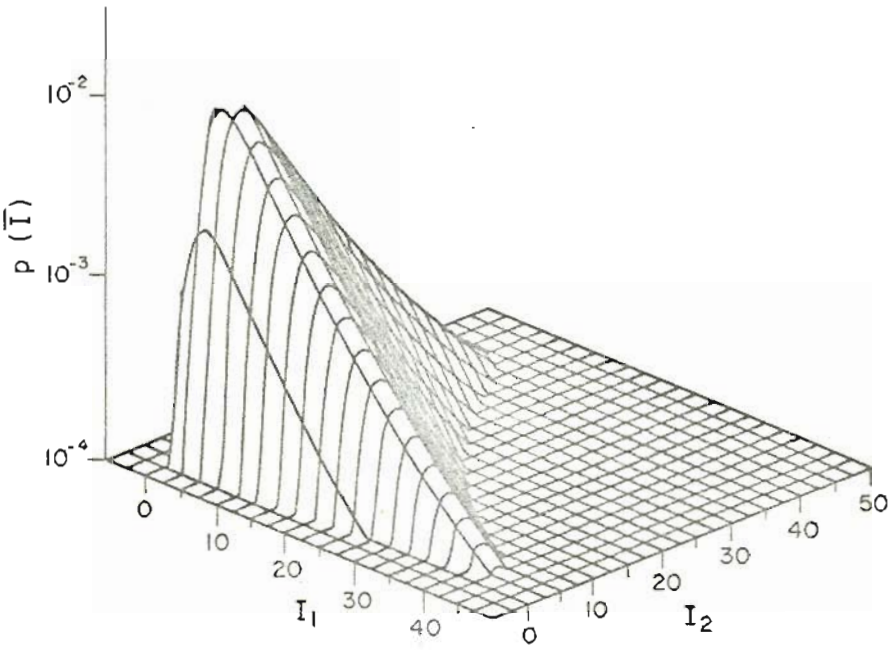

Fig. 6.6a: Plot of theoretical $p(\vec{I})$ vs. (I_1, I_2) for case of Fig. 6.5.

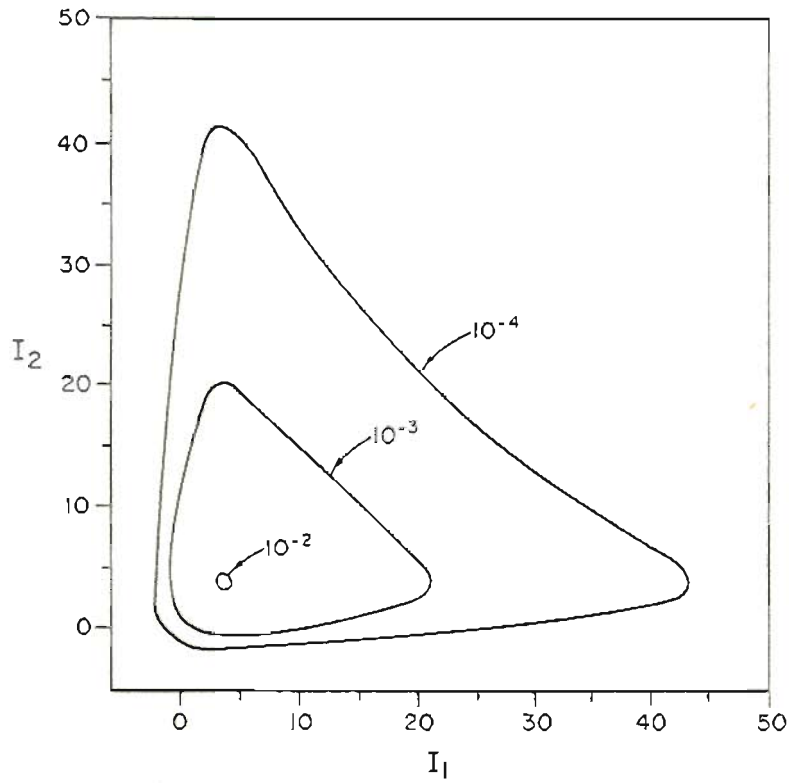

Fig. 6.6b: Contour plot of 6a.

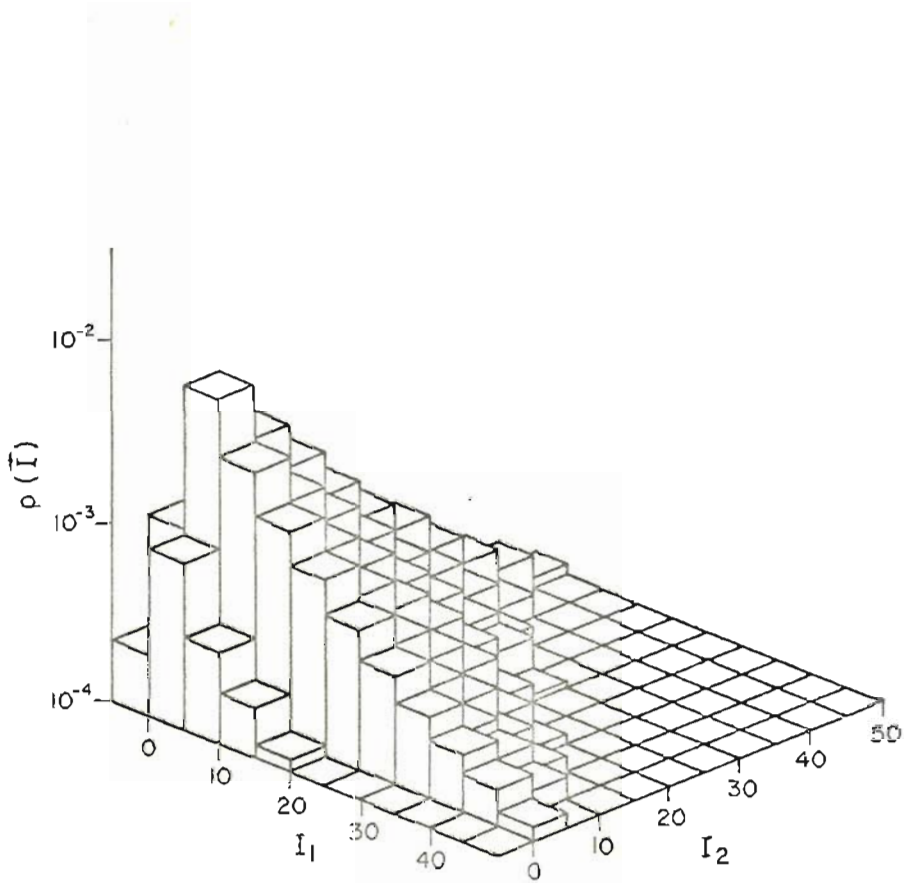

Fig. 6.7a: Same as Fig. 6.5 except that $\gamma_1 = 29$, $\gamma_2 = 28$, $\sigma_\chi = 0.8$, $D/r_o = 1$, $r_\chi = 0$, and $r_\Delta = 0.34$.

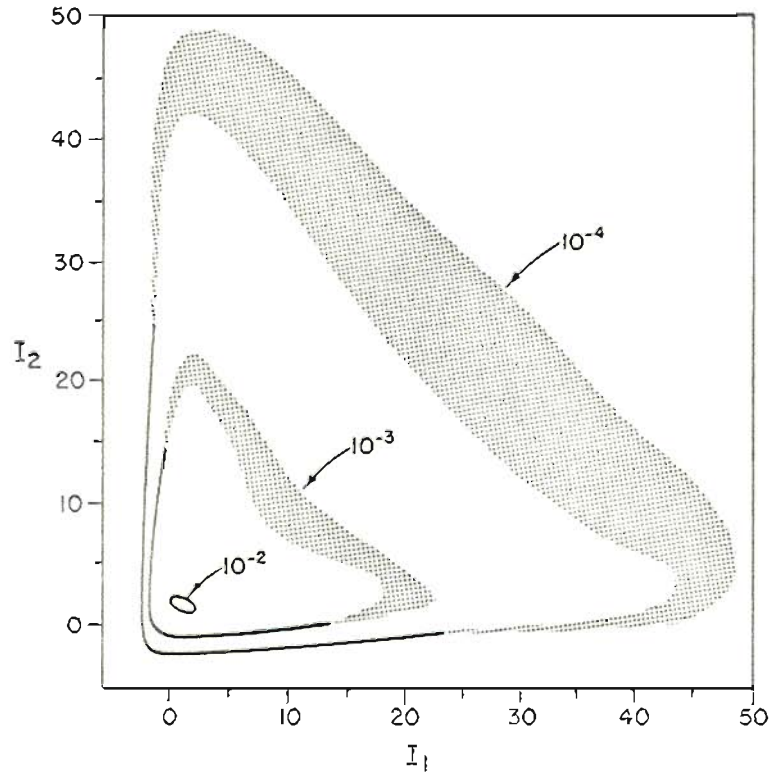

Fig. 6.7b: Contour plot of 7a.

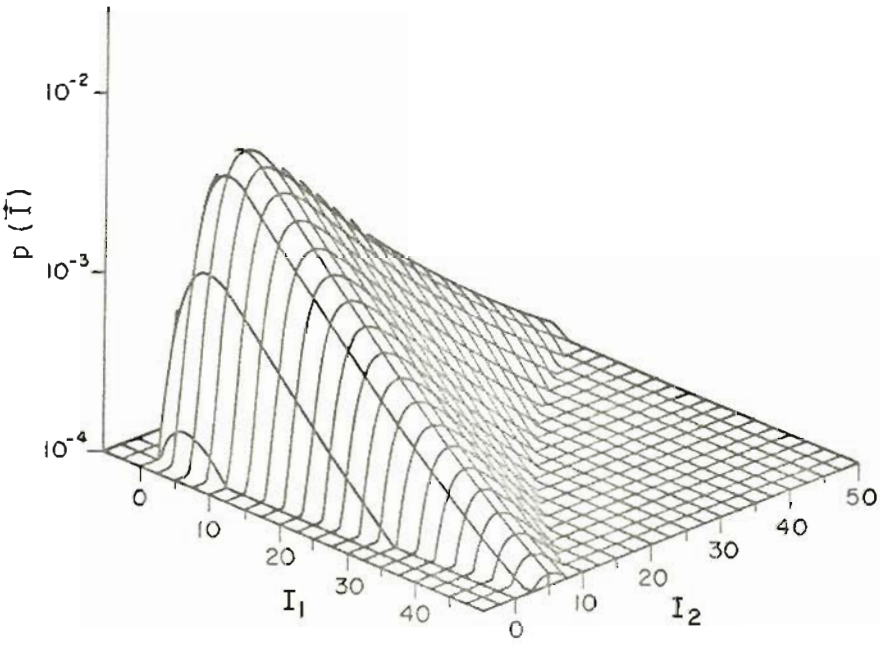

Fig. 6.8a: Plot of theoretical $p(\vec{I})$ vs. (I_1, I_2) for case of Fig. 6.7.

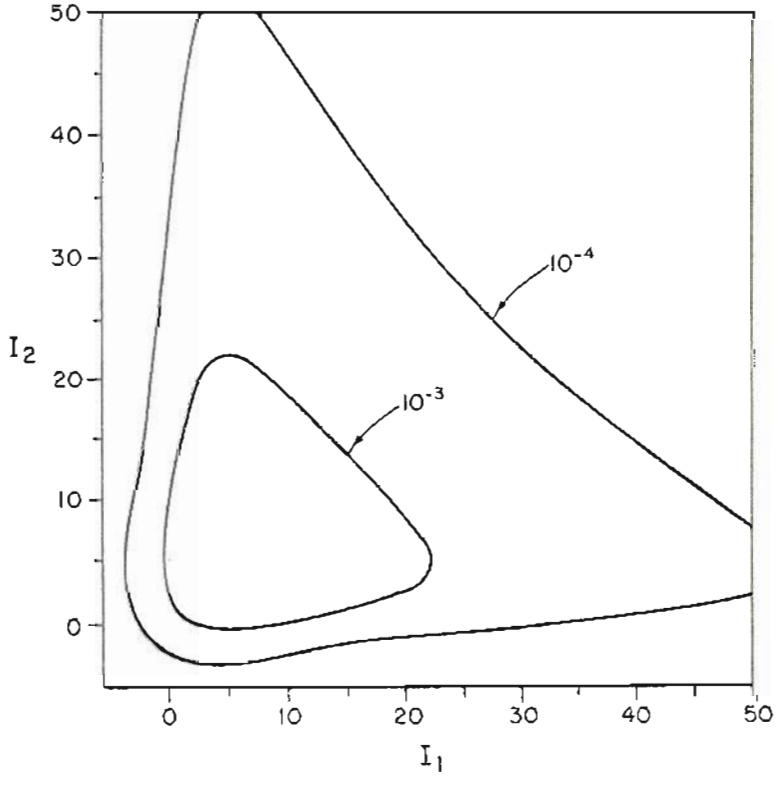

Fig. 6.8b: Contour plot of 8a.

7. SUMMARY

The focus of this work has been on optical communications through the clear-air turbulent atmosphere. Both single detector and detector array systems have been considered for photon counting receivers and also for optical heterodyne receivers. In this chapter the major conclusions that have resulted will be summarized.

In the direct detection case an averaged threshold receiver has been developed for symmetric binary, pulse-code modulated communications. In addition, a condition was derived for the number of bits that may be used in establishing the threshold. Bit error rates for this receiver were compared with those for previously developed optimum and suboptimum fixed threshold receivers for various combinations of turbulence strength, background radiation level, signal-to-noise ratio, number of diversity channels, and, in the newly developed processor, number of bits used for threshold averaging. This new receiver was seen to be a much simpler structure to implement. In addition, it was seen to result in a significantly lower bit error rate under most reasonable operating conditions.

Also introduced in this work is the concept of a partial tracking optical heterodyne array receiver. Using the average antenna gain as a measure of receiver performance, the relative effects of partial and full tilt tracking and of increased diversity on the performance of a heterodyne receiver were investigated. It was shown that the most effective method of increasing the array gain is by increasing the array size in far field applications, and by adding either partial or full tracking in near field applications. In the latter case, full tracking

results in a greater improvement, but is more difficult (and costly) to implement.

It was also noted that the expressions developed for the partial tracking heterodyne receiver could be applied directly to a problem in atmospheric imaging systems. This relationship was used to state explicity the dependence of image resolution and of the atmospheric modulation transfer function on exposure time.

The final area of investigation of this work was into the probability density function of the IF signal magnitude from an optical heterodyne receiver. Expanding the atmospherically distorted phase front in a series of othonormal polynomials across the detector aperture allowed the signal current to be found for arbitrary amplitude fading and phase front distortion. An integral expression for the probability density function including these two atmospheric effects and local oscillator shot noise was approximated using the method of steepest descents. This general approach was applied to one, two, and N detector arrays of non tracking receivers and also to single detectors with tilt tracking. Actual probability density functions were also measured on a system consisting of a HeNe laser transmitter operating at 632.8 nm, a 1.6 km propagation path through the open atmosphere, and a one or two detector, non tracking optical heterodyne receiver. The goal of this investigation was to develop a theoretical expression that is simple to evaluate, and at the same time, fairly accurately models the performance of a practical receiver configuration. Chapters 4 through 6 of this work demonstrate the realization of this goal, at least under the experimental conditions that were available.

REFERENCES

1. Aeschylus, Agamemnon, translated by Louis MacNeice, in "Ten Greek Plays," edited by L. R. Lind (The Riverside Press, Cambridge, 1957) p. 44.

2. A. Einstein, "Uber einen die Erzeugung und Verwandlung des Lichtes betreffenden heuristischen Gesichtspunkt," Ann. Physik 17, 132 - 148 (1905).

3. V. I. Tatarskii, The Effects of the Turbulent Atmosphere on Wave Propagation (Israel Program for Scientific Translations, Jerusalem, 1971).

4. R. S. Lawrence and J. W. Strohbehn, "A Survey of Clear-Air Propagation Effects Relevant to Optical Communications," Proc. IEEE 58, 1523 - 1545 (1970).

5. Paul Diament and M. C. Teich, "Photodetection of Low-Level Radiation through the Turbulent Atmosphere," J. Opt. Soc. Am. 60, 1489 - 1494 (1970).

6. M. C. Teich and S. Rosenberg, "N-Fold Joint Photocounting Distribution for Modulated Laser Radiation: Transmission Through the Turbulent Atmosphere," J. Opto-electron. 3, 63 - 76 (1971).

7. M. C. Teich and S. Rosenberg, "Photocounting Array Receivers for Optical Communication Through the Lognormal Atmospheric Channel. 1: Optimum and Suboptimum Receiver Structures," Appl. Opt. 12, 2616 - 2624 (1973).

8. S. Rosenberg and M. C. Teich, "Photocounting Array Receivers for Optical Communication Through the Lognormal Atmospheric Channel. 2: Optimum and Suboptimum Receiver Performance for Binary Signaling," Appl. Opt. 12, 2625 - 2635 (1973).

9. E. V. Hoversten, R. O. Harger, and S. J. Halme, "Communication Theory for the Turbulent Atmosphere," Proc. IEEE 58, 1626 - 1650 (1970).

10. W. K. Pratt, Laser Communications Systems (Wiley, New York, 1969), Chap. 9.

11. R. M. Gagliardi and S. Karp, Optical Communications (Wiley, New York, 1976), Chap. 5.

12. S. Karp and J. R. Clark, "Photon Counting: A Problem in Classical Noise Theory," IEEE Trans. Inform. Theory IT-16, 672 - 680 (1970).

13. D. L. Fried, G. E. Mevers, and M. P. Keister, Jr., "Measurements of Laser-Beam Scintillation in the Atmosphere," J. Opt. Soc. Am. 57, 787 - 797 (1967).

14. R. L. Mitchell, "Permanence of the Log-Normal Distribution," J. Opt. Soc. Am. 58, 1267 - 1272 (1968).

15. A. Papoulis, Probability, Random Variables, and Stochastic Processes (McGraw-Hill, New York, 1965), Chap. 16.

16. H. L. Van Trees, Detection, Estimation, and Modulation Theory (Wiley, New York, 1968), Chap. 2.

17. H. E. Slazer, R. Zucker, and R. Capuano, in "Handbook of Mathematical Functions," edited by M. Abramowitz and I. Stegun (Dover, New York, 1965), P. 924.

18. David L. Fried, "Optical Heterodyne Detection of an Atmospherically Distorted Signal Wave Front," Proc. IEEE 55, 57 - 67 (1967).

19. I. Goldstein, P. A. Miles, and A. Chabot, "Heterodyne Measurements of Light Propagation Through Atmospheric Turbulence," Proc. IEEE 53, 1172 - 1180 (1965).

20. David L. Fried, "Effects of Atmospheric Turbulence on Static and Tracking Optical Heterodyne Receivers/Average Antenna Gain and Antenna Gain Variation," Optical Science Consultants Report TR-027 (1971).

21. David M. Chase, "Power Loss in Propagation Through a Turbulent Medium for an Optical-Heterodyne System with Angle Tracking," J. Opt. Soc. Am. 56, 33 - 44 (1966).

22. David L. Fried, "Statistics of a Geometrical Representation of Wavefront Distortion," J. Opt. Soc. Am. 55, 1427 - 1435 (1965); 56, 410 (1966).

23. David L. Fried, "Optical Resolution Through a Randomly Inhomogeneous Medium for Very Long and Very Short Exposures," J. Opt. Soc. Am. 56, 1372 - 1379 (1966).

24. R. E. Hufnagel and N. R. Stanley, "Modulation Transfer Function Associated with Image Transmission Through Turbulent Media," J. Opt. Soc. Am. 54, 52 - 61 (1964).

25. M. T. Tavis and H. T. Yura, "Short-Term Average Irradiance Profile of an Optical Beam in a Turbulent Medium," Appl. Opt. 15, 2922 - 2931 (1976).

26. R. F. Lutomirski and H. T. Yura, "Wave Structure Function and Mutual Coherence Function of an Optical Wave in a Turbulent Atmosphere," J. Opt. Soc. Am. 61, 482 - 487 (1971).

27. D. A. DeWolf, "Strong Irradiance Fluctuations in Turbulent Air: Plane Wave," J. Opt. Soc. Am., 63, 171 - 179 (1973).

28. D. L. Fried and R. A. Schmeltzer, "The Effect of Atmospheric Scintillation on an Optical Data Channel - Laser Radar and Binary Communications," Appl. Opt. 6, 1729 - 1737 (1967).

29. G. K. Born, R. Bogenberger, K. D. Erben, F. Frank, F. Mohr, and G. Sepp, "Phase-front Distortion of Laser Radiation in a Turbulent Atmosphere," Appl. Opt. 14, 2857 - 2863 (1975).

30. H. T. Yura, "Mutual Coherence Function of a Finite Cross Section Optical Beam Propagating in a Turbulent Medium," Appl. Opt. 11, 1399 - 1406 (1972).

31. J. Richard Kerr, "Experiments on Turbulence Characteristics and Multiwavelength Scintillation Phenomena," J. Opt. Soc. Am. 66, 1040 - 1049 (1972).

32. S. F. Clifford, G. R. Ochs, and R. S. Lawrence, "Saturation of Optical Scintillation by Strong Turbulence," J. Opt. Soc. Am. 64, 148 - 154 (1974).

33. James A. Dowling and Peter M. Livingston, "Behavior of Focused Beams in Atmospheric Turbulence: Measurements and Comments on the Theory," J. Opt. Soc. Am. 63, 846 - 858 (1973).

34. J. E. Pearson, "Comparison of Scintillometer and Microthermometer Measurements of C_n^2," J. Opt. Soc. Am. 65, 938 - 941 (1975).

35. John W. Strohbehn, "Line-of-Sight Wave Propagation Through the Turbulent Atmosphere," Proc. IEEE 56, 1301 - 1318 (1968).

36. Phillip M. Morse and Herman Feshback, Methods of Theoretical Physics (McGraw-Hill, New York, 1953), Chap. 4.

Appendix A

In the averaged threshold receiver structure of Eq.(18) of Chapter 2, the fading was assumed to be constant during a period of time given by $T = N/R$ which will be true, for all practical purposes, if we can expect ΔZ, the fluctuation in Z during T, to be much less than the error in $\hat{Z}$, the receiver estimate of the fading. In other words, we will require that:

$$\langle(\Delta Z)^2\rangle << \langle(\Delta\hat{Z})^2\rangle \tag{A1}$$

If ΔZ is small we can let $\Delta Z \approx (dZ/dt)\,T$. Then, using Taylor's frozen turbulence hypothesis and assuming a homogeneous, locally isotropic atmosphere with stationarity of the log-amplitude variance, it can easily be shown that:

$$\langle(\Delta Z)^2\rangle = \left\langle\left(\frac{dZ}{dt}\right)^2\right\rangle \frac{N^2}{R^2} = \frac{24.6\ v_\perp^{\,2}\ \sigma^2 N^2}{(\lambda L)^{5/6}\ l_o^{\,1/9}\ R^2} \tag{A2}$$

For the right side of the inequality we look at the variance of $\bar{n}$ and transform this to the variance of $\hat{Z}$ with the result that:

$$\langle(\Delta\hat{Z})^2\rangle = \frac{4}{N\ N_S^{\,2}}\left(\frac{1}{2}N_S + N_B + e^{\sigma^2}\ N_S^{\,2}\right) \tag{A3}$$

Solving for the number of averaging bits, we have the requirement that:

$$N << 0.546\ (\lambda L)^{5/18}\ l_o^{\,1/9}\left(\frac{R}{v_\perp\ \sigma\ N_S}\right)^{2/3}\left(\frac{1}{2}N_S + N_B + e^{\sigma^2}\ N_S^{\,2}\right) \tag{A4}$$

In order to show this graphically, we make the assumptions that 1) $l_o^{\,1/9} \approx (2\text{mm})^{1/9}$ and 2) $\frac{1}{2}N_S + N_B << e^{\sigma^2}N_S^{\,2}$, so that the right side of this inequality reduces to:

$$N_{max} \approx 0.274\ (\lambda L)^{5/18}\left(\frac{R}{v_\perp}\right)^{2/3}\left(\frac{e^{\sigma^2}}{\sigma^2}\right)^{1/3} \tag{A5}$$

This is shown in Fig. A.1 for a wide range of parameter values where rationalized MKS units have been used exclusively. Note that N_{max} is a minimum for $\sigma = 1.0$ and that the values at $\sigma = 0.5$ and 1.5 are virtually identical. Logarithmic interpolation and extrapolation of $\sqrt{\lambda L}$ values are valid.

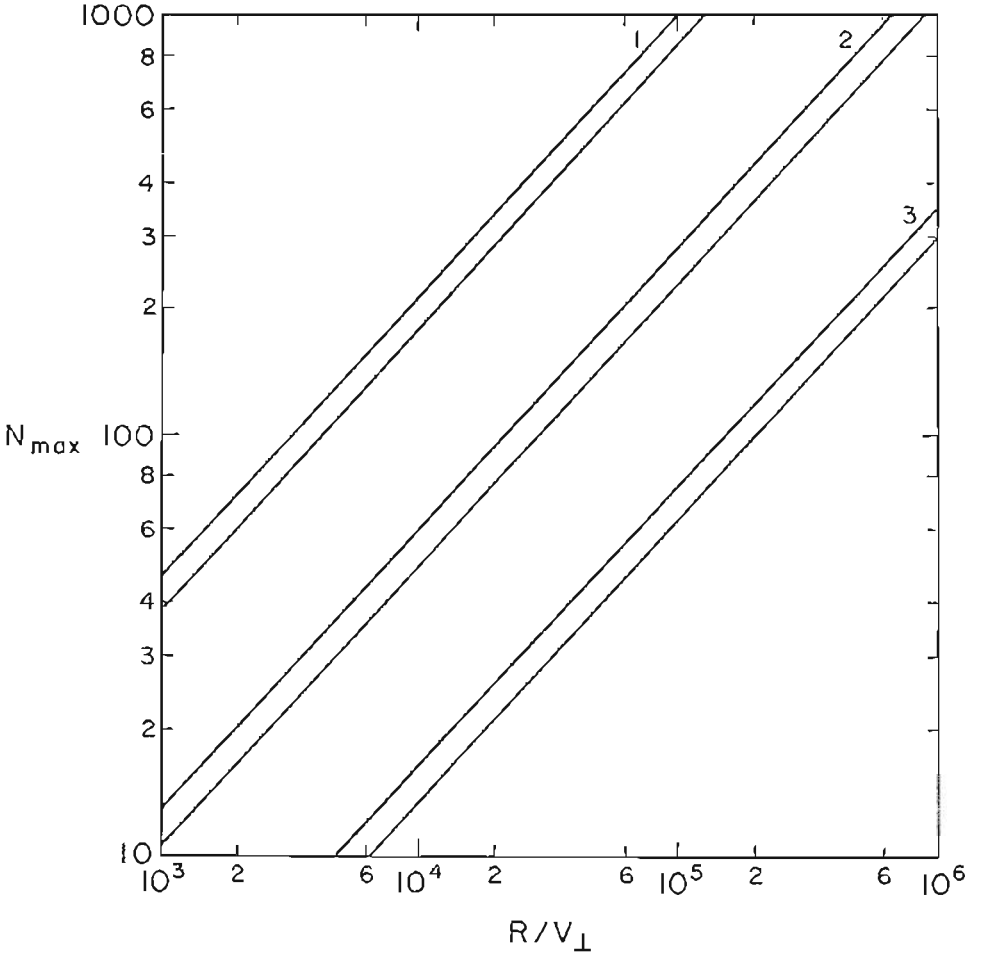

Fig. A.1. Upper bound on number of averaging bits, N_{max}, vs. ratio of data rate to perpendicular wind velocity, $R/v_\perp$ with dependence on log-intensity standard deviation, σ and Fresnel zone size, $\sqrt{\lambda L}$, shown parametrically. Lower curve in each doublet corresponds to $\sigma = 1.0$ and the upper one to $\sigma = 0.5$ or 1.5, where the doublets are labeled by 1) for $\sqrt{\lambda L} = 1.0$, 2) for $\sqrt{\lambda L} = 0.1$, and 3) for $\sqrt{\lambda L} = 0.01$.

Appendix B

Three separate FORTRAN computer codes were used in Chapter 2 to generate the bit error rate curves in the one detector case. This appendix presents listings of these codes, each followed by a partial glossary of variable names. The extention of each to multiple detectors was straightforward in all cases and the multiple detector codes are, therefore, not included.

The first listing was used to find the probability of error for the approximate optimum and MAP receivers from the relationship

$$P(E) = \tfrac{1}{2} \sum_{n=0}^{n_T} p(n|H_1) + \tfrac{1}{2}\left[1 - \sum_{n=0}^{n_T} p(n|H_0) \right] \qquad \text{(B1)}$$

where n_T is the largest integer for which L is less than zero in the case of each receiver. The steepest descents approximation to $p(n|H_1)$ given by Eq.(7) was used.

If, in the averaged threshold receiver, an infinite number of averaging bits can be used, the instantaneous fading can be known exactly. The second listing is of a program to calculate, for this case,

$$P(E) = \tfrac{1}{2} \int_0^\infty dZ\ p(Z) \sum_{n=0}^{n_T} p(n|H_1,Z) + \tfrac{1}{2} \int_0^\infty dZ\ p(Z) \sum_{n=n_T+1}^{\infty} p(n|H_0,Z) \qquad \text{(B2)}$$

using the trapezoidal rule for numerical integration. In the multiple detector cases the Hermite approximation to the integral over $p(\vec{Z})$ was used due to run time limitations.

For a finite number of averaging bits the result is a more complex expression:

$$P(E) = \tfrac{1}{2}\int_0^\infty dZ \sum_{n=0}^{\infty} p(n|H_1,Z)\left[1 - \sum_{k=0}^{\bar{n}_T} p(\bar{n}|k,Z)\right]$$
$$+ \tfrac{1}{2}\int_0^\infty dZ \sum_{n=0}^{\infty} p(n|H_0,Z) \sum_{k=0}^{\infty} p(k) \sum_{\bar{n}=0}^{\bar{n}_T} p(\bar{n}|k,Z) \qquad \text{(B3)}$$

where k, the number of "1" bits during the average time, is a Binomially distributed random variable. The threshold $\bar{n}_T$ is the largest integer value of $\bar{n}$ for which L is less than zero in Eq.(18). The third program performs the operations indicated in Eq.(B3) after making the simplifying assumption that $\bar{n}$ is large enough to approximate its actual conditional distribution, which is Poisson, by a Gaussian so that the sum over $\bar{n}$ can be replaced by the error function.

```
C     P(ERROR) FOR APPROXIMATE OPTIMUM AND MAP RECEIVERS
C           WITH D = 1
C
      DOUBLE PRECISION PNS, RNF
      CALL SEARCH (1,'INPUT',1,0)
      CALL SEARCH (2,'OUTPUT',2,0)
   10 FORMAT (3E10.4)
      READ (5,10) SD, RNS, RNB
   20 FORMAT ('  SD = ', F5.2 , '  NS = ', F4.0 , '  NB = ', F4.0)
      WRITE (6,20) SD, RNS, RNB
      VAR = SD*SD
      RNF = 1.0
      FMAP = -1.0
      FOPT = -1.0
      CALL FZO (SD, RNS, RNB, 0.0, ZO)
      PS = (EXP(-ZO*RNS-RNB - 0.5*(ALOG(ZO)+0.5*VAR)*(ALOG(ZO)+0.5*VAR)
     1      /VAR)) / SQRT(1.0+VAR*ZO*RNS)
      PNS = EXP(-RNB)
      ENB = PNS
      DO 500 I = 1,200
      RN = I
      RNF = RNF * RN
      CALL FZO (SD, RNS, RNB, RN, ZO)
      HPS = (ZO*RNS+RNB)**RN * EXP(-ZO*RNS-RNB-0.5* (ALOG(ZO)
     1     +0.5*VAR)* (ALOG(ZO)+0.5*VAR)/VAR) / (RNF * SQRT(1.0
     2     -VAR*ZO*RNS* (RN*RNB/((ZO*RNS+RNB)*(ZO*RNS+RNB))-1.0)))
      HPNS = ((RNB**RN)/RNF)*ENB
      RL = RN * ALOG(ZO*RNS/RNB+1.0) - ZO*RNS - 0.5*(ALOG(ZO)
     1   +0.5*VAR)*(ALOG(ZO)+0.5*VAR)/VAR - 0.5*ALOG(1.0 -
     2     VAR*ZO*RNS*(RN*RNB/((ZO*RNS+RNB)*(ZO*RNS+RNB))-1.0))
      IF (RL.GT.0.0) GO TO 400
  200 CALL MAP (RNS, RNB, RN, ZO, R)
      IF (R.LT.0.0) GO TO 450
      IF (FMAP.GT.0.0) GO TO 260
  250 FORMAT ('    MAP ','  KT = ', F12.2/'  P(S) = ',
     1    E12.5,'  P(NS) = ',E12.5,'  P(E) = ',E12.5)
      PNS1 = 1.0 - PNS
      ERR = 0.5 * (PS+PNS1)
      WRITE (6,250) RN, PS, PNS1, ERR
      FMAP = FMAP + 2.0
  260 IF (FOPT) 450, 450, 600
  400 IF (FOPT.GT.0.0) GO TO 440
  410 FORMAT ('    OPT ','  KT = ',F12.2/'  P(S) = ',
     1     E12.5,'  P(NS) = ',E12.5,'  P(E) = ',E12.5)
      PNS1 = 1.0 - PNS
      ERR = 0.5 * (PS+PNS1)
      WRITE (6,410) RN, PS, PNS1, ERR
      FOPT = FOPT + 2.0
  440 IF (FMAP) 200, 200, 600
  450 PS = PS + HPS
      PNS = PNS + HPNS
  500 CONTINUE
  600 CONTINUE
      CALL SEARCH (4,0,1,0)
      CALL SEARCH (4,0,2,0)
```

```
      CALL EXIT
      END
C
C     CALCULATES STATIONARY POINT ZO USING NEWTON'S METHOD
C
      SUBROUTINE FZO (SD, RNS, RNB, RN, X2)
      X2 = ABS(RN - RNB * 0.001) / RNS
   24 X1 = X2
      F = RN*X1*RNS / (X1*RNS+RNB) -X1*RNS - ALOG(X1) / (SD*SD) -0.5
      F1 = RN*RNB*RNS/ ((X1*RNS+RNB)* (X1*RNS+RNB))-RNS-1./(X1*SD*SD)
      X2 = X1 - F/F1
      IF (X2) 25, 25, 26
   25 X2 = X1/2.0
      GO TO 24
   26 CONTINUE
      IF (ABS((X2-X1) /X2) - 1.0E-05) 28, 28, 24
   28 CONTINUE
      RETURN
      END
C
C     CALCULATES MAP RECEIVER LIKELIHOOD FUNCTION R
C
      SUBROUTINE MAP (RNS, RNB,  RN, ZO, R)
      R =  RN * ALOG(ZO*RNS/RNB + 1.0) - ZO * RNS
      RETURN
      END
```

ERR	P(E)
FMAP	MAP threshold flag
FOPT	approximate optimum threshold flag
HPNS	$p(n\|H_0)$
HPS	$p(n\|H_1)$
PNS1	P(False Alarm)
PS	P(Miss)
R	MAP L (Eq. 12)
RL	approximate optimum L (Eq.11)
RN	n
RNB	N_B
RNF	n!
RNS	N_S
SD	σ
ZO	Z_o or $\hat{Z}$

```
C     P(ERROR) FOR AVERAGED THRESHOLD RECEIVER
C        WITH D = 1 AND INFINITE THRESHOLD AVERAGING
C
      DOUBLE PRECISION PN0(200), FACT(200), DNB, DNS, PH0,
     1                 PH1, PE0, PE1, DSD, VAR, Z
      CALL SEARCH (1,'INPUT',1,0)
      CALL SEARCH (2,'OUTPUT',2,0)
   10 FORMAT (3E10.4)
      READ (5,10) SD, RNS, RNB
   20 FORMAT (/'    D = 1 ',' SD = ',F5.3,'  NS = ',F5.0,
     1            '  NB = ',F5.0)
      WRITE (6,20) SD, RNS, RNB
      DNB = RNB
      DNS = RNS
      DSD = SD
      VAR = DSD * DSD
      PE1 = 0.0
      PE0 = 0.0
C
C     P (N / NO SIGNAL)
C
      FACT(1) = 1.0
      PN0(1) = DEXP(-DNB)
      DO 100 K = 2,200
      RN = K - 1
      FACT(K) = FACT(K-1) * RN
      PN0(K) = (DNB**RN / FACT(K)) * PN0(1)
  100 CONTINUE
C
C     Z INTEGRATION
C
      Z = 0.5D-03
      DO 600 I = 1,5000
      PH1 = DEXP(-Z*DNS - DNB)
      PH0 = 0.0
C
      DO 500 J = 1,198
      RN = J
      RL = RN*DLOG(Z*DNS/DNB+1.0) -Z*DNS
      IF (RL) 450, 460, 470
  450 PH1=PH1+((Z*DNS+DNB)**RN/FACT(J+1))*DEXP(-Z*DNS-DNB)
      GO TO 500
  460 PH1=PH1+0.5*((Z*DNS+DNB)**RN/FACT(J+1))*DEXP(-Z*DNS-DNB)
      PH0 = PH0 + 0.5*PN0(J+1)
      GO TO 500
  470 PH0 = PH0 + PN0(J+1)
      IF (PN0(J+1)/PH0.LT.1.0D-05) GO TO 510
  500 CONTINUE
C
  510 PH1 = PH1*DEXP(-0.5*(DLOG(Z)+0.5*VAR)*(DLOG(Z)+0.5*VAR)/VAR)/
     1     (2.50663*DSD*Z)
      PH0 = PH0*DEXP(-0.5*(DLOG(Z)+0.5*VAR)*(DLOG(Z)+0.5*VAR)/VAR)/
     1     (2.50663*DSD*Z)
      PE0 = PE0 + PH0
      PE1 = PE1 + PH1
```

```
      IF (PE1.EQ.0.0) GO TO 590
      IF (PH1/PE1.GT.1.0D-05) GO TO 590
      IF (PH0/PE0.LT.1.0D-05) GO TO 610
  590 Z = Z + 1.0D-03
  600 CONTINUE
C
  610 PE1 = PE1*1.0D-03
      PE0 =  PE0*1.0D-03
      PEE = 0.5 * (PE0+PE1)
  620 FORMAT (/'  APPROXIMATE MAP RECEIVER ',' KT = ',
     1    I5/'  P(MISS) = ',D15.5,'  P(FALSE ALARM) = ',D15.5,
     2     '  P(E) = ',E15.5)
      WRITE (6,620) I, PE1, PE0, PEE
      CALL SEARCH (4,0,1,0)
      CALL SEARCH (4,0,2,0)
      CALL EXIT
      END
```

FACT(n+1)	n!
PEO	P(False Alarm)
PE1	P(Miss)
PEE	P(E)
PHO	$p(Z) \sum_{n=n_T+1}^{\infty} p(n\|H_0,Z)$
PH1	$p(Z) \sum_{n=0}^{n_T} p(n\|H_1,Z)$
PNO(n+1)	$p(n\|H_0)$
RL	L (Eq.18)
RN	n
RNB	N_B
RNS	N_S
SD	σ

```
C      P(ERROR) FOR AVERAGED THRESHOLD RECEIVER
C         WITH D = 1 AND FINITE THRESHOLD AVERAGING
C
       DIMENSION FACT(1000), POIS(1000), RNT(1000), P(1000)
       CALL SEARCH (1,'INPUT1',1,0)
       CALL SEARCH (2,'OUTPUT',3,0)
C
    40 FORMAT (3E10.4,I10)
       READ (5,40) RNS,RNB,SD,NAVE
       NDSUM = RNS + RNB
       VAR = SD*SD
       RNAV = NAVE
       NAV1 = NAVE + 1
       PMIS = 0.0
       PFA = 0.0
       FACT(1) = 0.0
       POIS(1) = EXP(-RNB)
       RNT(1) = RNB
C
C       GENERATES FACTORIAL AND THRESHOLDS
C
       DO 110 N = 2, NDSUM
       RN = N - 1
       FACT(N) = FACT(N-1) + ALOG(RN)
       POIS(N) = POIS(N-1) * RNB / RN
       IF (RN-RNB) 50, 50, 60
    50 RN2 = RNB
       GO TO 110
    60 RN1 = RN + RNB / RNS
       DO 100 I = 1, 50
       F = RN * ALOG(RN1/RNB) - RN1 + RNB
       F1 = RN/RN1 - 1.0
       RN2 = RN1 - F/F1
       IF (ABS(RN1-RN2) .LT. 1.0E-4*RN2) GO TO 110
   100 RN1 = RN2
   110 RNT(N) = RN2
C
C       GENERATES BINOMIAL DISTRIBUTION
C
       P(1) = 0.5 ** RNAV
       DO 150 K = 2, NAV1
       RK = K - 1
   150 P(K) = P(K-1) * (RNAV-RK+1.0) / RK
C
C         INTEGRAL OVER Z
C
       DO 700 IZ = 1, 100
       Z = IZ
       Z = 0.01 * Z
C
C       SUM OF DISTRIBUTION OVER N
C
       P1H1 = 0.0
       P1H2 = 0.0
       P0H1 = 0.0
```

```
      P0H2 = 0.0
      DO 600 N = 1, NDSUM
      RN = N - 1
C
C       SUM OVER K
C
      PH1 = 0.0
      PH2 = 0.0
      DO 500 K = 1, NAV1
      RK = K - 1
      RKT = 50.0 * RNAV * (RNT(N) -2.0*RK*Z*RNS/RNAV -RNB)
     1    / SQRT(RK*Z*RNS +RNAV*RNB)
C  ERF IS ERROR FUNCTION SUBROUTINE
      PNLT = ERF(RKT)
      PH1 = PH1 + P(K) * PNLT
      RKT = 50.0 * RNAV * (RNT(N) -2.0*RK*RNS/(Z*RNAV) -RNB)
     1    / SQRT(RK*RNS/Z +RNAV*RNB)
      PNLT = ERF(RKT)
  500 PH2 = PH2 + P(K) * PNLT
C
      P1H1 = P1H1 + EXP( RN*ALOG(Z*RNS+RNB) - Z*RNS-RNB
     1             - FACT(N) ) * (1.0-PH1)
      A = RN*ALOG(RNS/Z+RNB) - RNS/Z-RNB - FACT(N)
      IF (A .LT. -100.0) GO TO 550
      P1H2 = P1H2 + EXP(A) * (1.0-PH2)
  550 CONTINUE
      P0H1 = P0H1 + POIS(N) * PH1
      P0H2 = P0H2 + POIS(N) * PH2
  600 CONTINUE
C
      PZ = EXP(-0.5* (ALOG(Z)+0.5*VAR) * (ALOG(Z)+0.5*VAR)
     1   / VAR) / (2.50663 * SD * Z)
      PZINV = EXP(-0.5* (ALOG(Z)-0.5*VAR) * (ALOG(Z)-0.5*VAR)
     1       / VAR) / (2.50663 * SD * Z)
      PMIS = PMIS + PZ*P1H1 + PZINV*P1H2
      PFA = PFA + PZ*P0H1 + PZINV*P0H2
  700 CONTINUE
C
      PMIS = (PMIS - 0.5*PZ*P1H1 - 0.5*PZINV*P1H2) / 100.0
      PFA = (PFA - 0.5*PZ*P0H1 - 0.5*PZINV*P0H2) / 100.0
      PE = 0.5 * (PMIS + PFA)
  800 FORMAT(3E15.5)
      WRITE (7,800) PMIS, PFA, PE
 2000 CONTINUE
      CALL SEARCH (4,0,1,0)
      CALL SEARCH (4,0,3,0)
      CALL EXIT
      END
```

FACT(n+1)	ln(n!)
NAVE	N
P(k+1)	p(k)
PE	P(E)
PFA	P(False Alarm)
PMIS	P(Miss)
POIS(n+1)	$p(n \mid H_0)$
PZ	p(Z)
PZINV	p(1/Z)
RNB	N_B
RNS	N_S
SD	σ

Appendix C

What follows is a listing of the FORTRAN computer code that was used to evaluate the integral in Eq.(8) of Chapter 3. For each value of D/r_o (DRO), the corresponding value for <G> (SNR) is printed, along with their respective logarithms (ALD and ALP) to simplify plotting. The program to evaluate Eq.(12) is identical except for statement number 100 and was, therefore, not presented.

```
C  SNR FOR HETERODYNE RECEIVER WITH PARTIAL
C    ANGLE-OF-ARRIVAL TRACKING. TRAPEZOIDAL RULE
C      INTEGRATION OF EQ.8.
C
      CALL SEARCH (2,'OUTPUT',2,0)
   10 FORMAT (E15.5)
      READ (1,10) C
C       C = DT / D                (NEAR FIELD)
C       C = 8 * DT / D             (FAR FIELD)
      DO 300 ND = 1, 30
        ALD = ND
        ALD = ALD * 0.1 - 1.0
        DRO = 10.0 ** ALD
C          DRO = D / R0
      SNR = 0.0
      DO 100 NU = 1, 1000
        U = NU
        U = U * 0.001
  100 SNR = SNR + U * ( ATAN(SQRT(1.0-U*U)/U) - SQRT(1.0-U*U)
     1     * U ) * EXP(-1.29 * (U*DRO)**1.6666667
     2           * (1.0-(U/C)**0.3333333))
      SNR = 5.09206E-3 * DRO*DRO * SNR
      ALP = ALOG10(SNR)
  200 FORMAT (4E15.5)
      WRITE (6,200) DRO, ALD, ALP, SNR
  300 CONTINUE
      CALL SEARCH (4,0,2,0)
      CALL EXIT
      END
```

Appendix D

This appendix contains listings of the FORTRAN computer codes that were used to generate the figures of Chapter 4, each followed by a partial glossary of variable names. The first two of these calculate p(I) values for the static and tracking receivers, respectively. In each case Newton's method is used in order to obtain the stationary points.

The third program calculates the function

$$g(I) = \int_{3.83}^{7.02} \int_{-\infty}^{\infty} dX\, d\Delta\, p(X)\, p(\Delta)\, \frac{1}{\sqrt{2\pi}}\, \exp\left[-\tfrac{1}{2}\,(I - 2\gamma Z J_1(\Delta)/\Delta)^2\right] \tag{D1}$$

using a steepest descents approximation to the integral over X and trapezoidal rule integration over Δ. The correction term for a particular I is then found to be, from Eq.(40) of Chapter 4, g(-I) - g(I).

```
C    P(I) FOR HETERODYNE RECEIVER WITHOUT ANGLE-OF-ARRIVAL
C          TRACKING   (FROM EQ. 28)
C
      CALL SEARCH (1,'INPUT',1,0)
      CALL SEARCH (2,'OUTPUT',2,0)
   50 FORMAT (4E10.4)
      READ (5,50) SX, SD, DI, GA
        X1 = - SX*SX
        DEL1 = SD
        RIHD = 2.0 * GA * EXP(X1) * AJ1(DEL1) / DI
          IHD = RIHD
        RIHD = IHD * DI
      DO 500 I = 1, 3000
         RI = I - 1
        RI = RIHD +  RI * DI
      CALL XODO (X1,DEL1,RI,GA,SX,SD,XO,DELO,B,ZO,RIBAR)
      P1 = EXP(-0.5 * (RI-RIBAR) * (RI-RIBAR)
     1   - 0.5 * (XO/SX+SX) * (XO/SX+SX)
     2     - 0.5 * DELO * DELO / (SD*SD))
     3       * DELO / (SQRT(B) * SX * SD*SD)
  400 FORMAT (F15.2, E15.5)
      WRITE (6,400) RI, P1
      IF (RI .LT. GA) GO TO 500
      IF (P1 .LT. 1.0E-5) GO TO 600
  500 CONTINUE
            PAUSE 4
  600 CONTINUE
        X1 = - SX*SX
        DEL1 = SD
        RIHD = 2.0 * GA * EXP(X1) * AJ1(DEL1) / DI
          IHD = RIHD
        RIHD = IHD * DI
      DO 1500 I = 1, 3000
         RI = I
        RI = RIHD -  RI * DI
      CALL XODO (X1,DEL1,RI,GA,SX,SD,XO,DELO,B,ZO,RIBAR)
      P1 = EXP(-0.5 * (RI-RIBAR) * (RI-RIBAR)
     1   - 0.5 * (XO/SX+SX) * (XO/SX+SX)
     2     - 0.5 * DELO * DELO / (SD*SD))
     3       * DELO / (SQRT(B) * SX * SD*SD)
      WRITE (6,400) RI, P1
      IF (P1 .LT. 1.0E-5) GO TO 1600
 1500 CONTINUE
            PAUSE 4
 1600 CONTINUE
      CALL SEARCH (4,0,1,0)
      CALL SEARCH (4,0,2,0)
      CALL EXIT
      END
C
C     CALCULATES STATIONARY POINTS XO AND DELO
C       FROM EQS. 25 USING NEWTON'S METHOD
C
      SUBROUTINE XODO (X1,DEL1,RI,GA,SX,SD,XO,DELO,B,ZO,RIBAR)
      DO 100 L = 1, 100
```

```
      XO = X1
      ZO = EXP(XO)
      DELO = DEL1
      RIBAR = 2.0 * GA * ZO * AJ1(DELO)
C          AJ1 IS FIRST ORDER BESSEL FUNCTION DIVIDED BY
C                       ARGUMENT
      RIBO  = 2.0 * GA * ZO * AJ0(DELO)
C          AJ0 IS ZERO ORDER BESSEL FUNCTION
      FX = (RI-RIBAR) * RIBAR - XO/(SX*SX) - 1.0
      FD = (RI-RIBAR) * (RIBO-2.0*RIBAR) / DELO
     1  - DELO/(SD*SD) + 1.0/DELO
      F2XX = (RI-2.0*RIBAR) * RIBAR - 1.0/(SX*SX)
      F2XD = (RI-2.0*RIBAR) * (RIBO-2.0*RIBAR) / DELO
      F2DD = (RI-RIBAR) * (6.0*RIBAR-DELO*DELO*RIBAR-3.0*RIBO)
     1   / (DELO*DELO) - 1.0/(SD*SD) - 1.0/(DELO*DELO)
     2       - (RIBO-2.0*RIBAR) * (RIBO-2.0*RIBAR) / (DELO*DELO)
      B = F2DD*F2XX - F2XD*F2XD
      X1 = XO + (FD*F2XD-FX*F2DD) / B
      DEL1 = DELO + (FX*F2XD-FD*F2XX) / B
      IF (ABS((X1-XO)/XO) .GT. 1.0E-4) GO TO 100
      IF (ABS((DEL1-DELO)/DELO) .GT. 1.0E-4) GO TO 100
        RETURN
  100 CONTINUE
          PAUSE 3
        RETURN
      END
```

B	determinant B (Eq.26)
DELO	Δ_o
DI	resolution of results
F2DD	$\partial^2 f/\partial\Delta^2$ (Eq.27c)
F2XD	$\partial^2 f/\partial X\partial\Delta$(Eq.27b)
F2XX	$\partial^2 f/\partial X^2$ (Eq.27a)
FD	$\partial f/\partial\Delta$ (Eq.25b)
FX	$\partial f/\partial X$ (Eq.25a)
GA	γ
P1	p(I) (Eq.28)
RI	I
SD	σ_Δ
SX	σ_X
XO	X_o
ZO	Z_o

```
C     P(I) FOR HETERODYNE RECEIVER WITH ANGLE-OF-ARRIVAL
C          TRACKING     (FROM EQ. 37)
C
      COMMON CCOS(21), CSIN(21), CJO(21)
      CALL SEARCH (1,'INPUT',1,0)
      CALL SEARCH (2,'OUTPUT',2,0)
    5 FORMAT (4E10.4)
      READ (5,5) SX, SA, GA, DI
      CCOS(1) = 1.0
      CSIN(1) = 1.0
      CJO(1) = 1.0
      DO 100 K = 2, 21
         RK = K - 1
      CCOS(K) = - 0.5 * CCOS(K-1) / (2.0*RK*RK-RK)
      CSIN(K) = - 0.5 * CSIN(K-1) / (2.0*RK*RK+RK)
      CJO(K) = - CJO(K-1) / (RK*RK)
  100 CONTINUE
        X1 =  -SX*SX
        A41 = 0.0
        AQ1 = SA
       RBB = GA * EXP(X1) * C(A41,AQ1) / DI
            IRBB = RBB
        RBB = IRBB * DI
C
      DO 700 I = 1, 200
        RI = I
        RI = RBB -  RI * DI
      DO 500 KNT = 1, 100
C          LOOP CALCULATES STATIONARY POINTS X0, A40, AND AQ0
C             FROM EQS. 33 USING NEWTON'S METHOD
        X0 = X1
        Z0 = EXP(X0)
        A40 = A41
        AQ0 = AQ1
        C0 = C(A40,AQ0)
        S0 = S(A40,AQ0)
        C41 = DC4(A40,AQ0)
        S41 = DS4(A40,AQ0)
        CQ1 = DCQ(A40,AQ0)
        SQ1 = DSQ(A40,AQ0)
        C42 = D2C4(A40,AQ0)
        S42 = D2S4(A40,AQ0)
        CQ2 = D2CQ(A40,AQ0)
        SQ2 = D2SQ(A40,AQ0)
        C22 = D2CQ4(A40,AQ0)
        S22 = D2SQ4(A40,AQ0)
      RIB = SQRT(C0*C0 + S0*S0)
      RIBAR = GA * Z0 * RIB
      W4 = GA * Z0 * (C0*C41 + S0*S41) / RIB
      WQ = GA * Z0 * (C0*CQ1 + S0*SQ1) / RIB
        FX = (RI-RIBAR) * RIBAR - X0/(SX*SX) - 1.0
        F4 = (RI-RIBAR) * W4 - A40/(SA*SA)
        FQ = (RI-RIBAR) * WQ - 2.0*AQ0/(SA*SA) + 1.0/AQ0
      F2XX = (RI-2.0*RIBAR) * RIBAR - 1.0/(SX*SX)
      F244 = -W4*W4 + (RI-RIBAR) * GA*Z0/RIB
```

```
     1   * (-W4*W4/(GA*GA*ZO*ZO) + CO*C42 + SO*S42 + C41*C41 + S41*S41)
     2     - 1.0/(SA*SA)
      F2QQ = -WQ*WQ + (RI-RIBAR) * GA*ZO/RIB
     1   * (-WQ*WQ/(GA*GA*ZO*ZO) + CO*CQ2 + SO*SQ2 + CQ1*CQ1 + SQ1*SQ1)
     2     - 2.0/(SA*SA) - 1.0/(AQO*AQO)
      F2X4 = (RI-2.0*RIBAR) * W4
      F2XQ = (RI-2.0*RIBAR) * WQ
      F2Q4 = -W4*WQ + (RI-RIBAR) * (-W4*WQ/RIBAR
     1   + GA*ZO/RIB * (CO*C22 + SO*S22 + C41*CQ1 + S41*SQ1))
        B = DET(F2XX, F2X4, F2XQ, F2X4, F244, F2Q4, F2XQ, F2Q4, F2QQ)
      X1 = XO - DET(FX, F4, FQ, F2X4, F244, F2Q4,
     1   F2XQ, F2Q4, F2QQ) / B
      A41 = A4O - DET(F2XX, F2X4, F2XQ, FX, F4, FQ,
     1   F2XQ, F2Q4, F2QQ) / B
      AQ1 = AQO - DET(F2XX, F2X4, F2XQ, F2X4, F244, F2Q4,
     1   FX, F4, FQ) / B
C
      IF (ABS((X1-XO)/XO) .GT. 1.0E-5) GO TO 500
      IF (ABS((AQ1-AQO)/AQO) .LT. 1.0E-5) GO TO 600
  500 CONTINUE
              PAUSE 1
  600 CONTINUE
      P1 = 2.0 * AQO * EXP( -0.5*(RI-RIBAR)*(RI-RIBAR)
     1   - 0.5*(XO+SX*SX)*(XO+SX*SX)/(SX*SX)
     2     - 0.5*(A4O*A4O+2.0*AQO*AQO)/(SA*SA) )
     3       / (SX * SA*SA*SA * SQRT(-B))
  650 FORMAT (F15.3, E15.5)
      WRITE (6,650) RI, P1
      IF (P1 .LT. 1.0E-7) GO TO 800
  700 CONTINUE
  800 CONTINUE
        X1 =  -SX*SX
        A41 = 0.0
        AQ1 = SA
       RBB = GA * EXP(X1) * C(A41,AQ1) / DI
            IRBB = RBB
        RBB = IRBB * DI
C
      DO 1700 I = 1, 200
        RI = I - 2
        RI = RBB +  RI * DI
      DO 1500 KNT = 1, 100
        XO = X1
        ZO = EXP(XO)
        A4O = A41
        AQO = AQ1
        CO = C(A4O,AQO)
        SO = S(A4O,AQO)
        C41 = DC4(A4O,AQO)
        S41 = DS4(A4O,AQO)
        CQ1 = DCQ(A4O,AQO)
        SQ1 = DSQ(A4O,AQO)
        C42 = D2C4(A4O,AQO)
        S42 = D2S4(A4O,AQO)
        CQ2 = D2CQ(A4O,AQO)
        SQ2 = D2SQ(A4O,AQO)
```

```
        C22 = D2CQ4(A40,AQ0)
        S22 = D2SQ4(A40,AQ0)
      RIB = SQRT(C0*C0 + S0*S0)
      RIBAR = GA * Z0 * RIB
      W4 = GA * Z0 * (C0*C41 + S0*S41) / RIB
      WQ = GA * Z0 * (C0*CQ1 + S0*SQ1) / RIB
        FX = (RI-RIBAR) * RIBAR - X0/(SX*SX) - 1.0
        F4 = (RI-RIBAR) * W4 - A40/(SA*SA)
        FQ = (RI-RIBAR) * WQ - 2.0*AQ0/(SA*SA) + 1.0/AQ0
      F2XX = (RI-2.0*RIBAR) * RIBAR - 1.0/(SX*SX)
      F244 = -W4*W4 + (RI-RIBAR) * GA*Z0/RIB
     1   * (-W4*W4/(GA*GA*Z0*Z0) + C0*C42 + S0*S42 + C41*C41 + S41*S41)
     2     - 1.0/(SA*SA)
      F2QQ = -WQ*WQ + (RI-RIBAR) * GA*Z0/RIB
     1   * (-WQ*WQ/(GA*GA*Z0*Z0) + C0*CQ2 + S0*SQ2 + CQ1*CQ1 + SQ1*SQ1)
     2     - 2.0/(SA*SA) - 1.0/(AQ0*AQ0)
      F2X4 = (RI-2.0*RIBAR) * W4
      F2XQ = (RI-2.0*RIBAR) * WQ
      F2Q4 = -W4*WQ + (RI-RIBAR) * (-W4*WQ/RIBAR
     1   + GA*Z0/RIB * (C0*C22 + S0*S22 + C41*CQ1 + S41*SQ1))
        B = DET(F2XX, F2X4, F2XQ, F2X4, F244, F2Q4, F2XQ, F2Q4, F2QQ)
      X1 = X0 - DET(FX, F4, FQ, F2X4, F244, F2Q4,
     1   F2XQ, F2Q4, F2QQ) / B
      A41 = A40 - DET(F2XX, F2X4, F2XQ, FX, F4, FQ,
     1   F2XQ, F2Q4, F2QQ) / B
      AQ1 = AQ0 - DET(F2XX, F2X4, F2XQ, F2X4, F244, F2Q4,
     1   FX, F4, FQ) / B
C
      IF (ABS((X1-X0)/X0) .GT. 5.0E-5) GO TO 1500
      IF (ABS((AQ1-AQ0)/AQ0) .LT. 1.0E-5) GO TO 1600
 1500 CONTINUE
             PAUSE 1
 1600 CONTINUE
      P1 = 2.0 * AQ0 * EXP( -0.5*(RI-RIBAR)*(RI-RIBAR)
     1   - 0.5*(X0+SX*SX)*(X0+SX*SX)/(SX*SX)
     2     - 0.5*(A40*A40+2.0*AQ0*AQ0)/(SA*SA) )
     3       / (SX * SA*SA*SA * SQRT(-B))
      WRITE (6,650) RI, P1
      IF (P1 .LT. 1.0E-7) GO TO 1800
 1700 CONTINUE
 1800 CONTINUE
      CALL SEARCH (4,0,1,0)
      CALL SEARCH (4,0,2,0)
      CALL EXIT
      END
C
C  C(A,B) =  INTEGRAL 0 TO 1 OF COS(AT) * J0(BT) DT
C
      FUNCTION C(A,B)
      COMMON CCOS(21), CSIN(21), CJ0(21)
        X = A * A
        Y = 0.25 * B * B
        C = 0.0
      IF (A.EQ.0.0) GO TO 10
      DO 5 K = 1, 21
        RK = K - 1
```

```
      DO 5 L = 1, 21
        RL = L - 1
    5 C = C + CCOS(K) * CJO(L) * X**RK * Y**RL / (RL+RK+0.5)
      C = 0.5 * C
      RETURN
   10 DO 15 L = 1, 21
        RL = L - 1
   15 C = C + CJO(L) * Y**RL / (RL+0.5)
      C = 0.5 * C
      RETURN
      END
C
C   S(A,B) =  INTEGRAL 0 TO 1 OF SIN(AT) * J0(BT) DT
C
      FUNCTION S(A,B)
      COMMON CCOS(21), CSIN(21), CJO(21)
      IF (A.EQ.0.0) GO TO 10
        X = A * A
        Y = 0.25 * B * B
        S = 0.0
      DO 5 K = 1, 21
        RK = K - 1
      DO 5 L = 1, 21
        RL = L - 1
    5 S = S + CSIN(K) * CJO(L) * X**RK * Y**RL / (RL+RK+1.0)
      S = 0.5 * A * S
      RETURN
   10 S = 0.0
      RETURN
      END
C
C    DC4 = DC/DA
C
      FUNCTION DC4(A,B)
      COMMON CCOS(21), CSIN(21), CJO(21)
      IF (A.EQ.0.0) GO TO 10
        X = A * A
        Y = 0.25 * B * B
        C = 0.0
      DO 5 K = 1, 21
        RK = K - 1
      DO 5 L = 1, 21
        RL = L - 1
    5 C = C + CCOS(K) * CJO(L) * X**RK * Y**RL * RK / (RL+RK+0.5)
      DC4 = C / A
      RETURN
   10 DC4 = 0.0
      RETURN
      END
C
C     DS4 = DS/DA
C
      FUNCTION DS4(A,B)
      COMMON CCOS(21), CSIN(21), CJO(21)
        X = A * A
        Y = 0.25 * B * B
```

```
        S = 0.0
      IF (A.EQ.0.0) GO TO 10
      DO 5 K = 1, 21
        RK = K - 1
      DO 5 L = 1, 21
        RL = L - 1
    5 S = S + CSIN(K) * CJO(L) * X**RK * Y**RL * (RK+0.5) / (RL+RK+1.0)
      DS4 = S
      RETURN
   10 DO 15 L = 1, 21
        RL = L - 1
   15 S = S + CJO(L) * Y**RL * 0.5 / (RL+1.0)
      DS4 = S
      RETURN
      END
C
C    DCQ = DC/DB
C
      FUNCTION DCQ(A,B)
      COMMON CCOS(21), CSIN(21), CJO(21)
        X = A * A
        Y = 0.25 * B * B
        C = 0.0
      IF (A.EQ.0.0) GO TO 10
      DO 5 K = 1, 21
        RK = K - 1
      DO 5 L = 1, 21
        RL = L - 1
    5 C = C + CCOS(K) * CJO(L) * X**RK * Y**RL * RL / (RL+RK+0.5)
      DCQ = C / B
      RETURN
   10 DO 15 L = 1, 21
        RL = L - 1
   15 C = C + CJO(L) * Y**RL * RL / (RL+0.5)
      DCQ = C / B
      RETURN
      END
C
C     DSQ = DS/DB
C
      FUNCTION DSQ(A,B)
      COMMON CCOS(21), CSIN(21), CJO(21)
      IF (A.EQ.0.0) GO TO 10
        X = A * A
        Y = 0.25 * B * B
        S = 0.0
      DO 5 K = 1, 21
        RK = K - 1
      DO 5 L = 1, 21
        RL = L - 1
    5 S = S + CSIN(K) * CJO(L) * X**RK * Y**RL * RL / (RL+RK+1.0)
      DSQ = A * S / B
      RETURN
   10 DSQ = 0.0
      RETURN
      END
```

```
C
C    D2C4 = D2C/DA2
C
      FUNCTION D2C4(A,B)
      COMMON CCOS(21), CSIN(21), CJO(21)
        X = A * A
        Y = 0.25 * B * B
        C = 0.0
      IF (A.EQ.0.0) GO TO 10
      DO 5 K = 2, 21
        RK = K - 1
      DO 5 L = 1, 21
        RL = L - 1
    5 C = C + CCOS(K) * CJO(L) * X**(RK-1.0) * Y**RL
     1    * RK * (RK-0.5) / (RL+RK+0.5)
      D2C4 = 2.0 * C
      RETURN
   10 DO 15 L = 1, 21
        RL = L - 1
   15 C = C + CJO(L) * Y**RL * 0.5 / (RL+1.5)
      D2C4 = -C
      RETURN
      END
C
C     D2S4 = D2S/DA2
C
      FUNCTION D2S4(A,B)
      COMMON CCOS(21), CSIN(21), CJO(21)
      IF (A.EQ.0.0) GO TO 10
        X = A * A
        Y = 0.25 * B * B
        S = 0.0
      DO 5 K = 1, 21
        RK = K - 1
      DO 5 L = 1, 21
        RL = L - 1
    5 S = S + CSIN(K) * CJO(L) * X**RK * Y**RL
     1    * RK * (RK+0.5) / (RL+RK+1.0)
      D2S4 = 2.0 * S / A
      RETURN
   10 D2S4 = 0.0
      RETURN
      END
C
C    D2CQ = D2C/DB2
C
      FUNCTION D2CQ(A,B)
      COMMON CCOS(21), CSIN(21), CJO(21)
        X = A * A
        Y = 0.25 * B * B
        C = 0.0
      IF (A.EQ.0.0) GO TO 10
      DO 5 K = 1, 21
        RK = K - 1
      DO 5 L = 1, 21
        RL = L - 1
```

```
     5 C = C + CCOS(K) * CJO(L) * X**RK * Y**RL
       1    * RL * (RL-0.5) / (RL+RK+0.5)
         D2CQ = 2.0 * C / (B*B)
         RETURN
    10 DO 15 L = 1, 21
         RL = L - 1
    15 C = C + CJO(L) * Y**RL * RL * (RL-0.5) / (RL+0.5)
         D2CQ = 2.0 * C / (B*B)
         RETURN
         END
C
C     D2SQ = D2S/DB2
C
         FUNCTION D2SQ(A,B)
         COMMON CCOS(21), CSIN(21), CJO(21)
         IF (A.EQ.0.0) GO TO 10
           X = A * A
           Y = 0.25 * B * B
           S = 0.0
         DO 5 K = 1, 21
           RK = K - 1
         DO 5 L = 1, 21
           RL = L - 1
     5 S = S + CSIN(K) * CJO(L) * X**RK * Y**RL
       1    * RL * (RL-0.5) / (RL+RK+1.0)
         D2SQ = 2.0 * A * S / (B*B)
         RETURN
    10 D2SQ = 0.0
         RETURN
         END
C
C     D2CQ4 = D2C/DADB
C
         FUNCTION D2CQ4(A,B)
         COMMON CCOS(21), CSIN(21), CJO(21)
         IF (A.EQ.0.0) GO TO 10
           X = A * A
           Y = 0.25 * B * B
           C = 0.0
         DO 5 K = 1, 21
           RK = K - 1
         DO 5 L = 1, 21
           RL = L - 1
     5 C = C + CCOS(K) * CJO(L) * X**RK * Y**RL
       1    * RK * RL / (RL+RK+0.5)
         D2CQ4 = 2.0 * C / (A*B)
         RETURN
    10 D2CQ4 = 0.0
         RETURN
         END
C
C     D2SQ4 = D2S/DADB
C
         FUNCTION D2SQ4(A,B)
         COMMON CCOS(21), CSIN(21), CJO(21)
           X = A * A
```

```
      Y = 0.25 * B * B
      C = 0.0
      IF (A.EQ.0.0) GO TO 10
      DO 5 K = 1, 21
        RK = K - 1
      DO 5 L = 1, 21
        RL = L - 1
    5 S = S + CSIN(K) * CJO(L) * X**RK * Y**RL
     1    * RL * (RK+0.5) / (RL+RK+1.0)
      D2SQ4 = 2.0 * S / B
      RETURN
   10 DO 15 L = 1, 21
        RL = L - 1
   15 S = S + CJO(L) * Y**RL * RL * 0.5 / (RL+1.0)
      D2SQ4 = 2.0 * S / B
      RETURN
      END
C
C    DET : 3 X 3 DETERMINANT
C
      FUNCTION DET(A1,A2,A3,B1,B2,B3,C1,C2,C3)
      DET = A1 * (B2*C3 - B3*C2)
     1     - A2 * (B1*C3 - B3*C1)
     2     + A3 * (B1*C2 - B2*C1)
      RETURN
      END
```

A40	α_o	
AQ0	β_o	
C22	$\partial^2 C/\partial\alpha\partial\beta$	
C41	$\partial C/\partial\alpha$	
C42	$\partial^2 C/\partial\alpha^2$	
CCOS	coefficients of Taylor's expansion of cosine function	
CJO	coefficients of Taylor's expansion of zero order Bessel function	
CQ1	$\partial C/\partial\beta$	
CQ2	$\partial^2 C/\partial\beta^2$	
CSIN	coefficients of Taylor's expansion of sine function	
DI	resolution of results	
F244	$\partial^2 f/\partial\alpha^2$	(Eq.36c)
F2Q4	$\partial^2 f/\partial\alpha\partial\beta$	
F2QQ	$\partial^2 f/\partial\beta^2$	(Eq.36d)
F2X4	$\partial^2 f/\partial X\partial\alpha$	
F2XQ	$\partial^2 f/\partial X\partial\beta$	(Eq.36b)
F2XX	$\partial^2 f/\partial X^2$	(Eq.36a)

F4	$\partial f/\partial\alpha$	(Eq.33b)
FQ	$\partial f/\partial\beta$	(Eq.33c)
FX	$\partial f/\partial X$	(Eq.33a)
GA	γ	
P1	p(I)	(Eq.37)
RI	I	
S22	$\partial^2 S/\partial\alpha\partial\beta$	
S41	$\partial S/\partial\alpha$	
S42	$\partial^2 S/\partial\alpha^2$	
SA	σ_α	
SQ1	$\partial S/\partial\beta$	
SQ2	$\partial^2 S/\partial\beta^2$	
SX	σ_X	
XO	X_o	
ZO	Z_o	

```
C     CORRECTION TERM FOR NON-TRACKING P(I)     (EQ. 40)
C
      CALL SEARCH (1,'INPUT',1,0)
      CALL SEARCH (2,'OUTPUT',2,0)
   10 FORMAT (4E10.4)
      READ (5,10) SX, SD, DI, GA
         TGA = 2.0 * GA
         VX = SX * SX
         VD = SD * SD
         IEND = 10.0 / DI
      DO 300 I = 1, IEND
         RI = I
         RI = -5.0 + RI * DI
         XO = - VX
      P =      3.83171 * EXP(-0.5 * (RI*RI + 14.682 /VD))
      P = P + 7.01559 * EXP(-0.5 * (RI*RI + 49.2185/VD))
      P = 0.5 * SX * P
      DO 100 K = 1, 99
         D = K
         D = 3.83171 + 3.18388E-2 * D
      CALL FXO (XO, TGA, D, RI, VX, VD, RIBAR, FXX)
      P = P + D * EXP(-0.5* ((RI-RIBAR)*(RI-RIBAR)
     1    + (XO+VX)*(XO+VX)/VX + D*D/VD)) / SQRT(-FXX)
  100 CONTINUE
      P = 0.398942 * 3.18388E-2 * P / (SX*VD)
  200 FORMAT (F10.2, E15.5)
      WRITE (6,200) RI, P
  300 CONTINUE
      CALL SEARCH (4,0,1,0)
      CALL SEARCH (4,0,2,0)
      CALL EXIT
      END
C
C    CALCULATION OF STATIONARY POINT FOR STEEPEST DESCENTS
C         INTEGRATION OVER X
C
      SUBROUTINE FXO(XO, TGA, D, RI, VX, VD, RIBAR, FXX)
      DO 1000 L = 1, 100
         X1 = XO
         RIBAR = TGA * EXP(X1) * AJ1(D)
C             AJ1 IS FIRST ORDER BESSEL FUNCTION DIVIDED
C                   BY ARGUMENT
      FX = (RI-RIBAR) * RIBAR - (X1+VX)/VX
      FXX = (RI-2.0*RIBAR) * RIBAR - 1.0/VX
      XO = X1 - FX / FXX
      IF (ABS((X1-XO)/X1) .GT. 1.0E-5) GO TO 1000
         RETURN
 1000 CONTINUE
         PAUSE 1
         RETURN
         END
```

DI	resolution of results
FX	$\partial f/\partial X$
FXX	$\partial^2 f/\partial X^2$
GA	γ
P	g(I) (Eq.D1)
RI	I
SD	σ_Δ
SX	σ_X
XO	stationary point

Appendix E

In the final two chapters of this work, experimental results have been presented for the signal distribution from an optical heterodyne receiver which was described briefly in the text of these chapters. In this appendix the actual receiver that was used is described in more detail, including design schematics. These are given in Figs. E1 through E13 with a few words of explanation below.

Fig. E1. Receiver Block Diagram.

In this figure the main functional blocks of the frequency lock loop, the four signal channels, the photomultiplier tube power distribution, and the current monitoring circuitry are outlined showing their interrelationships. The following figures detail the design of each of these blocks.

Fig. E2. Optics.

The signal is collected by the telescope and mixed with the local oscillator laser at the surface of a ten per cent reflecting beamsplitter. Separation of the signal into four channels is begun by the four independent steering mirrors and the process is completed by the four aperture slide plate located in front of the detector boxes. The optics form an image of the front of the telescope at this slide plate that is reduced by a factor of 5.3. The virtual apertures at the telescope form a square 10 cm. on a side with each having a diameter that can be varied from 0.21 cm. to 5.1 cm.

Fig. E3. Loop Photomultiplier Tube.

The photomultiplier tube anode feeds a tuned circuit centered at 29.5 MHz and with -3dB points at 28.8 MHz and 30.3 MHz. The IF signal,

taken from a 50 ohm tap on the inductor, is fed into the frequency discriminator block while the D.C. component of the current is low pass filtered and fed into the current monitoring circuit.

Fig. E4. Discriminator.

The signal is next fed into an RGH Electronics IF package which amplifies and then envelope demodulates it. The amplified IF signal is put through an RGH discriminator package with center frequency at 29.5 MHz and the frequency demodulated signal is sent to the sample and hold circuitry. The amplitude demodulated signal from the IF strip is fed into the sample and hold control circuit.

Fig. E5. Sample and Hold Control.

A sample and hold circuit was designed into the system so that the loop would lock onto its last known value during periods when the optical signal was blocked by the chopping wheel. The discriminator output is sampled whenever either 1) the switch in the control circuit is in the "continuous" mode, or 2) the amplitude demodulated signal from the IF strip is greater than the comparator threshold with the switch in the "chopped" mode. In attempting to adjust the comparator threshold, however, it was discovered that the frequency demodulation of the IF signal was more sensitive than the amplitude demodulation. In addition, the tuned circuit at the photomultiplier anode insured that the peak frequency of the noise spectrum was the same as the lock-on frequency so that the loop did not drift rapidly during periods of no signal. The result was that the best performance was obtained by running the loop in the "continuous" mode.

Fig. E6. Sample and Hold.

The sample and hold circuitry, always sampling in the "continuous" mode, feeds into a gain of one amplifier which operates in either an

"inverting" or a "non-inverting" mode. The local oscillator frequency will be higher or lower than that of the signal depending on the position of this switch. This makes no practical difference in the operation of the loop or in the signal channels, however.

Fig. E7. Loop Gain Control.

A two stage amplifier controls the loop gain. The first stage is a low voltage amplifier with gain continuously variable from 0 to 2.5. The second stage is capable of 0 to 300 V outputs and has a switchable gain control. Optimum loop performance occurs with this switch in a gain 100 position which results in an overall loop response of about one kHz. The loop is locked by manually sweeping the adjustable offset voltage of the high voltage amplifier stage. The gain control output is fed into the control electronics of a Spectra Physics' 119 laser which acts as a voltage controlled oscillator, completing the loop.

Fig. E8. Oscillator.

This circuit generates a 28.5 MHz electrical signal and feeds it to each of the four signal channels.

Fig. E9. Signal Photomultiplier Tube Box.

In each of the four signal channels the photomultiplier anode current feeds into a tuned circuit identical to that in the loop detector. The D.C. component is fed to the monitoring circuit while the IF component is mixed with the oscillator output. The resultant 1MHz signal is passed to the rectifier through a line driver and transmission cable.

Fig. E10. Rectifier.

This is one of the four identical full wave rectifiers that begin envelope demodulation of the signals.

Fig. E11. Low Pass Filter.

The final stage of envelope demodulation is accomplished with an eight pole Bessel filter. The -3dB point of the filter is at 200 kHz.

The final two figures give details of the photomultiplier tube power distribution and of the metering circuit that was used to monitor the D.C. anode current through the tubes.

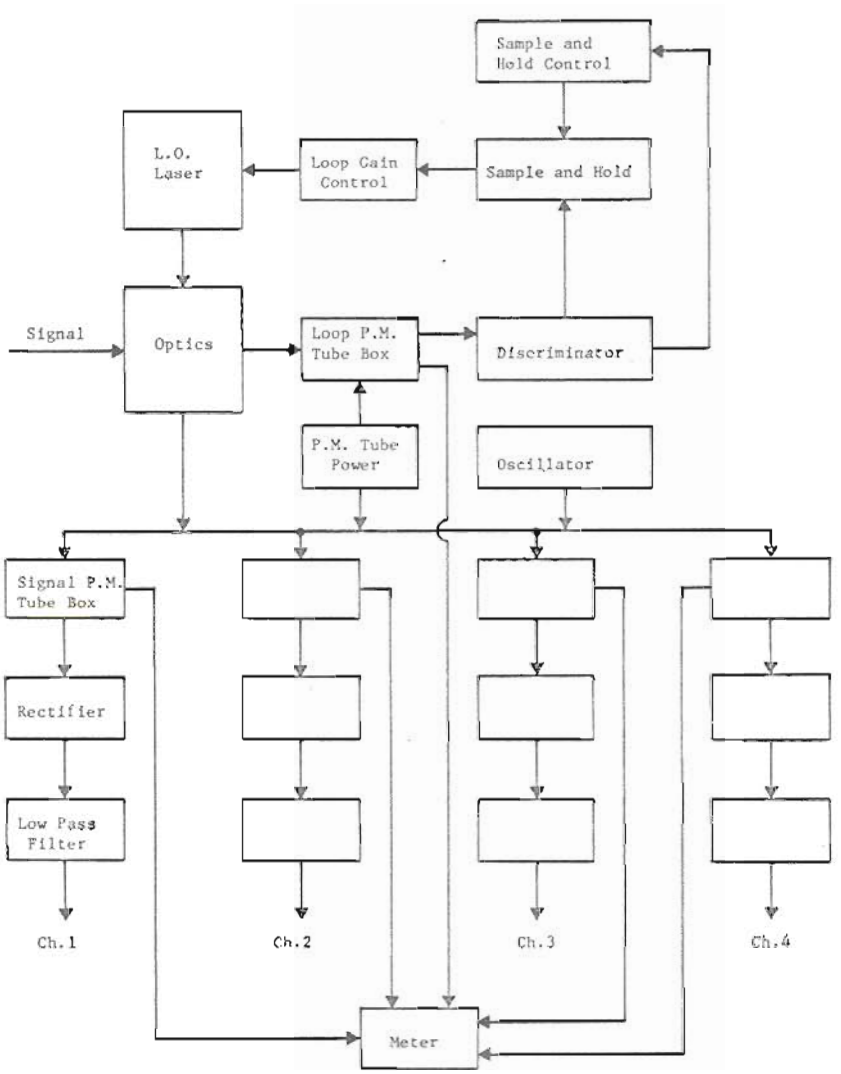

Fig. E1. Receiver block diagram.

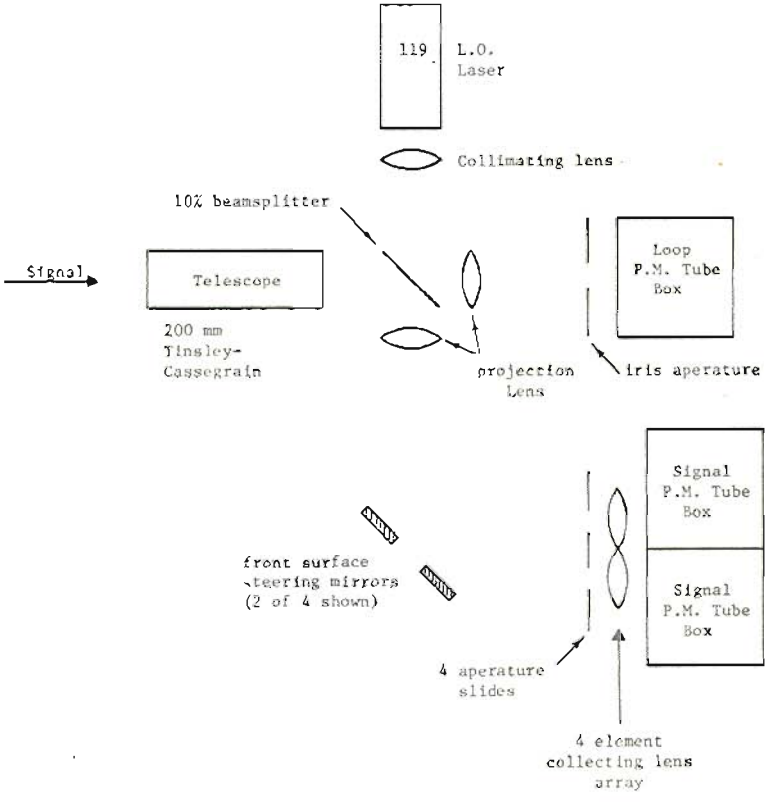

Fig. E2. Optics

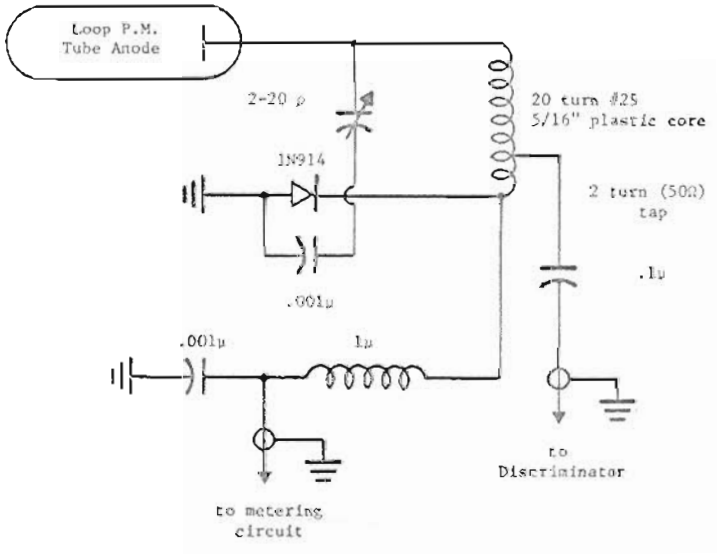

Fig. E3. Loop photomultiplier tube

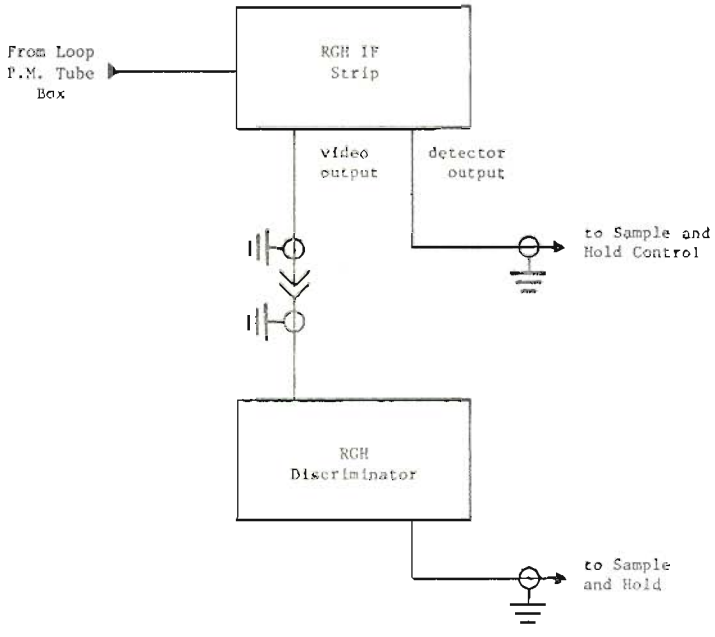

Fig. E4. Discriminator

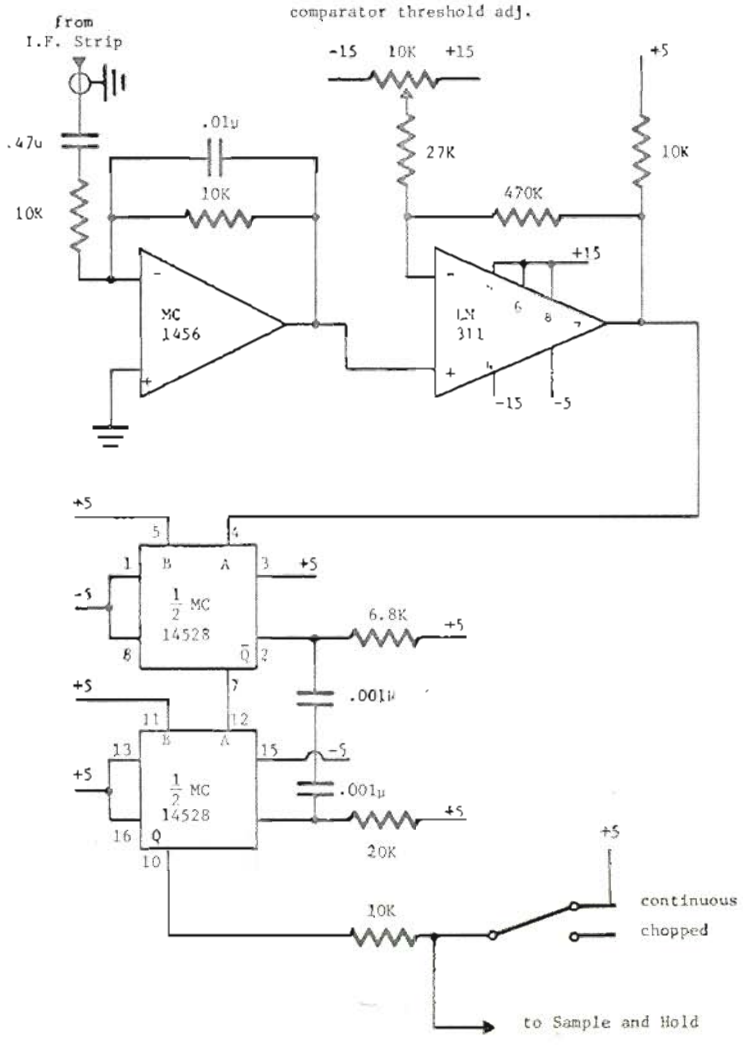

Fig. E5. Sample and hold control

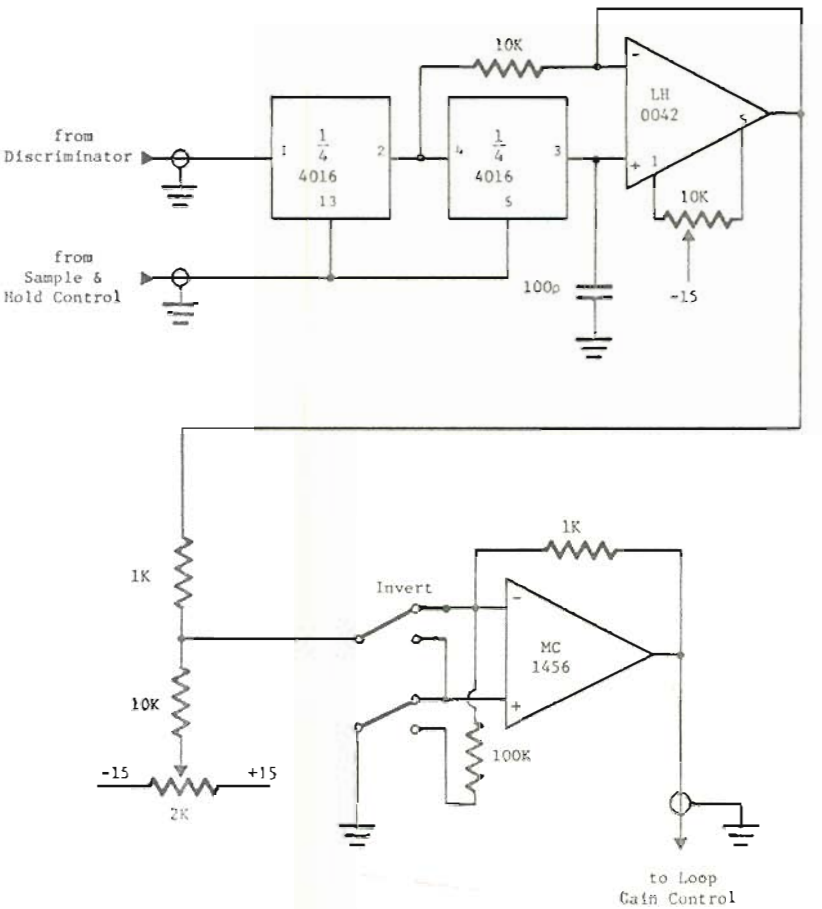

Fig. E6. Sample and hold

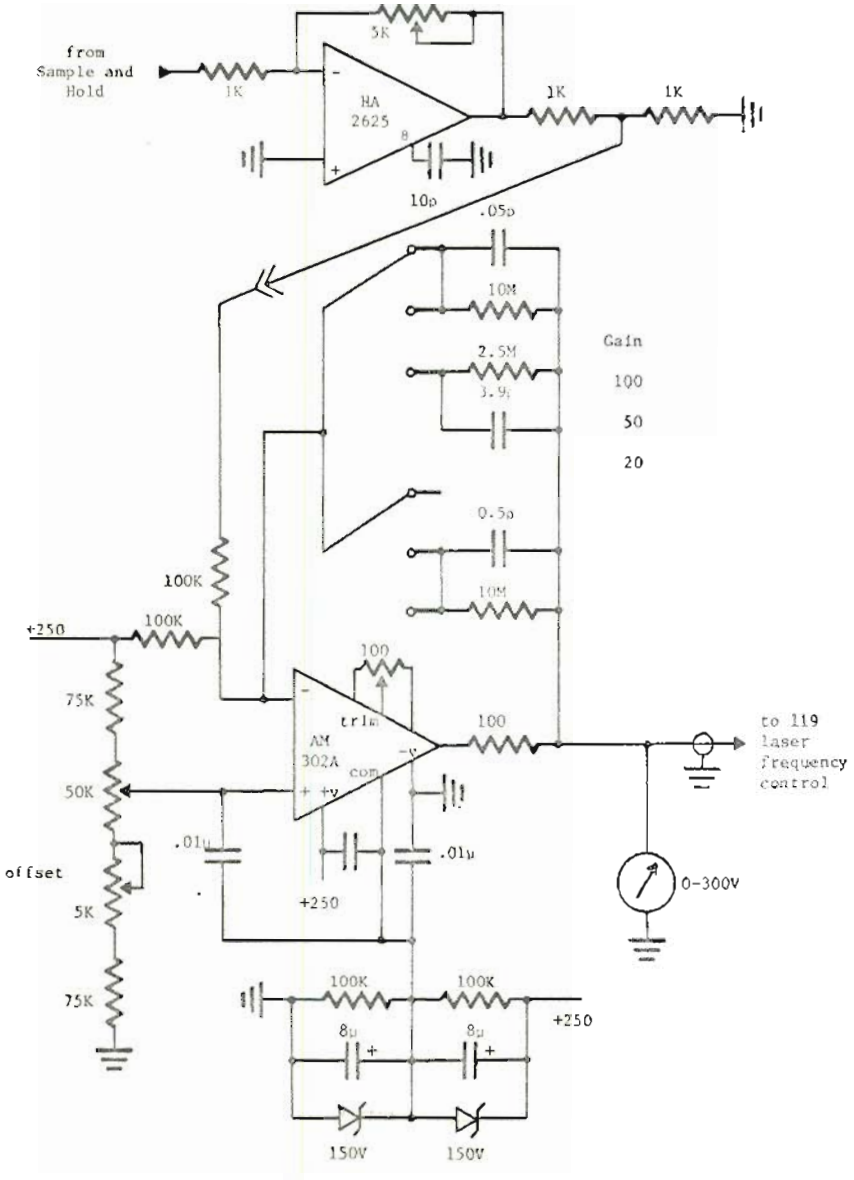

Fig. E7. Loop gain control

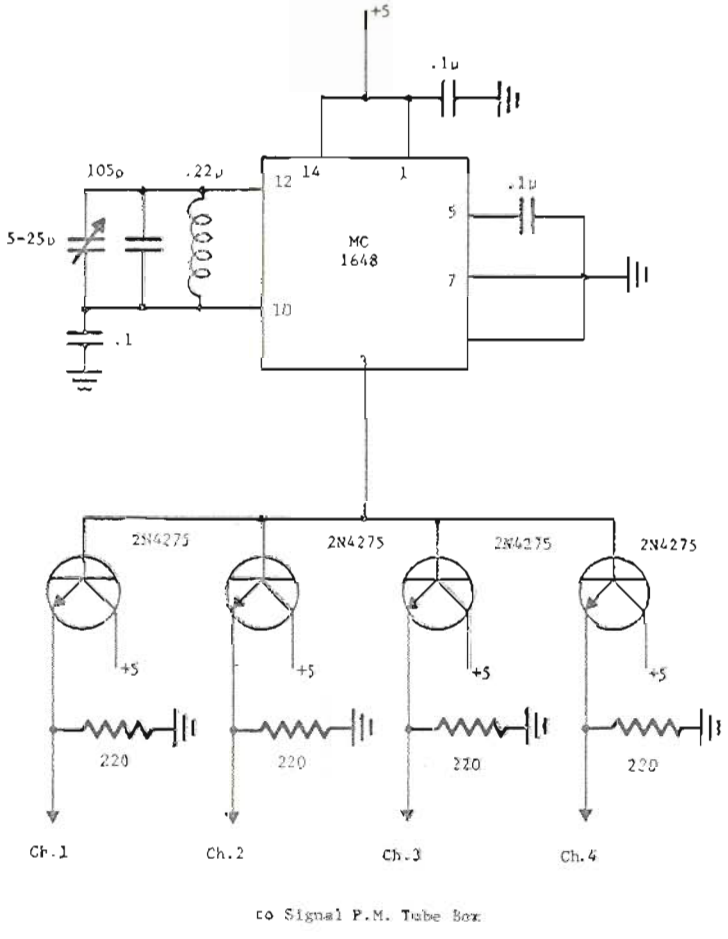

Fig. E8. Oscillator

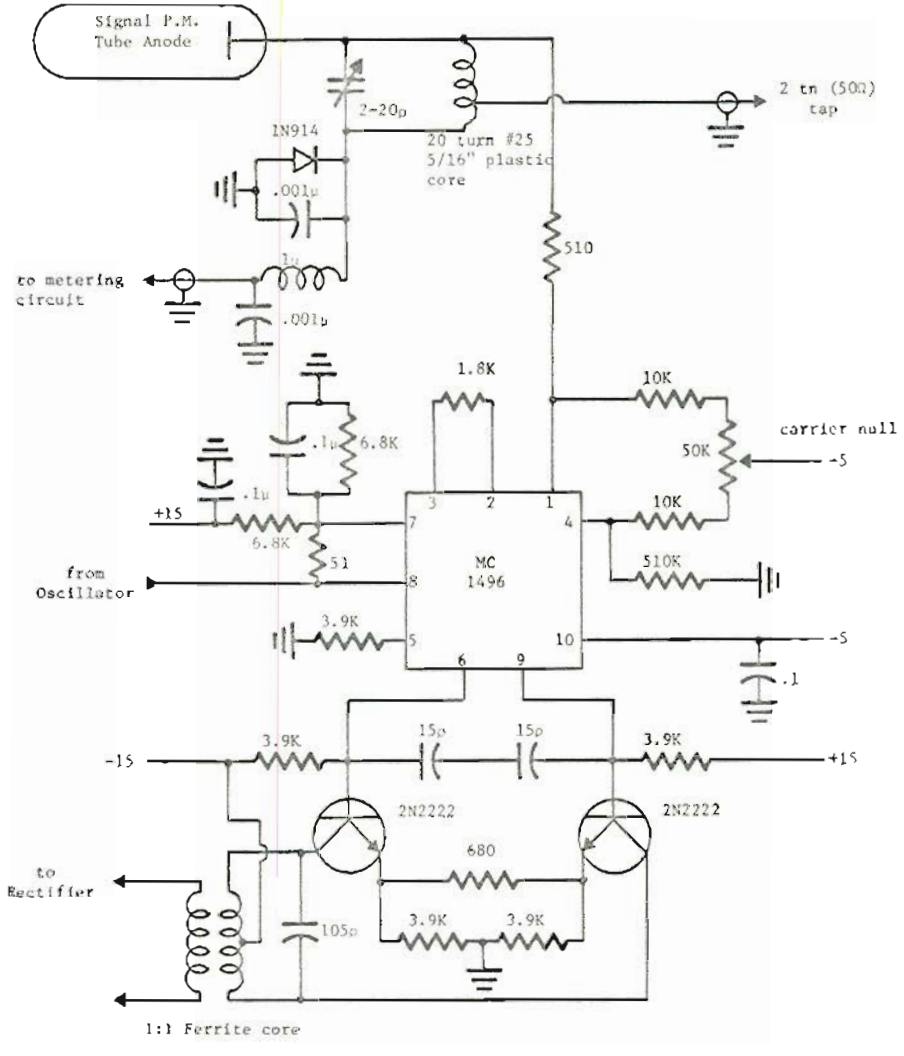

Fig. E9. Signal photomultiplier tube box

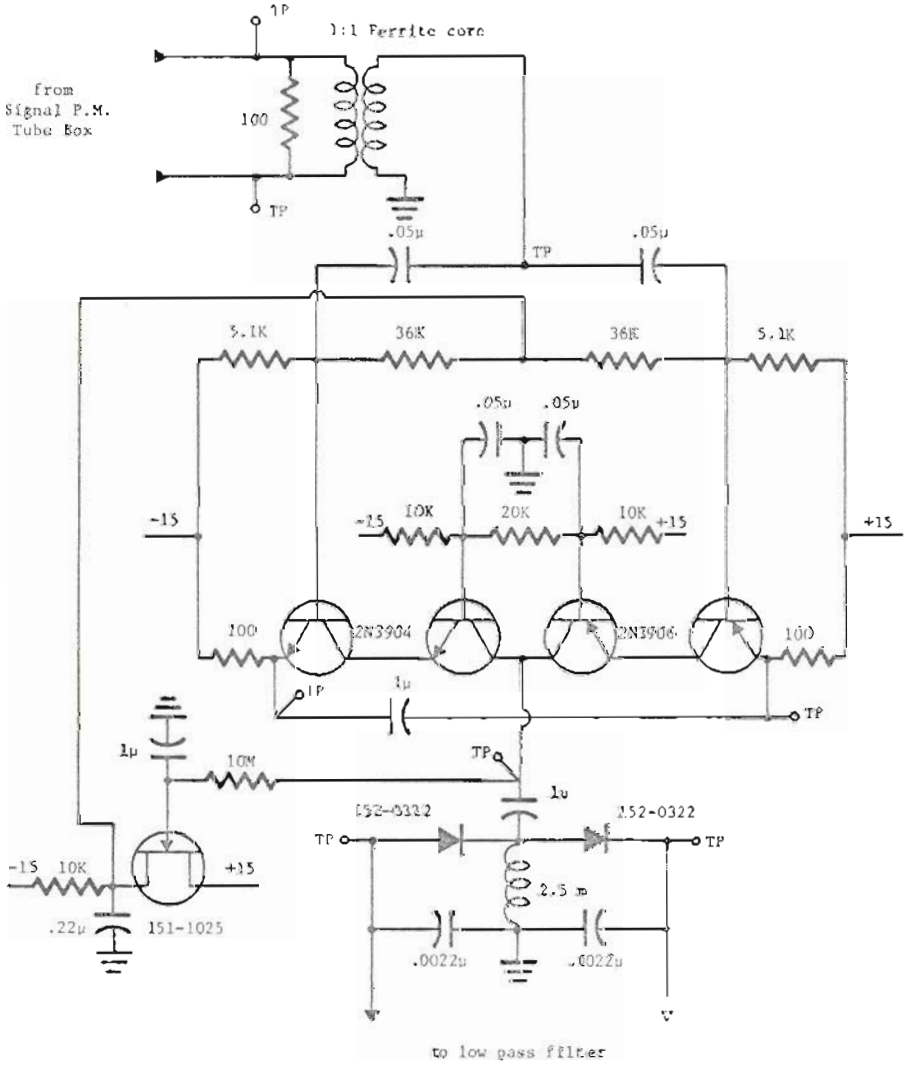

Fig. E10. Rectifier

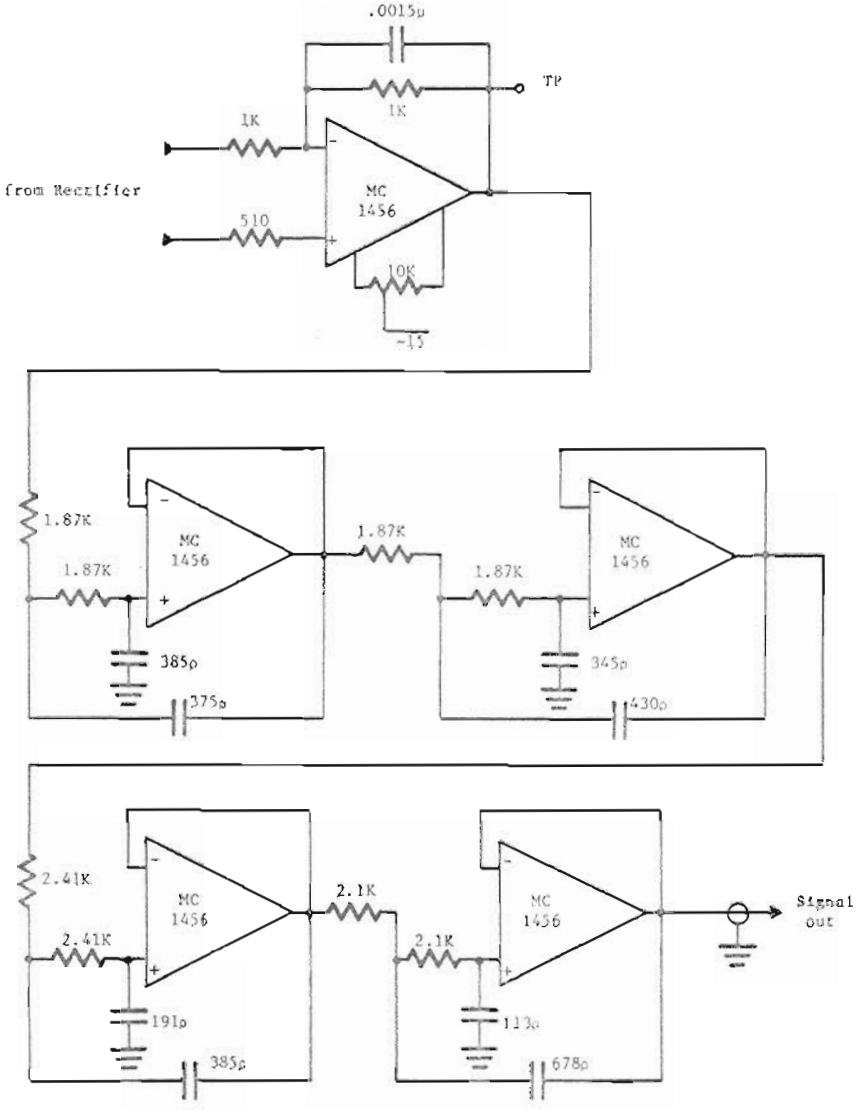

Fig. E11. Low pass filter

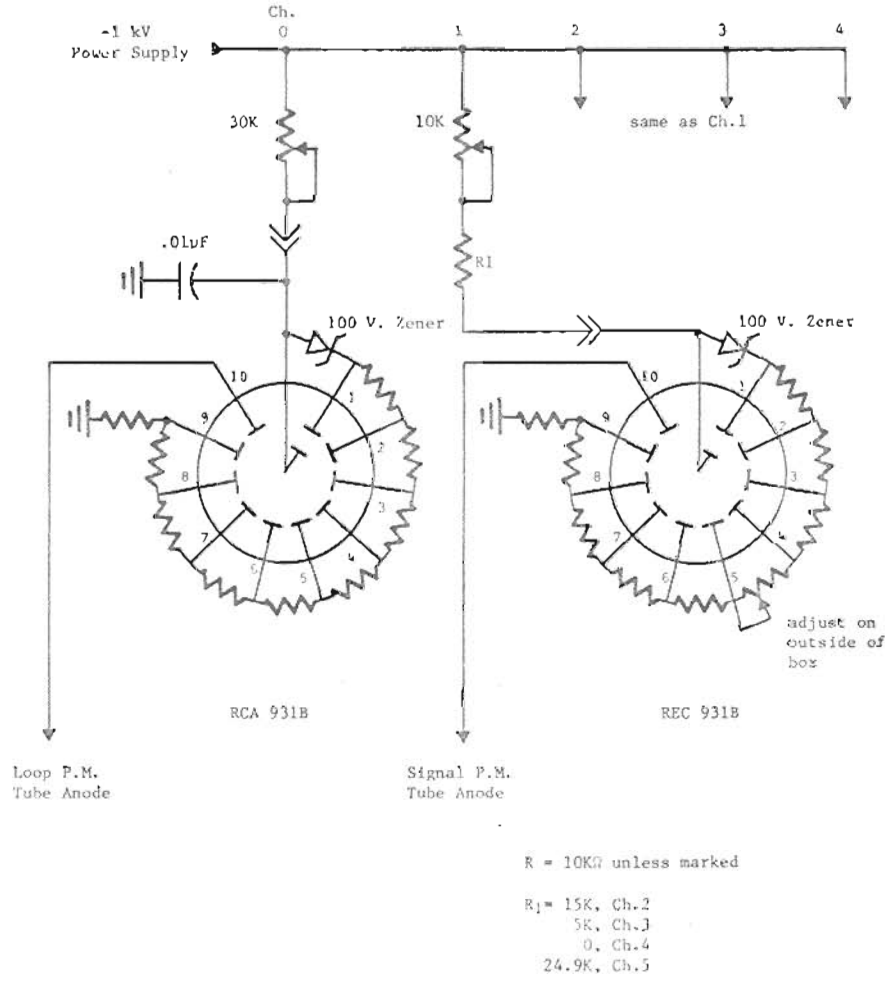

Fig. E12. Photomultiplier tube power distribution

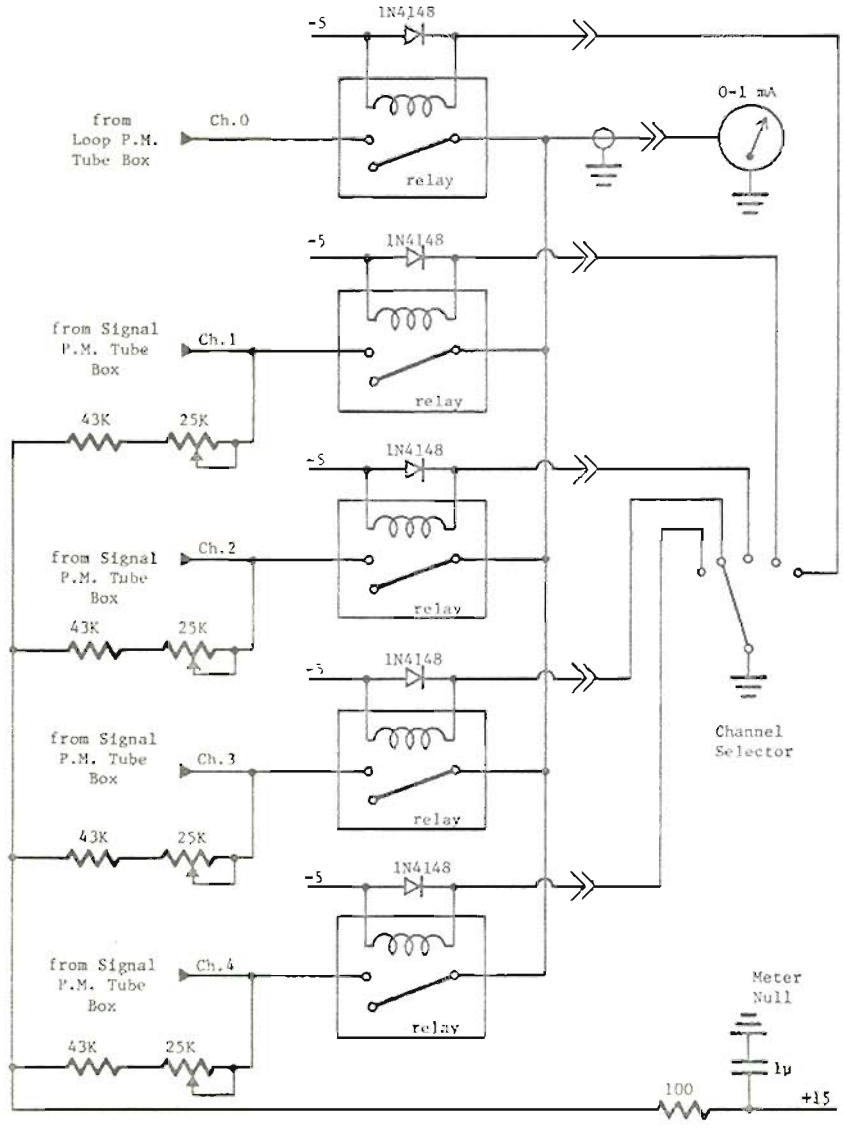

Fig. E13. Current Metering circuit

Appendix F

Since $\vec{\Delta}_x$ and $\vec{\Delta}_y$ are independent random vectors, we have, from Eq.(2) of Chapter 6

$$p(\vec{\Delta}_x, \vec{\Delta}_y) = (2\pi)^{-N} |C_{\Delta_x}|^{-\frac{1}{2}} |C_{\Delta_y}|^{-\frac{1}{2}} \exp\left(-\tfrac{1}{2} \vec{\Delta}_x^{\dagger} C_{\Delta_x}^{-1} \vec{\Delta}_x^{2}\right) \tag{F1}$$

$$- \tfrac{1}{2} \vec{\Delta}_y^{\dagger} C_{\Delta_y}^{-1} \vec{\Delta}_y)$$

Changing to polar corrdinates

$$\Delta_i = (\Delta_{xi}^2 + \Delta_{yi}^2)^{\frac{1}{2}} \tag{F2}$$

$$\theta_i = \tan^{-1}(\Delta_{yi}/\Delta_{xi})$$

and integrating over the N angular variables yields

$$p(\vec{\Delta}) = (2\pi)^{-N} |C_{\Delta_x}|^{-\frac{1}{2}} |C_{\Delta_y}|^{-\frac{1}{2}} \int_0^{2\pi} \cdots \int \Delta_1 d\theta_1 \cdots \Delta_N d\theta_N \tag{F3}$$

$$X \exp\left[-\tfrac{1}{2} \sum_{i=1}^{N} \sum_{j=1}^{N} \Delta_i \Delta_j \left(C_{\Delta_{xij}}^{-1} \cos\theta_i \cos\theta_j + C_{\Delta_{yij}}^{-1} \sin\theta_i \sin\theta_j\right)\right]$$

If we assume an isotropic atmosphere, so that $C_{\Delta_{xii}}^{-1} = C_{\Delta_{yii}}^{-1}$, this can be rearranged to give

$$p(\vec{\Delta}) = |C_{\Delta_x}|^{-\frac{1}{2}} |C_{\Delta_y}|^{-\frac{1}{2}} \prod_{i=1}^{N} \left[\Delta_i \exp(-\tfrac{1}{2} C_{\Delta_{xii}}^{-1} \Delta_i^2)\right]$$

$$X \left\{ (2\pi)^{-N} \int_0^{2\pi} \cdots \int d\theta_1 \ldots d\theta_N \exp\left[-\tfrac{1}{2} \sum_{\substack{i=1 \\ i\neq j}}^{N} \sum_{j=1}^{N} \Delta_i \Delta_j \right. \right. \tag{F4}$$

$$\left. \left. X \left(C_{\Delta_{xij}}^{-1} \cos\theta_i \cos\theta_j + C_{\Delta_{yij}}^{-1} \sin\theta_i \sin\theta_j\right)\right]\right\}$$

Comparison of F4 with Eq.(3), therefore, implies that $G_N(\vec{\Delta})$ is defined by the expression contained within the curly brackets.

Evaluation of $G_N(\vec{\Delta})$ for the general case is seen to be rather complex. If all off-diagonal elements of C_{Δ_x} and C_{Δ_y} are zero, however, the trivial result is obtained that $G_N(\vec{\Delta}) = 1$ for independent Δ_i and also, therefore, that $G_1(\vec{\Delta}) = 1$. The probability density function then reduces to the product of N Rayleigh density functions.

Another case that can be evaluated is $G_2(\vec{\Delta})$. First we make the observations that $C_{\Delta x12} = C_{\Delta x21}$ from symmetry considerations, and that without loss of generality, we can align the detectors so that they lie along the line y = x. This last condition allows us to consider the case where $C_{\Delta_x} = C_{\Delta_y}$ so that

$$G_2(\vec{\Delta}) = \frac{1}{4\pi^2} \int_0^{2\pi} \int_0^{2\pi} d\theta_1 \, d\theta_2 \exp\left[- C_{\Delta x12} \, \Delta_1 \, \Delta_2 \cos(\theta_1 - \theta_2) \right]$$

$$= I_o \left(C_{\Delta x12} \, \Delta_1 \, \Delta_2 \right) \qquad \text{(F5)}$$

where I_o is the modified Bessel function of order zero.

For three or more detectors the form of the covariance matrices depends on the geometry of the receivers and the integration becomes more complex. In all probability numerical evaluation of $G_N(\vec{\Delta})$ and of its derivatives would be necessary in these cases.

Appendix G

In Eq.(11) of Chapter 6 it was stated that

$$C_{\Delta x} = \sigma_{\Delta}^2 \begin{pmatrix} 1 & r_{\Delta} \\ r_{\Delta} & 1 \end{pmatrix} \tag{G1}$$

which implied that the phase parameter variance and correlation coefficient are given by

$$\sigma_{\Delta}^2 = C_{\Delta x11} = \langle \Delta_{x1}^2 \rangle$$

$$r_{\Delta} = C_{\Delta x12} \,/\, C_{\Delta x11} = \frac{1}{\sigma_{\Delta}^2} \langle \Delta_{x1} \Delta_{x2} \rangle \tag{G2}$$

since, from symmetry considerations, $\langle \Delta_{x1} \rangle = \langle \Delta_{x2} \rangle = 0$.

Let $\phi(a)$ be the phase angle of the signal at the point labeled "a" in Fig. G1. The average x-direction component of the tilt across detector 1 can be approximated, in this notation, by

$$\Delta_{x1} \approx \tfrac{1}{2} [\phi(a) - \phi(a')] \tag{G3}$$

so that

$$\sigma_{\Delta}^2 = \tfrac{1}{4} \langle [\phi(a)-\phi(a')]^2 \rangle = \tfrac{1}{4} D_s(D) \tag{G4}$$

where D is the detector aperture diameter and D_s, the structure function of phase, is defined by Eq.(G4). In a similar manner,

$$4 \sigma_{\Delta}^2 r_{\Delta} = \langle [\phi(a)-\phi(a')][\phi(b)-\phi(b')] \rangle \tag{G5}$$

Some algebraic manipulation yields

$$\sigma_{\Delta}^2 r_{\Delta} = \tfrac{1}{8} \Big\{ \langle [\phi(a)-\phi(b')]^2 \rangle + \langle [\phi(a')-\phi(b)]^2 \rangle - \langle [\phi(a)-\phi(b)]^2 \rangle - \langle [\phi(a')-\phi(b')]^2 \rangle \Big\} \tag{G6}$$

which, considering the geometry of Fig. G1, results in

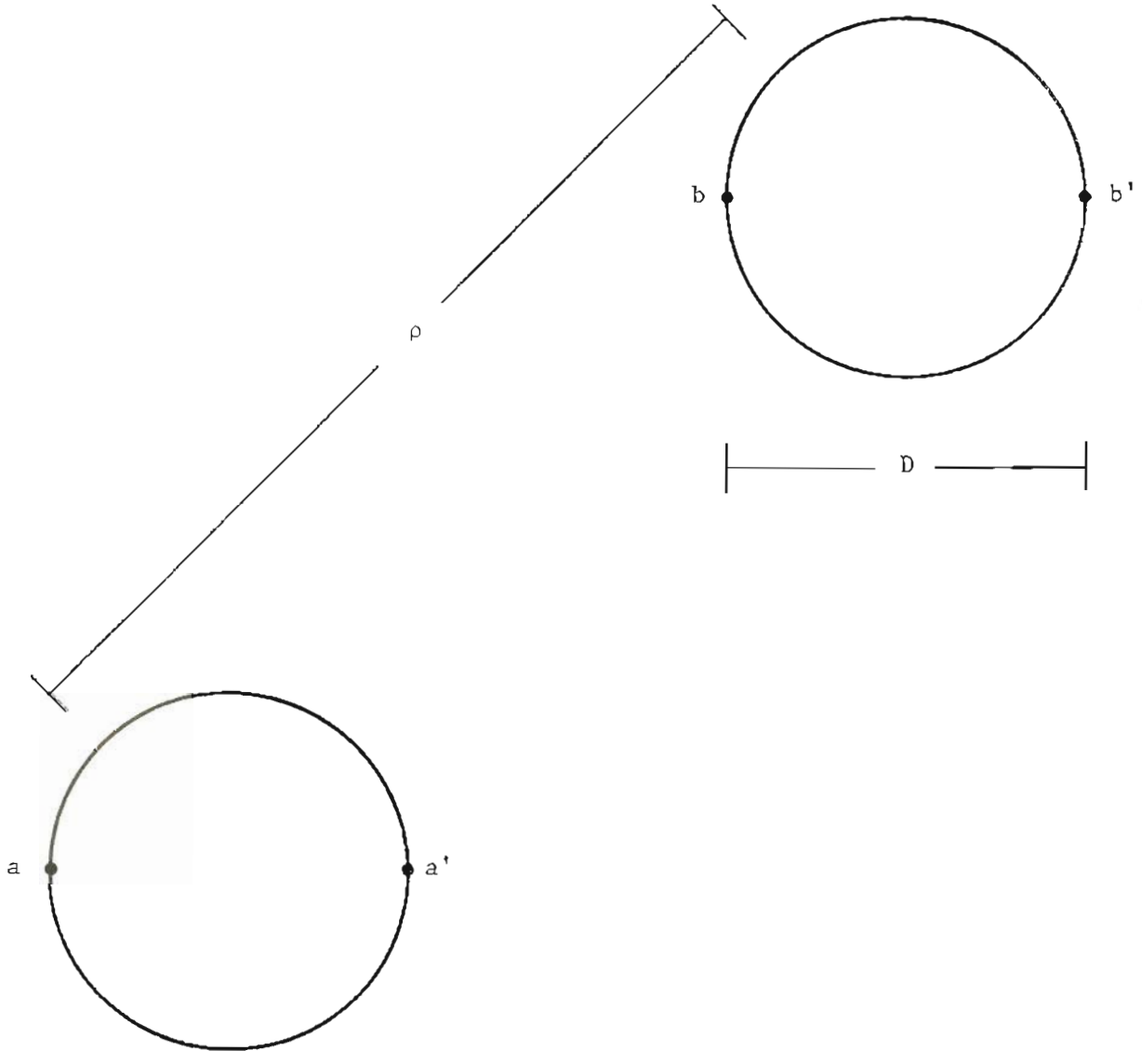

Fig. G1: Geometry used for calculation of $r_{\triangle}$.

(G7)

$$\sigma_\Delta^2 \, r_\Delta = \tfrac{1}{8} \mathcal{D}_s \left[(\rho^2+D^2+\sqrt{2}\,\rho\,D)^{\frac{1}{2}} \right] + \tfrac{1}{8} \mathcal{D}_s \left[(\rho^2+D^2-\sqrt{2}\,\rho\,D)^{\frac{1}{2}} \right.$$

$$\left. - \tfrac{1}{4} \mathcal{D}_s(\rho) \right.$$

It is helpful at this point to define the characteristic coherence diameter of the atmosphere by

$$r_o = 3.31 \, z \left[\mathcal{D}(z) \right]^{-5/3} \tag{G8}$$

where $\mathcal{D}(z)$ is the total wave structure function. For the cases of plane and spherical wave propagation, this is given by

$$r_o = \begin{cases} 1.73 \, k^{-6/5} \, L^{-3/5} \, C_n^{-6/5} & \text{(plane wave)} \\ 3.11 \, k^{-6/5} \, L^{-3/5} \, C_n^{-6/5} & \text{(spherical wave)} \end{cases} \tag{G9}$$

where k is the wavenumber of the signal, L is the propagation distance, and C_n^2 is the structure constant of refractive index fluctuations.

The assumption that $\mathcal{D}_s(z) \approx \mathcal{D}(z)$ is a very good approximation for near field applications[3] ($D \gg \sqrt{2\pi L/k}$) and also under conditions of saturated amplitude fluctuations.[29] Since, even when these conditions are not met, this approximation overestimates phase fluctuations by no more than a factor of two, it will be used here. This leads to

$$\sigma_\Delta^2 = 1.72 (D/r_o)^{5/3} \tag{G10}$$

$$r_\Delta = \tfrac{1}{2} \left(1 + \frac{\rho^2}{D^2} + \sqrt{2}\frac{\rho}{D} \right)^{5/6} + \tfrac{1}{2} \left(1 + \frac{\rho^2}{D^2} - \sqrt{2}\frac{\rho}{D} \right)^{5/6} - \left(\frac{\rho}{D} \right)^{5/6}$$

for spherical or plane wave propagation.

BIOGRAPHICAL NOTE

The author was born 29 August 1951 in Seattle, Washington. He received his Bachelor of Science degree in Physics and Mathematics from Whitworth College in 1974, with his undergraduate work including, in 1973, a four month Fellowship at McDonnell-Douglas Laboratories working on safety analysis of a nuclear powered heart pacemaker.

Since 1974, he has been a student at the Oregon Graduate Center, where his work in optical communications through the atmosphere has led to the following publications:

1. J.H. Churnside and C.M. McIntyre, "Averaged Threshold Receiver for Direct Detection of Optical Communications Through the Lognormal Atmospheric Channel," Appl. Opt. 16, October 1977.
2. J.H. Churnside and C.M. McIntyre, "Partial Tracking Optical Heterodyne Receiver Arrays," J. Opt. Soc. Am.68, June 1978.
3. J.H. Churnside and C.M. McIntyre, "Signal Current Probability Distribution for Optical Heterodyne Receivers in the Turbulent Atmosphere. 1: Theory, " Appl. Opt. 17, 1 August 1978.
4. J.H. Churnside and C.M. McIntyre, "Signal Current Probability Distribution for Optical Heterodyne Receivers In the Turbulent Atmosphere. 2: Experiment," Appl. Opt. 17, 1 August 1978.

5. J.H. Churnside and C.M. McIntyre, "Joint Signal Probability Distribution of an Optical Heterodyne Array," Proc. SPIE 142, March 1978.

6. C.M. McIntyre and J.H. Churnside, "Heterodyne Receiver for Visible Radiation Through the Atmosphere," Proc. SPIE 142, March 1978.